Development of cell-type specific ligands and dendrons comprising a defined number of different functional groups for targeted gene therapy

Inaugural-Dissertation
to obtain the academic degree
Doctor rerum naturalium (Dr. rer. nat.)

submitted to the Department of Biology, Chemistry, Pharmacy
of Freie Universität Berlin

by

Melanie Kraß

2023

The following PhD thesis was carried out from October 2020 until October 2023 in the research group of Prof. Dr. Hendrik Fuchs at the Institute of Diagnostic Laboratory Medicine, Clinical Chemistry and Pathobiochemistry of the Charité.

1st reviewer:
Prof. Dr. Hendrik Fuchs
Charité – Universitätsmedizin Berlin
Institute of Diagnostic Laboratory Medicine, Clinical Chemistry and Pathobiochemistry
Augustenburger Platz 1
13353 Berlin Germany

2nd reviewer:
Prof. Dr. Rainer Haag
Freie Universität Berlin
Institute of Chemistry and Biochemistry
Takustraße 3
14195 Berlin Germany

Date of defence: 01.02.2024

Acknowledgement

First, I would like to thank Prof. Dr. Hendrik Fuchs, for allowing me to complete my doctoral thesis in his research group, but above all, for his continuous support. He always had an open door, and I could exchange ideas and discuss the progress of the project with him at any time.

Next, I would like to express my gratitude to Prof. Dr. Rainer Haag, who took on the role of the second examiner and thus enabled me to pursue my doctoral studies at the Freie Universität Berlin.

I also want to extend my thanks to my amazing ENDOSCAPE team at Charité (Hendrik, Gregor, Philipp, Lena). It was an honour to work with you. We were a fantastic team and tackled all challenges together. Our business trips were always filled with fun and joy. A special thanks goes to Meike from FU Berlin. I am very grateful and proud of our great collaboration. Thanks also to the rest of the ENDOSCAPE consortium for productive meetings, discussions, and support.

Of course, I would like to thank the entire AG Fuchs, both the "official" members (Nicole, Alex, Shikha, Gregor, Philipp, Lena, Alessio, Gaurav) and our "adopted" ones (Maria, Tuyen, Robert), our former students, and the AG Dernedde (Jens, Marten, Burak). It was always a pleasure to work with you and exchange scientific ideas. Thank you for your professional and personal support and friendship.

I would also like to thank my university friends (Max, Felix, Simon, Ruben, and Franzi). Without you, my studies wouldn't have been nearly as fun and successful. A huge thank you goes to my best friend, Mara. Even though you live over 500 km away, you managed to take a lot of burden off my shoulders and always supported me.

I also want to thank my boyfriend and partner, Constantin. You have always been my safe haven where I could relax after work. Thank you for your unconditional love and support in all aspects of my life.

Last but not least, I want to express my gratitude to my parents, who have made me the person I am today and who loved me unconditionally. They taught me to always see things positively and not to fear new challenges. They supported me throughout my entire life and always believed in me. Thank you for everything Mom and Dad!

This project has received funding from the European Union’s Horizon 2020 research and innovation programme under grant agreement No 825730.

Declaration of Authorship

Herewith I certify that I have prepared and written my thesis independently and that I have not used any sources and aids other than those indicated by me. I also declare that I have not submitted the dissertation in this or any other form to any other institution as a dissertation.

_____

Berlin, 12.10.2023

Table of contents

Zusammenfassung

Gentherapie ist eine leistungsfähige und vielversprechende therapeutische Methode zur Behandlung einer Vielzahl von Krankheiten. Um die sichere und effiziente Übertragung des genetischen Materials zu gewährleisten und einen Abbau zu verhindern, hat sich die Verwendung kationischer dendritischer Vektoren besonders bewährt, da sie negativ geladenes genetisches Material komplexieren und Polyplexe bilden können. Verzweigte kationische Polymere, auch Dendrimere genannt, wie Poly(amidoamin) (PAMAM) haben bereits vielversprechende Ergebnisse beim Gentransport gezeigt. PAMAM wurde jedoch auch mit Zytotoxizität und Heterogenität in Verbindung gebracht. Um diese Einschränkungen zu überwinden, wurden in dieser Arbeit vier definierte Dendrone auf Polylysinbasis mit unterschiedlichen funktionellen Gruppen mittels Festphasen-Peptidsynthese auf reproduzierbare Weise synthetisiert. Darüber hinaus ist die zielgerichtete Therapie ein wertvolles Instrument für die spezifischere Behandlung von Krebs oder anderen Krankheiten, ohne dass gesunde Zellen zerstört oder geschädigt werden. In dieser Arbeit wurden als Proof of Concept, sowohl Leber- als auch Krebszellen als Zielzellen untersucht. Als leberspezifische Zielstrukturen wurden das vom Hepatitis-Virus B abgeleitete große Oberflächenprotein (LSP) und seine preS1-Bindungsdomäne sowie das Apolipoprotein A1 (ApoA1), das Teil des High-Density-Lipoproteins (HDL) ist, ausgewählt. Der epidermale Wachstumsfaktor (EGF) wurde als zielgerichteter Ligand für Krebs verwendet. Um Vernetzungen zu vermeiden und eine homogene Plattform zu erhalten, wurden die Ligandenplasmide so konzipiert, dass sie nur eine einzige Konjugationsstelle aufweisen. Zwei Ligandenvarianten wurden erfolgreich rekombinant in *Escherichia coli* Rosetta(DE3) (K-EGF^{RR}) und NiCo21(DE3) (C-ApoA1) mit einer Ausbeute von 4–6 mg/L Ansatz exprimiert. Die Ligand-Zell-Interaktion wurde mittels Durchflusszytometrie und Fluoreszenzmikroskopie bewertet, während die Ligand-Rezeptor-Interaktion mittels enzymgekoppelten Immunabsorptionstest und Oberflächenplasmonenresonanz untersucht wurde. Die Affinität der EGF-Variante war sogar höher als die des Wildtyp-EGF (K_D: 5,9 vs 7,3 nM). Darüber hinaus wurden heterobifunktionelle Polyethylenglykol-Linker eingeführt, um eine orthogonale Klick-Konjugation des Proteins an ein beliebiges Ziel, in diesem Fall die synthetisierten Dendrons, zu ermöglichen. Die Dendrons wurden mit Plasmid-DNA, die für das verstärkt grün fluoreszierenden Protein (eGFP) oder Luziferase kodiert, in verschiedenen N/P-Verhältnissen (0,5–16) polyplexiert, wobei N für die Anzahl der terminalen Aminogruppen steht und P für die Phosphatgruppen der DNA. Darüber hinaus wurden K-EGF^{RR} in unterschiedlichen EGF/DNA-Gewichtsverhältnissen (0,1; 1; 10) entweder elektrostatisch in den Polyplex eingebaut oder kovalent mit Hilfe von strain promoted azide-alkyne cycloadditon (SPAAC) gebunden. Die Polyplexe wurden mittels dynamischer Lichtstreuung analysiert (Größe: 270–1023 nm, Polydispersitätindex: 0,13–0,99) auf. Die Transfektionseffizienz wurde durch Messung der Expressionsniveaus von eGFP und Luziferase bewertet. Da die meisten DNA-Fragmente in Endolysosomen gefangen und

abgebaut werden, wurde das Saponin SO1861 (0,4 µM und 4 µM) als endosomaler Escape Enhancer entweder allein oder in zielgerichteter Form, konjugiert mit K-EGF^{RR} (SO1861-EGF) zu den Zellen gegeben. Während die Polyplexe mit den neu synthetisierten Polylysin-Dendronen keine erfolgreiche Transfektion des genetischen Materials aufwiesen, konnte gezeigt werden, dass PAMAM dazu in der Lage ist und dass die Effizienz der PAMAM-Polyplexe durch die Verwendung von SO1861-EGF erhöht werden kann.

Abstract

Gene delivery is a powerful and promising therapeutic tool for treating a wide range of diseases. To ensure the safe and efficient delivery of the genetic material and to prevent degradation, the use of cationic dendritic vectors is particularly popular because of their ability to complex negatively charged genetic material and to form polyplexes. Branched cationic polymers, also called dendrimers, like poly(amidoamine) (PAMAM) have already demonstrated promising results in gene delivery. However, PAMAM has also been associated with cytotoxic effects and heterogeneity. To overcome these limitations, in this thesis, four well-defined polylysine-based dendrons with different functional groups have been synthesised in a reproducible manner using solid-phase peptide synthesis. Targeted gene therapy is a valuable tool for the more specific treatment of cancer or other diseases without the destruction or damage of healthy cells. In this work, as a proof of concept, cancer and liver cells were investigated as targets. For liver targeting, the large surface protein (LSP) derived from hepatitis virus B and its preS1 binding domain, as well as apolipoprotein A1 (ApoA1), which is part of the high-density lipoprotein, were chosen as liver specific targeting moieties. The epidermal growth factor (EGF) was used as a cancer targeting ligand. To avoid cross-linking and to obtain a homogeneous platform, ligand plasmids were designed to have only a single conjugation site. Two ligand variants were successfully recombinantly expressed in *Escherichia coli* Rosetta (K-EGF^{RR}) and NiCo21 (C-ApoA1) with a yield of 4–6 mg/L expression approach. The ligand-cell interaction was evaluated by flow cytometry and fluorescence microscopy while the ligand-receptor interaction was evaluated by enzyme-linked immunosorbent assay and surface plasmon resonance. The affinity of the EGF variant was even higher than that of wild-type EGF (K_D: 5.9 vs 7.3 nM). In addition, heterobifunctional polyethylene glycol linkers were attached to the ligands to allow orthogonal click conjugation to a cargo of choice, in this case the synthesised dendrons. The dendrons were polyplexed with plasmid DNA encoding for enhanced green fluorescence protein (eGFP) or luciferase at different N (dendron amines)/P (DNA phosphates) ratios (0.5–16). In addition, K-EGF^{RR} was either electrostatically incorporated into the polyplex or covalently bound by strain promoted azide-alkyne cycloaddition using different EGF/DNA weight/weight ratios (0.1, 1, 10). The polyplexes were analysed by dynamic light scattering (size: 270–1412 nm and polydispersity index: 0.13–0.99). Transfection efficiency was assessed by measuring the expression levels of eGFP or luciferase. As most of the DNA cargos are trapped and degraded inside endolysosomes, the saponin SO1861 (0.4 µM and 4 µM) was added as an endosomal escape enhancer to the cells either alone (SO1861) or in targeted form conjugated to K-EGF^{RR} (SO1861-EGF). While the polyplexes containing the newly synthesizing polylysine dendrons did not show successful transfection of genetic material, it was demonstrated that PAMAM was able to do so and that the efficiency of PAMAM polyplexes was increased 6-fold by using SO1861-EGF.

List of figures

List of figures in appendix

List of tables

Abbreviations

2'-*O*-Me	2'-O-methyl
2'-*O*-MEO	2'-O-methoxyethyl
ACN	acetonitrile
AE	ArcticExpress
Amp	ampicillin
APC	allophycocyanin
ApoA1	apolipoprotein A1
BCA	bicinchoninic acid
BCN	bicyclononyne
Boc	butyloxycarbonyl
BOP	benzotriazol-1-yl-oxy-tris(dimethylamino)phosphonium hexafluorophosphate
CBD	chitin-binding domain
CICCA	p-chloro-α-cyanocinnamic acid
COMU	1-[(1-(cyano-2-ethoxy-2-oxoethylideneaminooxy)-dimethylamino-morpholino)] uronium hexafluorophosphate
CRISPR/Cas9	clustered regularly interspaced short palindromic repeats / CRISPR-associated protein 9
CuAAC	Cu(I) catalysed [3+2] azide-alkyne cycloaddition
Cy3	cyanine 3
Cy5	cyanine 5
D1, D2, D3, D4	dendron 1, 2, 3 ,4
DAPI	4',6-Diamidino-2-phenylindol
DBCO	dibenzocyclooctyne
DCC	N,N-dicyclohexylcarbodiimide
DCM	dichloromethane
DIC	N,N-diisopropylcarbodiimide
DIFO	difluorinated cyclooctyne
DIPEA	N,N-diisopropylethylamine
DLS	dynamic light scattering
DMC	dimethyl carbonate
DMEM	Dulbecco's modified eagle medium
DMF	dimethyl formamide
DMSO	dimethyl sulfoxide
DNA	deoxyribonucleic acid
DPBS	Dulbecco's phosphate buffered saline
dPL	dendritic polylysine
E. coli	*Escherichia coli*
ECL	enhanced chemiluminescence
EDTA	ethylenediaminetetraacetic acid
EEE	endosomal escape enhancers
EGF	epidermal growth factor
eGFP	enhanced green fluorescent protein

EGFR	epidermal growth factor receptor
ELISA	enzyme-linked immunosorbent assay
EMCH	(N-ε-maleimidocaproic acid hydrazide)
eq.	equivalents
ESI-MS	electrospray ionization mass spectrometry
FBS	fetal bovine serum
Fmoc	9-fluorenylmethyloxycarbonyl
FSC	forward scatter
FUB	Freie Universität Berlin
FXa	factor Xa
G	generation
GAR	goat anti rabbit
GFP	green fluorescent protein
h	hours
HATU	O-(7-azabenzotriazol-1-yl)-N,N,N′,N′-tetramethyluronium-hexafluorphosphat
HBTU	2-(1H-benzotriazol-1-yl)-1,1,3,3-tetramethyluronium-hexafluorophosphat
HDL	high-density lipoprotein
HEPES	4-(2-hydroxyethyl)-1-piperazineethanesulfonic acid
HER2	human epidermal growth factor receptor 2
HOAt	1-hydroxy-7-azabenzotriazol
HOBt	1-hydroxybenzotriazole
HPLC	high performance liquid chromatography
HRP	horse radish peroxidase
IMAC	immobilized metal ion affinity chromatography
IPTG	isopropyl-β-D-thiogalactopyranosid
K-EGF^{RR}	Lys-epidermal growth factor (lysines are replaced by arginines)
K_D	equilibrium dissociation constant
LB	lysogeny broth
LBAmp	lysogeny broth with ampicillin
LNA	locked nucleic acid
LP	linear positive mode
lPL	linear polylysine
LSP	large surface protein
M	method
mAB	monoclonal antibody
Mal	maleimide
MALDI-TOF-MS	matrix-assisted laser desorption ionization time-of-flight
MBHA	4-methylbenzhydrylamine hydrochloride
MBP	maltose binding protein
miRNA	micro RNA
MPI	Max Planck Institute
mRNA	messenger RNA

MTS	3-(4,5-dimethylthiazol-2-yl)-5-(3-carboxymethoxyphenyl)-2-(4-sulfophenyl)-2H-tetrazolium
MWCO	molecular weight cut-off
N/P	nitrogen / phosphate ratio
NaCl	sodium chloride
$NaCO_2CH_3$	sodium acetate
$NaH_2PO_4 \cdot 2\ H_2O$	sodium phosphate monobasic dihydrate
NAOH	sodium hydroxide
NHS	N-hydroxysuccinimide
NiNTA	nickel-nitriloacetic acid
NTCP	sodium taurocholate co-transporting polypeptide
nTPM	normalized transcripts per million
OD	optical density
OTC	ornithine transcarbamylase
PAMAM	poly(amidoamine)
PBS	phosphate-buffered saline
PBSB	PBS-Brij 58
PC	propylene carbonate
PDI	polydispersity index
pDNA	plasmid DNA
PEG	polyethylene glycol
pEGFP	enhanced green fluorescent protein plasmid
PEI	polyethylene imine
PL	polylysine
pp	polyplexed
PPI	polymethylene polyphenylene isocyanate
PyBOP	benzotriazol-1-yl-oxy-tripyrrolidinophosphonium hexafluorophosphate
RAM	rabbit anti mouse
RIP	ribosome-inactivating protein
RISC	RNA-induced silencing complex
RN	reflector negative mode
RNA	ribonucleic acid
RP	reflector positive mode
rpm	revolutions per minute
RU	resonance unit
SA	streptavidin
SDHB	super 2,5-dihydroxybenzoic acid
SDS-PAGE	sodium dodecyl-sulfate polyacrylamide gel electrophoresis
SEC	size exclusion chromatography
siRNA	small interfering RNA
SPAAC	strain-promoted azide-alkyne cycloaddition
SPPS	solid phase peptide synthesis
SPR	surface plasmon resonance
SR-B1	scavenger B1

StBu	*tert*-butylsulphenly
SYBR	Synergy Brands Inc.
TAE	tris-acetate-EDTA
TATU	O-(7-azabenzotriazole-1-yl)-N,N,N',N'-tetramethyluronium tetrafluoroborate
TBTU	2-(1H-benzotriazole-1-yl)-1,1,3,3-tetramethylaminium tetrafluoroborate
TCEP	tris(2-carboxyethyl)phosphine
TEMED	N,N,N′,N′ -tetramethylethylenediamine
TEV	tobacco etch virus
TFA	trifluoroacetic acid
TMB	3,3′,5,5′-tetramethylbenzidine
TRIS	tris(hydroxymethyl)aminomethane
UV/VIS	ultra violet / visible spectroscopy
vs.	versus
WB	western blot
wt	weight

1 Introduction

1.1 Gene delivery

Genetic diseases are caused by the alteration of genetic material or by disease-causing genes. They can be classified in monogenic or polygenic diseases. Monogenic diseases are also known as single-gene disorders, as the name implies, these diseases are caused by mutations in a single-gene. Examples for this type are haemophilia or Huntington disease [1-3]. In contrast, polygenic diseases, like diabetes or malignant tumours, are caused by the combined effects of multiple genetic variations along with environmental factors [4, 5]. Most genetic diseases are only treatable symptomatically. Approved treatment approaches include enzyme replacement therapy, hematopoietic stem cell transplantation, supplements, or medications [6, 7]. However, most of them also have major drawbacks like costly weekly intravenous infusions, adverse effects, or an increased risk of long-term complications like malignancy [8, 9]. Therefore, gene therapy is a potential and innovative treatment approach for genetic disorders. Here, the genetic material is transferred into the cell to repair, regulate, or replace the disease-causing genes [10, 11]. Nucleic acids, which can be used for this purpose include plasmid DNA (pDNA), small interfering RNA (siRNA), micro RNA (miRNA), antisense oligonucleotide and the CRISPR/Cas9 system [12-14]. pDNA and mRNA have great potential for gene editing, vaccines, or protein replacement therapy as they contain the genetic information for the expression of the desired protein [15, 16] whereas miRNA or siRNA can regulate or silence gene expression by inhibiting translation or promoting degradation of the target mRNA [17]. The most crucial step is the efficient delivery of the gene to the target tissue. Here, mRNA must bind to the ribosome, siRNA and miRNA must be loaded into the RNA-induced silencing complex (RISC) and DNA must be further transported into the nucleus to have its full effect (Figure 1). Especially for naked gene therapy drugs, where the genetic material is not associated with any carrier, there are several challenges for successful delivery: (1) degradation by RNase in serum, (2) immune detection from macrophages, (3) renal clearance, (4) poor tissue targeting and cell uptake capacity and (5) low endosomal escape leading to a low intracellular release efficiency (Figure 1) [18].

Chemical modifications and a suitable delivery system are essential to maintain the stability of genetic materials and thus their efficiency. The backbone of the nucleic acids can be modified, e.g. phosphorothioate, tetramethyl phosphoryl guanidine, and peptide nucleic acids can reduce the negative charge leading to degradation resistance and improvement of cellular uptake. Furthermore, the modification of the sugars including 2'-O-methyl (2'-O-Me), 2'-O-methoxyethyl (2'-O-MEO), locked nucleic acid (LNA), and 2'-fluoro, can improve the stability while the immunogenicity and toxicity are decreased [19, 20].

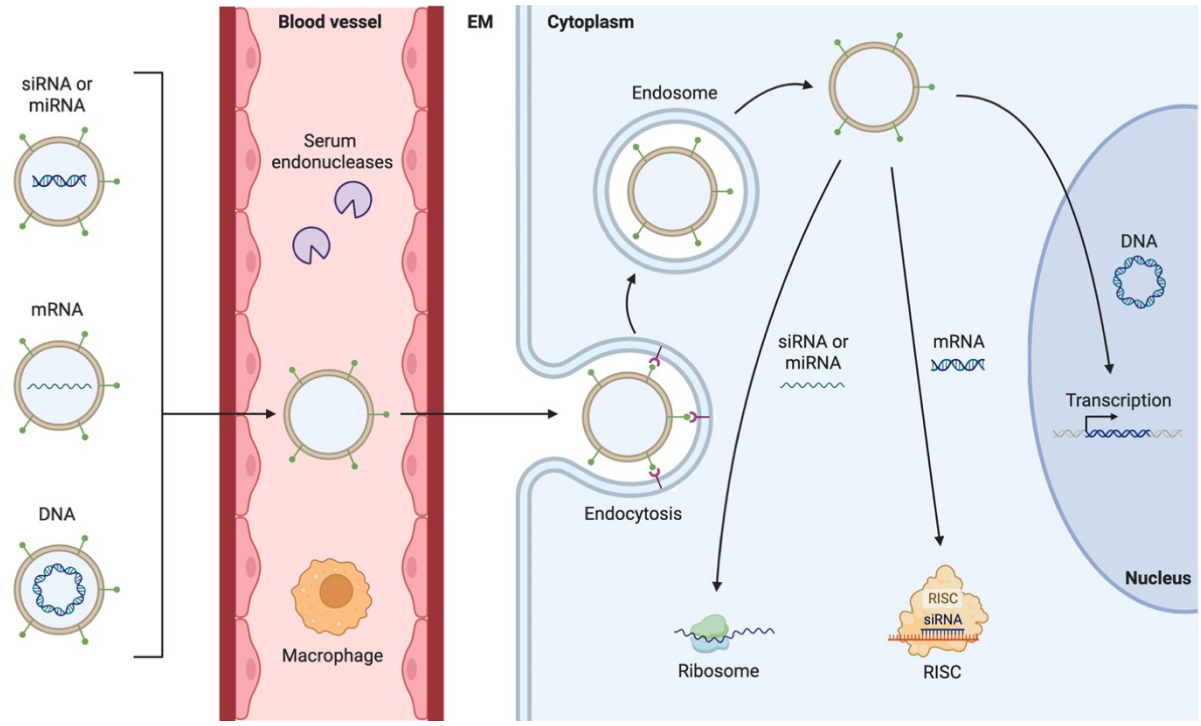

Figure 1: Delivery of genetic material to cells.
Therapeutically active nucleic acids like DNA, mRNA and siRNA or miRNA are travelling through the blood stream, where they can be degraded by macrophages or serum endonucleases. This limits the efficient delivery to the target cells. Additionally, the genetic material is often trapped in the endosome. This is restricting the transfection of the genetic material in the ribosome, RNA-induced silencing complex (RISC) or nucleus. The image is adapted from Yin et al. [21]. *Copyright © 2014, Springer Nature Limited. Created with BioRender.com*.

Another approach that does not require modification of the genetic material but can overcome the challenges described previously is to use gene delivery vehicles or molecular carriers called vectors, which can be viral or non-viral [22]. Viral vectors include herpes simplex virus [23], retrovirus [24], adenovirus [25], adeno-associated virus [26] and lentivirus [27]. All gene therapy drugs approved to date use viral vectors as they have a high transfection efficiency, since they infect dividing as well as non-dividing cells [28]. However, they have major drawbacks such as high immunogenicity, safety hazards, and the production in a larger scale is difficult [29]. Therefore, the increasing focus nowadays is on finding effective as well as safe non-viral vectors. Even though non-viral vectors have a lower transfection efficiency in comparison to viral vectors, they have several advantages such as low immunogenicity, large gene load capacity, high safety for larger scale production, and an easy modification for delivery purposes [10]. As non-viral vectors either liposomes [30], micelles [31], inorganic nanoparticles [32] or cationic polymers [33] can be used (Figure 2).

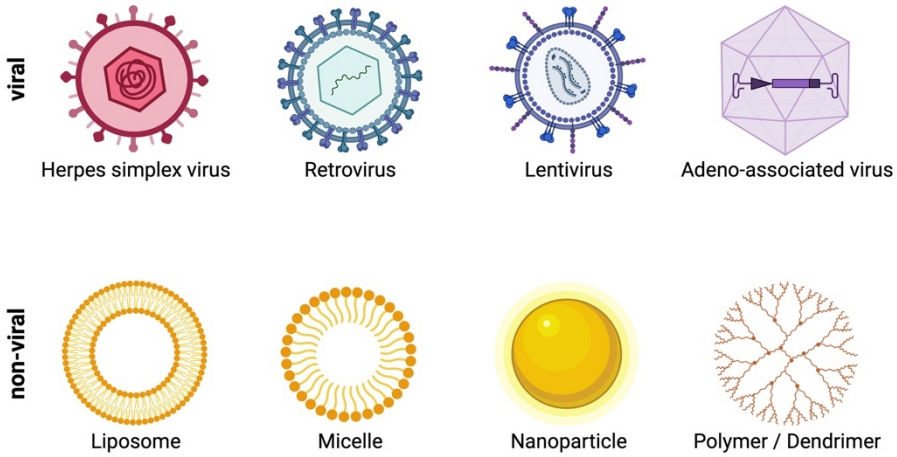

Figure 2: Viral and non-viral vectors for gene delivery.
Created with BioRender.com.

Liposomes are spherical vesicles composed of phospholipid bilayers, that can interact with the cell membrane to enhance cellular uptake due to their amphiphilic nature. Even though they have beneficial properties for being a good delivery platform, including biodegradability, biocompatibility, low toxicity, and immunogenicity, they also have a reduced delivery efficiency [34, 35]. This is due to structural destabilisation after non-specific binding of serum proteins and their reduced circulation life after uptake by the mononuclear phagocyte system [36]. Therefore, cationic polymers have emerged as promising gene delivery vehicles. Due to their positive surface charge, they can interact electrostatically with the negatively charged backbone of the nucleic acid to form so called polyplexes [33]. These polyplexes are spontaneously formed in a self-assembly manner and result commonly in spherical shape particles [37]. This condensation of the genetic material prevents it from degradation and facilitates an efficient delivery into the target cells [38, 39]. These polymers can occur in either linear or branched form. One famous example of a linear polymer used for gene transfection is polyethylene imine (PEI) and is considered as the gold standard. This is due to the fact, that it is one of the first polymers which demonstrates a high transfection efficiency and a great buffer capacity [40, 41]. PEI can prevent the degradation of the genetic material in the endosomes or lysosomes due to the proton sponge effect [42]. Here, protons are absorbed into intracellular endocytic vesicles by partially protonated polycations, which leads to an accompanied influx of chlorides. The osmotic swelling results in rupture of the vesicle and therefore, successful release of the genetic material [43]. The transfection efficiency grows with increasing molecular mass, but so does the cytotoxicity due to higher charge density [44]. Therefore, other cationic polymers must be investigated, like branched dendrimers, which are of great interest for successful gene delivery.

1.2 Dendritic delivery scaffold

Dendrimers are well-defined hyperbranched or tree-like polymers, where the main branches are called dendrons [45]. The common structure of dendrimers consists of three main components. (1) The central core, which is a single atom or molecule, (2) interior layers, also termed as generations, which are formed by repetitive branching units and (3) surface functional groups. The higher the generation the bigger the size and the number of terminal groups [46]. Biocompatibility, shape and size, degree of monodispersity, pharmacokinetics and interaction with the cell membrane are the main properties of dendrimers that have potential for drug delivery [47-49]. Dendrimers are synthesized through a repetitive stepwise progress, which can be either divergent or convergent. In the divergent approach the dendrimer is built from the core to the peripheral until the desired generation is reached. The convergent approach starts with the synthesis of single dendrons, which are then coupled to the core molecule. (Figure 3) [50, 51].

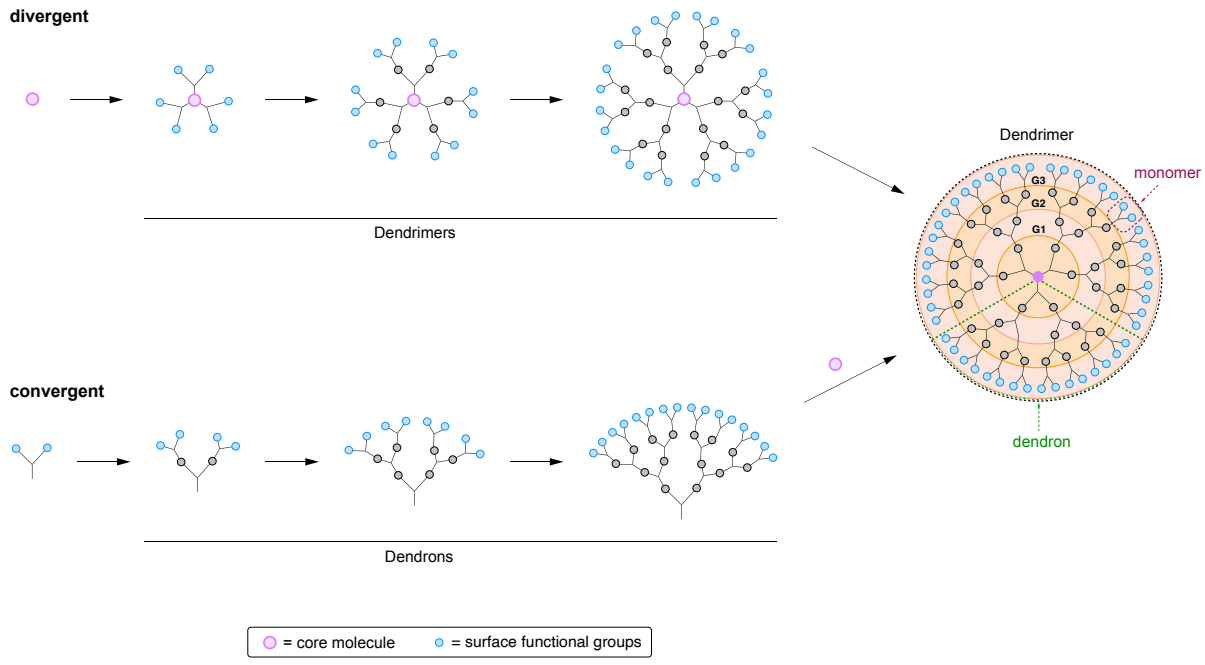

Figure 3: Synthesis strategies for dendrimers.
Divergent: Dendrimer is built from the core to the periphery. Convergent: Dendrons are first synthesized and then conjugated to a core molecule.

The first dendrimer was reported by Vögtle *et al.* in 1978 [45], they called their molecule cascade. This was followed by other dendrimers with terminal amine groups including Denkewalter *et al.* [52] with the first branched polylysine, Meijer *et al.* [53] with polypropylenimine (PPI) and Tomalia *et al.* [54] with the poly(amidoamine) (PAMAM).

PAMAM is a well-established dendrimer used in gene delivery. Like PEI, it can protect the genetic material by condensing the DNA with its positive surface charge and in addition promotes endosomal escape due to the proton sponge effect [42]. Compared to branched PEI, PAMAM has a larger nucleic acid loading capacity and a higher biocompatibility [55]. It is reported, that the higher the generation, the larger the size, the better the transfection efficiency. Nevertheless, with higher generations and the resulting higher surface charge, also the cytotoxicity is increasing [56, 57]. Therefore, it is necessary to either work with lower generations of PAMAM or shield the positive charge by PEGylation. Not only has polyethylene glycol (PEG) a positive effect on the toxicity, but it also reduces the interactions of polyplexes with blood components and increases the solubility in water [42, 58]. Additionally, the PAMAM surface can also be modified with targeting ligands, cell penetrating peptides or other molecules to improve their performance in gene delivery [59].

Another promising cationic polymer is polylysine, which is composed of repeating lysine units and exists in linear, hyperbranched or dendritic form [60, 61]. The linear form is well established and offers advantages such as facile synthesis, whereby the length is not limited due to steric hindrance [62]. Versatile surface modifications are possible like mentioned for PAMAM. However, it also has its limitations in terms of cytotoxicity or reduced endosomal escape. This can be overcome by using dendritic polylysine as it shows a lower toxic effect and enables the endosomal escape, due to its structure. Additionally, it also has a higher gene loading capacity [63]. The first dendritic polylysine was synthesized and patented by Denkewalter *et al.* in 1981 [52]. As lysine contains two amine functionalities, one at the α and one at the ε position, it is an excellent choice as a unit for controlled branching.

Polylysine or other peptide-based scaffolds can be synthesized using conventional solution-phase peptide synthesis or solid phase peptide synthesis (SPPS) [61]. SPPS offers advantageous features, like the completion of reactions by employing excess reagents leading to high reaction yields. Additionally, this approach facilitates the easy removal of these excess reagents and soluble by-product through simple consecutive washing and filtering of the resin. Consequently, SPPS provides a rapid and reliable way for generating diverse libraries of complex compounds.

The first SPPS was developed by Merrifield in 1963 for linear peptides [64]. The peptides are grown from C- to N-terminus on an insoluble polymeric material, also called resin. At this resin, the first amino acid is attached via its carboxyl group while the α-amino group (Nα) as well as the side chain are protected. These protecting groups can be either identical, so they can be removed simultaneously, or orthogonal, which means that they can be removed under different conditions. The two most common protecting groups for Nα are the acid labile tert-butyloxycarbonyl (Boc) and the base labile 9-fluorenylmethyloxycarbonyl (Fmoc) [65-67].

In the following section, the SPPS will be explained on linear and dendritic polylysine using the Fmoc strategy. SPPS is divided in three steps which are repeated until the desired peptide is generated. The first step is deprotection (1) of the amino acid attached to the resin, in case of Fmoc piperidine is used as basic cleavage reagent. Afterwards the amino acid which should be attached is activated (2) and coupled (3) under formation of an amide or peptide bond. For the activation and conjugation, coupling reagents like *O*-(7-Azabenzotriazol-1-yl)-N,N,N′,N′-tetramethyluronium-hexafluorphosphat (HATU) and diisopropylethylamine (DIPEA) are employed [68]. For linear peptides (Figure 4 A), the α-amino group and the functional groups of the side chain – which in case of lysine is the ε-amino group – are orthogonally protected, whereas for dendritic peptides an identically protected lysine can be used as branching units (Figure 4 B). Here, the ε- as well as the α-amine are protected by Fmoc. The steps (1)–(3) are repeated until the desired length or generation is obtained, then the peptide can be cleaved off from the resin [69]. Nevertheless, it is important to also mention the limitations associated with SPPS. Since isolation and characterization of intermediates cannot be performed without cleavage from the resin, which is resulting in product loss, it is challenging to eliminate by-products. They can occur because of incomplete coupling or deprotection reactions, as well as due to side reactions on the resin. Consequently, the monitoring of the reaction needs to be on-bead by colorimetric methods like Kaiser-Test [70].

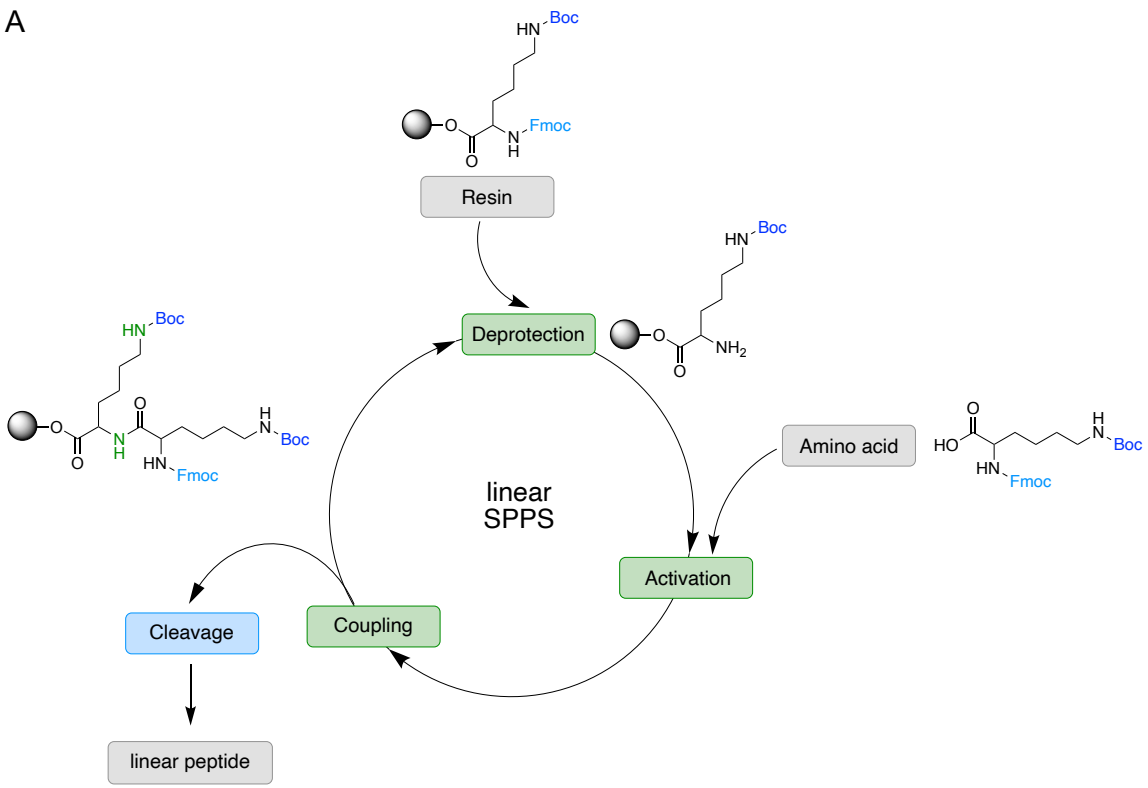

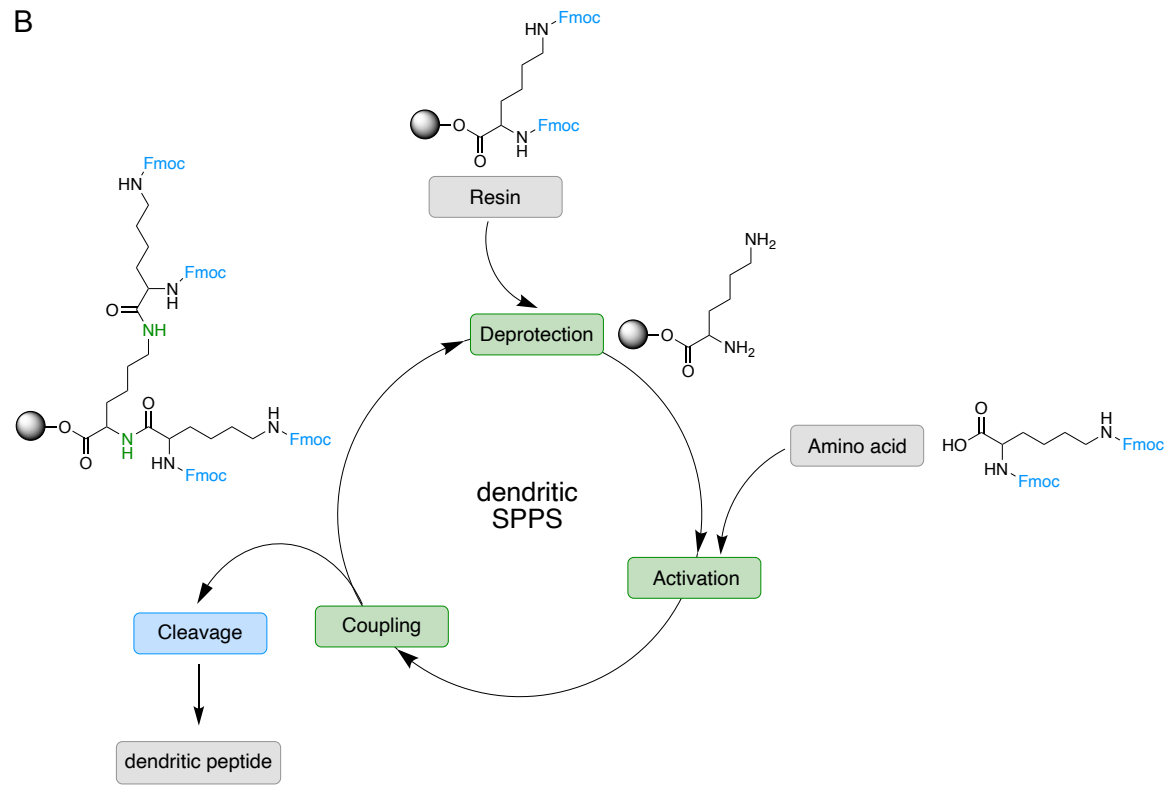

Figure 4: Linear versus dendritic solid phase peptide synthesis (SPPS).
The SPPS is following three main steps in a circular manner. (1) Deprotection of amino acid 1, (2) activation and (3) coupling of amino acid 2. (A) previous page; For linear SPPS the lysine is orthogonal protected with Boc and Fmoc. (B) For dendritic SPPS both amines of the lysine are protected with Fmoc. The lysine serves as a branching unit. After the desired length is obtained the linear or dendritic peptide is cleaved off.

1.3 Targeted therapy

As mentioned before, non-viral vectors or dendrimers can be equipped with targeting moieties, as these not only minimise the adverse effects of undirected treatment on healthy or off-targeted cells, but also broaden the therapeutic window, which allows the reduction of the therapeutic dose.

In this thesis, two different cell types should be addressed, cancer and liver cells. In case of cancer, targeting can occur through passive or active mechanisms. In passive drug targeting, macromolecules like liposomes or nanoparticles can accumulate and interact with tumour cells [71]. This is possible because tumour tissue, unlike normal tissue, tend to develop leaky blood vessels and lack a functional lymphatic system. The larger openings in the blood vessels allow molecules to diffuse more easily into the tumour while the absence of a lymphatic system makes it difficult for toxins to be evacuated, resulting in accumulation in the malignant tissue. This phenomenon is known as the enhanced permeability and retention (EPR) effect [72].

On the other hand, active targeting combines the drug with a specific targeting moiety that bind to its cognate receptor on the target cell membrane, which leads to the internalization of the drug [73]. Monoclonal antibodies (mABs) and small molecules are the main categories of active targeting therapies used in clinical trials. Already eight antibody drug conjugates have been approved so far [74].

In addition to antibodies, natural or modified protein ligands, such as transferrin, can be utilized as targeting moieties for drug delivery [75]. These ligands offer the advantage of being smaller in size and evolutionarily optimized to bind to their corresponding receptors. One well-known anti-cancer ligand is the epidermal growth factor (EGF) as many malignancies are overexpressing the EGF receptor (EGFR) [76, 77]. This receptor plays an important role in cell growth and proliferation and its abnormal activation can lead to cancer [78]. The EGFR is endocytosed when a ligand (e.g., EGF) binds and the activation of the receptor leads to conformational changes in which EGFR forms homo- or heterodimers with other receptors of the same family. This is followed by activation of the tyrosine kinase domain of EGFR and phosphorylation of its C-terminal tyrosine residues which in turn activates the downstream signalling pathway [79, 80]. Table 1 gives an overview of targeting moieties used for cancer targeting.

For liver targeting there are many receptors that can be addressed, like the sodium taurocholate co-transporting polypeptide (NTCP) for the preS1 domain of the hepatis B virus or the asialoglycoprotein receptor for galactosides or galactosamines and many others listed in Table 2. In case of NTCP, the 48 amino acids of the preS1 domain of the large surface protein of the hepatitis B virus binds to this receptor, which leads to the internalization of the virus [81, 82]. Another promising protein is the apolipoprotein A1 (ApoA1) as it addresses the high-density lipoprotein (HDL) receptor, also known as scavenger B1 (SR-B1) receptor, which is mainly found at the surface of liver cells. HDL plays an important role in the reverse transport of cholesterol. HDL conveys cholesterol and phospholipids from other tissues back to the liver [83, 84]. ApoA1 is one of the major structural proteins of HDL and plays a crucial role in lipid-binding and is also the key ligand for SR-B1 [85]. It is assumed that its amphiphilic α-helices are the recognition site for SR-B1 [86]. Target specific drug delivery to the liver can become important to treat diseases like haemophilia by addressing this receptor.

Table 1: Targeting moieties associated with targeting cancer cells.

Molecule	Ligand(s)	Target(s)	Cancer type(s)	Ref
Antibody	Anti-CD20	CD20	Burkitt'slymphoma	[87]
Antibody	Anti-CD47	CD47	Pancreas	[88]
Antibody	Anti-annexin A2	AnnexinA2	Breast, glioblastoma	[89]
Aptamer	AS1411	Nucleolin	Breast, non-small cell lung	[90]
Aptamer	HeA2_1 HeA2_3	HER2 receptor	Breast	[91]
Monosaccharide	Galactose	Asialoglycoprotein-receptor	Liver	[92]
Glycosaminoglycan	Hyaluronic acid	CD44	Melanoma, colon, lung	[93]
Vitamin	Cobalamin	Transcobalamin-receptor	Lung, breast, pancreas	[94]
Vitamin	Folate	Folate receptor	Ovarian, breast, kidney, brain	[95]
Peptide	RGD	Intergrins αvβ3, αvβ5, α5β1	Breast, glioblastoma, prostate, pancreas	[96]
Peptide	H2009.1	Intergrin αvβ6	Lung, ovarian, oral cavity	[97]
Peptide	RVG	CHRNA7	Brain	[98]
Peptide	Bombesin	GRP receptor	Breast, lung, prostate	[99]
Peptide	GE11	EGFR	Breast, lung, hepatoma	[87]
Tripeptide	NGR	Aminopeptidase N	Blood vessels	[100]
Protein	Transferrin	Transferrin-receptor	Metastatic and drug-resistant cancer cells	[101]
Protein	EGF	EGFR	Breast	[102]

Table 2: Ligands for liver targeting and their respective receptors.

Liver cell type	Ligand(s)	Target(s)	Ref
Hepatic stellate cells	Mannose-6-phosphate	Mannose-6-phosphate receptor	[103]
	Cyclic RGD	Type VI collagen receptor	[104]
	PDGF	PDGF receptor	[105]
	Human serum albumin	Scavenger receptor class A	[106]
Hepatocytes	Galactoside	Asialoglycoprotein receptor	[107]
	Galactosamine	Asialoglycoprotein receptor	[108]
	Linoleic acid	Plasma membrane fatty acid binding protein (Putative)	[109]
	Apolipoprotein A1	Scavenger receptor class B type I (SR-BI)	[110]
	preS1	IL-6 receptor and or immunoglobulin A binding protein (Putative)	[111]
	Glycyrrhizin	Glycyrrhizin receptors	[112]

1.4 Endosomal pathway and endosomal escape enhancer

As described before, not only the safe delivery of the genetic material to the cells plays a crucial role in successful transfection, but also the uptake of the drug into the cells. The uptake can occur through two primary mechanisms: membrane disruption-mediated including permeabilization and penetration, or carrier-mediated processes like fusion or endocytosis [113]. In case of clathrin-mediated endocytosis, the targeted drug binds to the cognate receptor on the cell membrane by its targeting moiety. This binding triggers a series of events: the membrane begins to invaginate, accompanied by the adaptor protein AP2 and clathrin, which coats the vesicle [114]. Once the vesicle is liberated from the AP2-clathrin coat, it enters the endosomal pathway, where the environment becomes progressively more acidic. The pH levels are shifting from 6.2 (early endosome) to 5.3 (late endosome) and 4.5–5.0 (lysosome) (Figure 5 A) [115]. The crucial step for a successful release of the drug which is internalized by the endosomal pathway is to escape from the endosomes or lysosomes to be released into the cytoplasm (Figure 5 B). Over 98% of the DNA/RNA cargos are not able to perform this step and are either recycled back to the cell surface together with the receptor or degraded in the lysosomes [116]. In order to facilitate the endosomal escape, enhancer molecules are required as they interact with the cell membranes, leading to a leakiness [113]. These so-called endosomal escape enhancers (EEE) can be either small chemical molecules, peptides, secondary metabolites, proteins, or detergents.

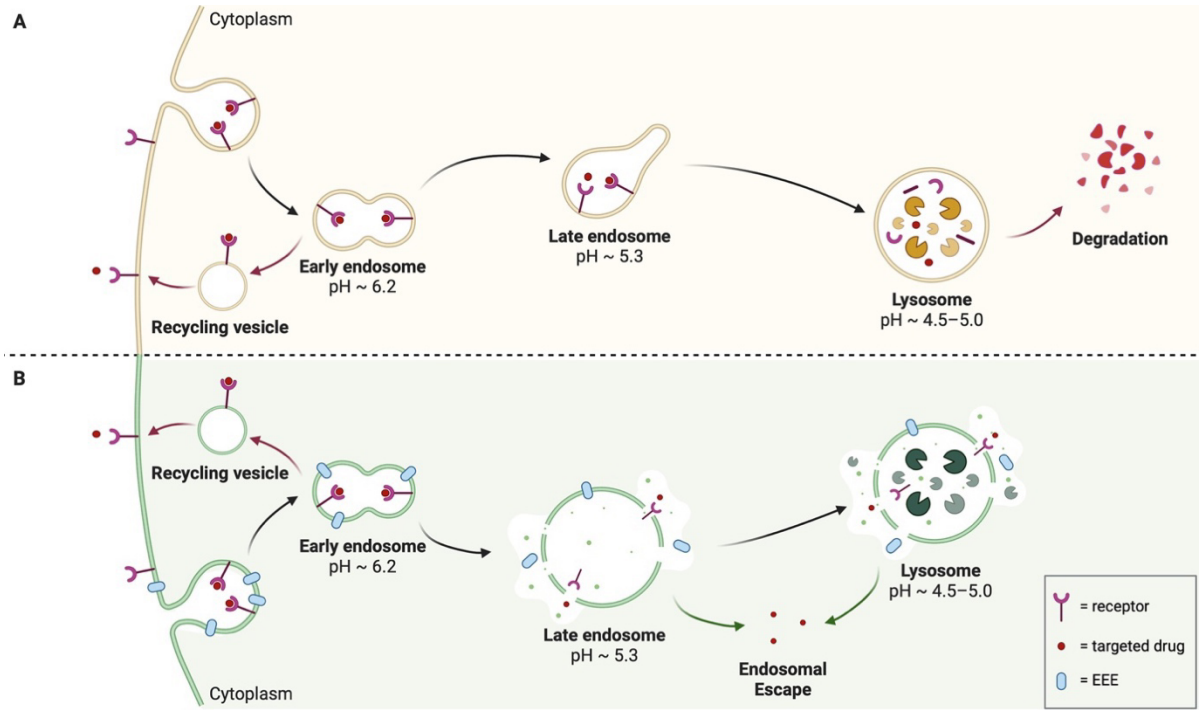

Figure 5: Endosomal pathway without (A) and with (B) endosomal escape enhancer.
After AP2 and clathrin assisted receptor-mediated endocytosis the vesicle is liberated from its coat and the drug is released form the receptor within the endosomes. Due to acidification the pH changes and the late endosome and lysosome are formed. (A) Here, the receptor and the entrapped toxin may become degraded. (B) The endosomal escape enhancers mediate the endosomal escape of the drug into the cytoplasm. Adapted from "Endocytic Pathway Comparison (Layout)", by BioRender.com (2023). Retrieved from https://app.biorender.com/biorender-templates.

Some promising endosomal escape enhancers belong to the group of glycosylated triterpenoids also known as saponins. They have the ability to decrease the degradation of drugs within the endolysosomal pathway, like type I ribosome-inactivating proteins (RIPs) (e.g. dianthin) by mediating the endosomal escape [117, 118]. The precise mechanism is still under investigation, but it is postulated that the protonated form of glucuronic acid in the EEEs interacts with the cholesterol found in the endosomal membrane, resulting in membrane disruption [119, 120]. Notably, for this interaction to occur, the EEE needs to be in its protonated state and therefore an acidic environment is required. This explains why endosomal escape is primarily observed in the late endosome or lysosome. Saponins offer certain advantages in this context, as they are biodegradable, stable, non-toxic at the concentrations required for the endosomal escape, and do not interfere with important metabolic pathways [121].

In vitro experiments, dependent on the specific cell line used, demonstrate a noteworthy enhancement of cytotoxicity for targeted toxins when combined with EEEs, ranging from 3000–4,000,000 fold increase, while *in vivo* tests performed on mice reveal a substantial enhancement in the range of 10–500 fold [117, 119, 122-126].

The reduction of the toxin concentration, down to 2% of the applied dose without EEE, serves to decrease immunogenicity and minimizes the occurrence of side effects. One noteworthy EEE, which exhibits remarkable efficiency enhancement for the targeted toxin dianthin-EGF without causing immunogenic responses, is the bidesmosidic saponin SO1861. This particular saponin is composed of the aglycon gypsogenin (Figure 6) and is extracted from *Saponaria officinalis* L. [127].

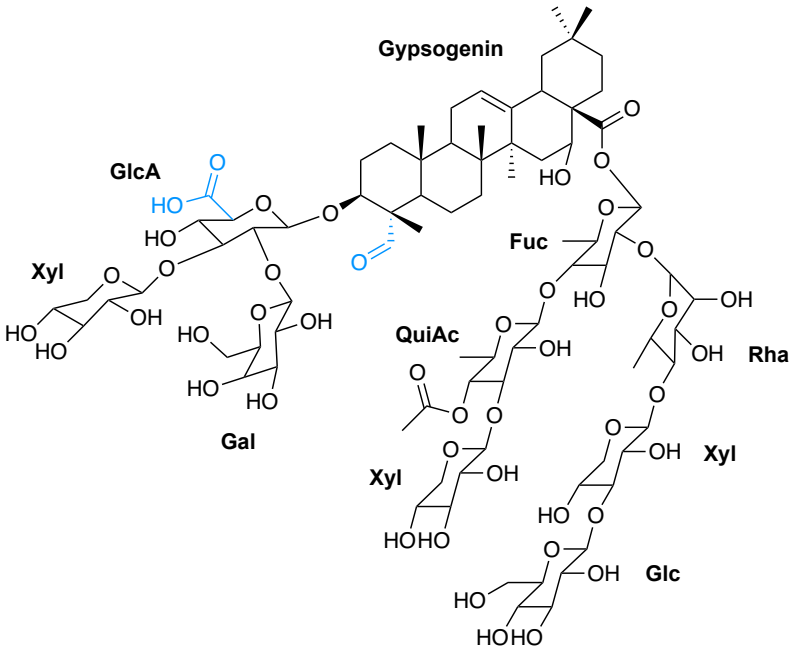

Figure 6: Structure of SO1861.
Consisting of aglyocon gypsogenin and two sugar chain residues. Sugar abbreviations: fucose (Fuc); galactose (Gal); glucose (Glc); glucuronic acid (GlcA); rhamnose (Rha); acetylated quinovose (QuiAc); xylose (Xyl). Blue indicates possible conjugation sites.

The major challenge in implementing an *in vivo* approach lies in the need to synchronize the pharmacokinetics of the targeted drug and the EEE SO1861. Both components must be simultaneously at effective concentrations within the cell at the side of action to induce the synergistic effect. Furthermore, these components follow different uptake mechanisms. EEEs enter cells through passive diffusion across the cell membrane, ultimately reaching the endosomes by interacting with cholesterol, whereas targeted drugs are internalized by receptor mediated endocytosis. Moreover, the process of absorption, metabolism, excretion, and release of the substances in living organisms vary. Considering these multifaceted factors, the timing of injections and the concentration of substances must be carefully considered for each individual organism. This complexity is currently a challenges that hinder the clinical application of this approach in patients.

1.5 ENDOSCAPE project

This thesis was part of the ENDOSCAPE project funded by the European Union's Horizon 2020 research and innovation programme. Twelve different partners from seven European countries were involved. The main goal of this project was to overcome the previously mentioned challenges and to make gene delivery safer, more efficient, and less costly. The ENDOSCAPE prototype consists of a non-viral vector which can complex the gene and can be additionally equipped with the EEE and a targeting moiety (Figure 7). As vectors, the consortium chose either a dendrimer, namely PAMAM, a linear polylysine, or a DNA origami scaffold.

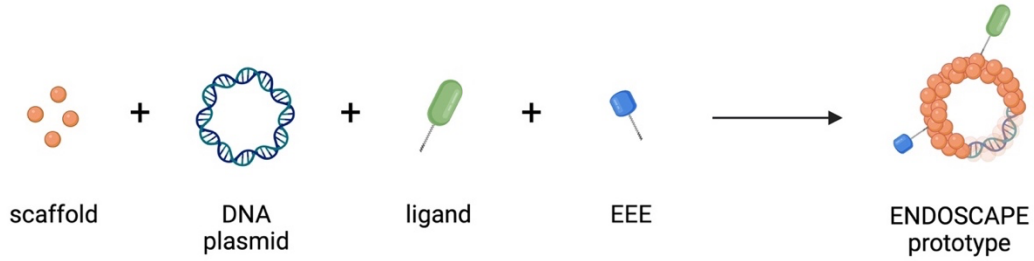

Figure 7: ENDOSCAPE prototype consisting of scaffold, DNA, ligand, and endosomal escape enhancer (EEE).
Created with BioRender.com.

To conjugate the ligand as well as the EEE to the scaffold, click chemistry was used. In 2022 K. Barry Sharpless, Morten Meldal and Carolyn Bertozzi have been awarded with the Nobel prize in chemistry for the development of click chemistry and biorthogonal chemistry. Click reactions exhibit several advantageous properties, including high yields with no side products, orthogonality, mild reaction conditions, rapid reaction kinetics, and regio- and stereo-specificity [128]. Particularly when it comes to modifying scaffolds, click chemistry emerges as a promising approach due to its high efficiency under mild conditions. These reactions can be performed near physiological pH, in aqueous medium, at room temperature, and often require only low reactant concentrations [129, 130]. The term 'click chemistry' was introduced by Sharpless *et al*. in 2001 [131], where he described the Cu(I) catalysed [3+2] azide-alkyne cycloaddition (CuAAC), which was also concurrently discovered by Meldal *et al*. While CuAAC is a well-established reaction in the field of chemistry, it comes with a major drawback when applied to protein conjugation. The use of Cu(I) as a catalyst raises concerns about toxicity when employed within living cells, as it mediates the generation of reactive oxygen species (ROS) from oxygen (O_2) [131, 132]. To address this issue, Bertozzi *et al.* developed a copper free strain-promoted [3+2] azide-alkyne cycloaddition (SPAAC) in 2004 [133]. In this alternative approach, difluorinated cyclooctyne (DIFO) is employed instead of a typical alkyne.

The increased ring strain in DIFO destabilises the alkyne, making it more reactive and eliminating the need for a copper catalyst.[134]. As an alternative to DIFO, bicyclononyne (BCN) or dibenzocyclooctyne (DBCO) can be used [135]. In this project SPAAC was used to conjugate the ligand containing the DBCO group, to the azide group of the scaffold (Figure 8). For this reason, a bifunctional 'click-adapter' was conjugated to the ligand bearing the DBCO group.

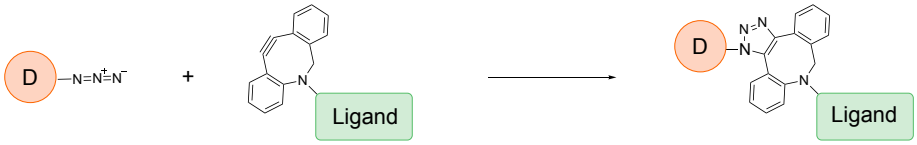

Figure 8: Conjugation of the ligand to the scaffold by SPAAC.

Another click reaction employed in the ENDOSCAPE project for the conjugation of SO1861 at the scaffold molecule is the thiol-ene reaction. This versatile reaction can occur through either a radical addition or a Michael-type addition [136]. In both cases it involves the reaction of the relatively weak sulphur-hydrogen bonds of thiols with the reactive C=C double bonds, known as 'Enes' [137]. In the radical addition, a thiyl radical is initiated, typically by light, heat or radical initiators. This radical then propagates with the alkene to form a carbon centred radical. Subsequently, in a chain-transfer step, a hydrogen radical from the thiol group is removed and binds to the carbon radical, resulting in the formation of a new thiyl radical. In this thesis, the Michael addition was performed. Here, a thiolate anion is generated and undergoes a Michael reaction with the alkene (Figure 9) [136].

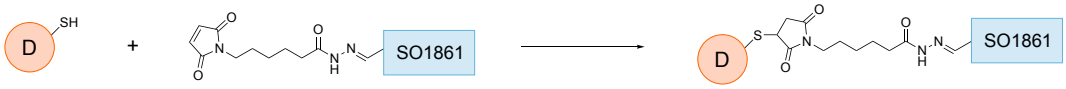

Figure 9: Conjugation of the EEE SO1861 to the scaffold using thiol-ene Michael addition.

Thiol-Michael reactions normally required catalysts like strong bases, metals or nucleophiles, to create the thiolate anion [138]. However, when employing maleimides as 'Enes' the need for a catalyst is eliminated. This is primarily due to the high reacivity of the C=C double bonds in maleimides, because of bond angle distortion, ring strain and two activating carbonyl groups in cis-conformation [139-141]. In addition, maleimides offer the advantage of being highly selective and biorthogonal, making them very efficient [142]. To introduce a maleimide into the SO1861 a bifunctional N-(ε-maleimidocaproic acid) hydrazide (EMCH) linker was used. This 'click-adapter' is attached to the aldehyde C-23 of SO1861 by the hydrazide group to form an acid labile hydrazone bond, which can be cleaved in the acidic environment of the late endosome or lysosome. This allows the endosomal release of the EEE.

1.6 Motivation

Major drawbacks of viral gene delivery platforms such as high immunogenicity, lead to an increasing interest in non-viral vectors for a more save and still efficient gene delivery. Dendrimers have demonstrated to successful transfect the genetic material. However, homogeneity is an important factor to consider when developing drug conjugates. In contrast to dendrimers like PAMAM, the aim in this thesis was to synthesize a dendron with a defined number of functional groups. This allows us to control the degree of functionalization and to decrease crosslinking in order to create a more homogeneous platform. Another aim was to create a less toxic dendron, as PAMAM tend to be cytotoxic due to its surface charge density.

Therefore, the idea was to build the dendrons from natural building blocks, like amino acids and to create a peptide dendron to have biodegradable components. Additionally, this dendron should be equipped with a targeting moiety, to act as a targeted drug delivery system. This cannot only reduce adverse effects due to unspecific treatment but can also increase the potency of the drug. Furthermore, to increase the efficiency of our gene delivery platform and to prevent the degradation of the genetic material in the endosomes or lysosomes, the endosomal escape enhancer SO1861 was aimed to be conjugated at the dendrons. Therefore, three different functional groups are required. (1) Amino groups, which are positively charged and therefore can interact electrostatically with the negatively charged DNA backbone. (2) Azide groups for the conjugation of the targeting moiety, which is equipped with a DBCO-linker by a strain-promoted azide-alkyne cycloaddition (SPAAC). (3) Thiol groups to attach the SO1861-EMCH by a thiol-ene Michael addition. The dendrons will be synthesised by solid phase peptide synthesis (SPPS), where the peptide dendron can be built from the amino acid attached to a resin in a simple and effective approach.

The next part of this thesis will focus on the production of the targeting ligands for the ENDOSCAPE prototypes. As proof of concept, two different diseases, namely cancer and haemophilia, should be addressed. Therefore, two different cell types will be targeted: cancer and liver cells. For the cancer cells the epidermal growth factor (EGF) was chosen, as the EGF receptor is overexpressed in many cancer cells. For liver cells the large surface protein (LSP) and its preS1 binding region from hepatitis B virus and the apolipoprotein A1 (ApoA1) of the high-density lipoprotein (HDL), which is involved in cholesterol transport to the liver, were chosen. Additionally, these protein ligands will be redesigned to insert a single conjugation site to reduce heterogeneity and aggregation. These ligands will be recombinantly expressed in *Escherichia coli* (*E. coli)*, purified, and afterwards equipped with the ‘click-adapter’ to attach them to the non-viral vector.

The interaction of the ligands with their respective receptor and internalization into the target cells will be tested by enzyme-linked immunosorbent assay (ELISA) and surface plasmon resonance (SPR) experiments as well as *in vitro* cell culture.

Furthermore, the ability of the dendrons to transfect plasmid DNA will be evaluated. For this purpose, plasmids encoding for enhanced green fluorescent protein (eGFP) and luciferase will be used as model plasmids. In addition, the targeting ligand will be incorporated into the polyplexes by electrostatic or covalent binding. The loading capacity of each dendron will be evaluated by Pico488 assay as well as agarose gel retardation assay. Not only homogeneity can have an impact on the success of the gene delivery, but also the size. It is known that a size of 100–200 nm is preferred, as these particles are small enough to avoid the filtration in spleen but large enough to be not taken up by the liver. Therefore, the size of the polyplexes will be determined by dynamic light scattering (DLS). Furthermore, the actual transfection efficiency will be evaluated by testing the targeted and non-targeted polyplexes co-administered with SO1861 or SO1861-EGF on receptor positive and negative control cell lines measuring the expression level of eGFP or luciferase. Additionally, the cytotoxicity of the polyplexes will be determined to reveal if they represent a potential non-viral gene delivery platform.

2 Material and Methods

2.1 Material

2.1.1 Chemicals

The following chemicals were used as purchased:

- 2-iminothiolane · HCl (Sigma Aldrich, St. Louis, US)
- acetic acid (Carl Roth, Karlsruhe, Germany)
- ACN (Carl Roth, Karlsruhe, Germany)
- acryl amide (Carl Roth, Karlsruhe, Germany)
- ammonium persulfate (Sigma Aldrich, St. Louis, US)
- ampicillin (Sigma Aldrich, St. Louis, US)
- amylose resin (New England Biolabs, Ipswich, US)
- ApoA1 (Merck, Darmstadt, Germany)
- bovine serum albumin (BSA) (Thermo Scientific, Waltham, US)
- Brij 58 (Sigma Aldrich, St. Louis, US)
- bromphenolblue (Serva, Heidelberg, Germany)
- Coomassie brilliantblue R-250 (Merck, Darmstadt, Germany)
- Cy3-NHS (Lumiprobe, Hannover, Germany)
- DBCO-PEG12-Mal (Lumiprobe, Hannover, Germany)
- DBCO-PEG12-NHS (Conju Probe, San Diego, US)
- DBCO-PEG3-hydrazon-Mal (Conju Probe, San Diego, US)
- DBCO-PEG3-S-S-NHS (Conju Probe, San Diego, US)
- DMEM medium (Lonza Group, Basel, Switzerland)
- DCM (Sigma Aldrich, St. Louis, US)
- dialysis tube 1.0 MWCO (Serva, Heidelberg, Germany)
- dialysis tube 3.5 MWCO (Spectrum Laboratories, East Tamaki, New Zealand)
- diethylether (Sigma Aldrich, St. Louis, US)
- Diluant A (BioLegend, San Diego, US)
- dimethylsulfoxide (DMSO, Carl Roth, Karlsruhe, Germany)
- DIPEA (Carl Roth, Karlsruhe, Germany)
- DMF (Carl Roth, Karlsruhe, Germany)
- Dulbecco's Phosphate Buffered Saline (DPBS) (Lonza Group, Basel, Switzerland)
- EDTA (Carl Roth, Karlsruhe, Germany)
- EGF (Gibco by life technologies, Carlsbad, US)
- EGFR (Acro, Newark, US)
- ethanol (Carl Roth, Karlsruhe, Germany)
- FBS (Bio&SELL GmbH, Nürnberg, Germany)
- Fmoc-Cys-S(tBu) (Sigma Aldrich, St. Louis, US)
- Fmoc-Cys-S(tBu) Wang resin (Bachem, Bubendorf, Switzerland)
- Fmoc-Lys-Boc Wang resin (Merck, Darmstadt, Germany)
- Fmoc-Lys-Fmoc (Carbolution, St. Ingbert, Germany)
- Fmoc-Lys-N3 (Carbolution, St. Ingbert, Germany)
- FXa (New England Biolabs, Ipswich, US)
- glycerol (Carl Roth, Karlsruhe, Germany)
- glycine (Carl Roth, Karlsruhe, Germany)
- HATU (Sigma Aldrich, St. Louis, US)
- HEPES (Carl Roth, Karlsruhe, Germany)
- hydrogen peroxide (Carl Roth, Karlsruhe, Germany)
- imidazole (Carl Roth, Karlsruhe, Germany)
- IPTG (Carl Roth, Karlsruhe, Germany)
- LB-Agar (Invitrogen, Waltham, US)
- lipofectamin (Invitrogen, Waltham, US)
- luminol (Sigma Aldrich, St. Louis, US)

- Luna® 5 µM C18(2) 100 Å 150 × 4.6 mm (Phenomenex, Torrance, US)
- Luna® 5 µM C18(2) 100 Å 250 × 10 mm (Phenomenex, Torrance, US)
- maltose (Merck, Darmstadt, Germany)
- mercaptoethanol (Sigma Aldrich, St. Louis, US)
- MTS solution (Abcam, Cambridge, UK)
- NaCl (Thermo Scientific, Waltham, US)
- NiNTA agarose (Macherey-Nagel, Düren, Germany)
- nitrocellulose membrane (Perkin Elmer, Waltham, US)
- oxidized glutathione (Carl Roth, Karlsruhe, Germany)
- p-coumarin acid (Sigma Aldrich, St. Louis, US)
- PD-10 columns (Cytiva, Marlborough, US)
- penicillin / streptomycin (Gibco by life technologies, Carlsbad, US)
- peptone (Carl Roth, Karlsruhe, Germany)
- Pico488 (Lumiprobe, Hannover, Germany)
- piperidine (Sigma Aldrich, St. Louis, US)
- ponceau S (Thermo Scientific, Waltham, US)
- reduced glutathione (Sigma Aldrich, St. Louis, US)
- RNase free water (Thermo Scientific, Waltham, US)
- RPMI medium (Gibco by life technologies, Carlsbad, US)
- SA sensor chip (Cytiva, Marlborough, US)
- SDS (Sigma Aldrich, St. Louis, US)
- skimmed milk (Carl Roth, Karlsruhe, Germany)
- SO1861-EMCH (Symeres, Nijmegen, Netherlands)
- Sodium acetat (Merck, Darmstadt, Germany)
- Sodium dihydrogen phosphate dihydrate (Carl Roth, Karlsruhe, Germany)
- Sodium hydroxide (Carl Roth, Karlsruhe, Germany)
- SR-BI (Acro, Newark, US)
- Steady-Glo® luciferase assay solution (Promega, Madison, US)
- streptavidin coated 96-well-plate (Thermo Scientific, Waltham, US)
- sucrose (Carl Roth, Karlsruhe, Germany)
- sulfo-Cy3-Mal (Lumiprobe, Hannover, Germany)
- sulfo-Cy3-NHS (Lumiprobe, Hannover, Germany)
- sulfo-Cy5-Mal (Lumiprobe, Hannover, Germany)
- sulfo-Cy5-NHS (Lumiprobe, Hannover, Germany)
- sulfuric acid (Carl Roth, Karlsruhe, Germany)
- surfactant P20 (Cytiva, Marlborough, US)
- SYBR green (Invitrogen, Waltham, US)
- T25 culture flask (Thermo Scientific, Waltham, US)
- TEMED (Sigma Aldrich, St. Louis, US)
- TFA (Carl Roth, Karlsruhe, Germany)
- TMB substrate (Sigma Aldrich, St. Louis, US)
- tricine (Carl Roth, Karlsruhe, Germany)
- TRIS (Carl Roth, Karlsruhe, Germany)
- TRIS HCl (Thermo Scientific, Waltham, US)
- Tritrack DNA loading dye (Thermo Scientific, Waltham, US)
- trypan blue (Gibco by life technologies, Carlsbad, US)

2.1.2 Antibodies

- anti-EGF (Abcam, Cambridge, UK)
- anti-ApoA1 (Invitrogen, Waltham, US)
- anti-preS1 (SantaCruz, Dallas, US)
- anti-MBP (New England BioLABS, Frankfurt, Germany)
- GAR (Dako, Jena, Germany)
- RAM (Dako, Jena, Germany)

2.1.3 Plasmids

Customized synthesis by BioCat (Heidelberg, Germany):
- pET11d-6×His-K-EGF^{RR}
- pET11d-6×His-OTC-Lk-LS protein
- pET11d-6×His-Tev-K-preS1-C
- pET11d-6×His-Tev-C-preS1-K
- pET11d-6×His-C-ApoA1
- pMAL-c5X-6×His-C-ApoA1

Obtained from FUB:
- pEGFP-N3
- npLuciferase

2.1.4 Bacterial strains

- *E. coli* DH5α (Life Technologies, Carslbad, CA, USA)
- *E. coli* ArcticExpress (DE3) (Agilent, Santa Clara, US)
- *E. coli* Rosetta (DE3) (Agilent, Santa Clara, US)
- *E. coli* BL21 (DE3) (Agilent, Santa Clara, US)
- *E. coli* NiCo21 (DE3) (New England BioLABS, Frankfurt, Germany)

2.1.5 Eucaryotic cells and associated media

- A431 (ATCC® CRL-1555™): DMEM
- HCT-116 (BioCat, Heidelberg, Germany): McCoy's 5 A
- HEK293-FT (Invitrogen™ R70007): DMEM
- Hepa 1-6 (ATCC® CRL-1830™): DMEM
- MDA-MB 468 (ATCC® HTB-132™): DMEM
- PC-9 (BioCat, Heidelberg, Germany): RPMI

2.1.6 Devices

- Cell counter device (Luna™, logos biosystems, Annandale, US)
- Centrifuge (Sorvall Evolution RC, Thermo Scientific, Waltham, US)
- DLS (Zetasizer Ultra, Malvern Panalytical, Malvern, UK)
- Flow cytometer (CytoFLEX, Beckmann Coulter, Krefeld, Germany)
- Fluorometer (Fluoroscan Ascent FL, Thermo Scientific, Waltham, US)
- French press (Thermo Scientific, Waltham, US)
- HPLC (1100 Series, Agilent, Santa Clara, US)
- Imaging system (Molecular Imager ® VersaDoc™, Bio-Rad, Hercules, US)
- Incubator (Certomat® BS-1, Sartorius, Göttingen, Germany)
- Live-cell analysis system (Incucyte® S3 Sartorius, Göttingen, Germany)
- Luminometer (Fluoroscan Ascent FL, Thermo Scientific, Waltham, US)
- Lyophilizer (Alpha 1-2 LD plus, Martin Christ Gefriertrocknungsanlagen GmbH)
- MALDI-TOF-MS (Ultraflex III, Bruker, Billerica, US)
- Absorbance microplate reader (SpectraMax 340P, Molecular Devices, San Jose, US)
- Rocker shaker (Rocky, Fröbel Labor Technik, Lindau, Germany)
- Rotary vacuum concentrator (RVC 2-25, Martin Christ, Osterode am Harz, Germany)
- Shaker (Thermomixer C, Eppendorf, Hamburg, Germany)
- SPR (Biacore X100, Cytavia, Marlborough, US)
- UV/Vis spectrometer (NanoDrop®ND 1000, Thermo Scientific, Waltham, US)

2.1.7 Kits

- BCA assay (Thermo Scientific, Waltham, US)
- Kaiser Test kit (Sigma Aldrich, St. Louis, US)
- MidiPrep (Macherey-Nagel, Düren, Germany)
- MiniPrep (Macherey-Nagel, Düren, Germany)

2.1.8 Computer software

- Biorender.com (Biorender, Toronto, Canada)
- ChemDraw Professional 16.0 / 19.0 (CambridgeSoft / PerkinElmer, Waltham, US)
- DLS Software (ZS XPLORER, Malvern Panalytical, Malvern, UK)
- GraphPad Prism 9 (GraphPad, San Diego, USA)
- IncuCyte® S3 Software (Essen BioScience, Ann Arbour, US)
- NanoDrop 1 000 Operating Software (ThermoFisher Scientific, Wilmington, US)
- SoftMax Pro (Molecular Devices Corporation, Sunnyvale, US)
- SPR Software (Biacore X100 Software, Cytavia, Marlborough, US)

2.2 Plasmid preparation

2.2.1 Transformation

LB medium:	10 g/L peptone, 5 g/L yeast extract, 10 g/L NaCl, pH 7.0; autoclaved
LB agar plates:	40 g/L LB-Agar
LB_{Amp} medium / LB_{Amp} agar plates:	50 µg/mL ampicillin; sterile filtered (0.22 µm)

A cell suspension of chemically competent *Escherichia coli (E. coli)* bacteria (Table 3) was thawed on ice, 1 µL plasmid DNA (0.2–0.8 µg/mL) was added and incubated (0 °C, 30 min). After heat shock (42 °C, 90 s) the suspension was treated with 300 µL LB medium and incubated in a shaking device (37 °C, 1 h, 250 rpm). Two different volumes in the range of 25 to 200 µL of the transformed cell suspension was plated on ampicillin containing lysogeny broth (LB_{Amp}) agar plates and incubated inverted (37 °C, 16 h). For plasmid preparation as well as for expression single colonies were picked and plates were stored overhead at 4 °C for a maximum of one month.

Table 3: Overview of *E. coli* strains used for different purposes.

Purpose	*E. coli*
Plasmid preparation	DH5α
Expression	ArcticExpress(DE3), BL21(DE3), NiCo21(DE3), Rosetta(DE3), Lemo21(DE3)

2.2.2 Plasmid preparation

For the overnight culture a single colony was inoculated in 100 mL LB_{Amp} media and shaken (37 °C, 16 h, 200 rpm). For the isolation of the plasmid DNA from the culture medium 100 mL MidiPrep Kit or 10 mL MiniPrep Kit were used, and procedures were followed according to the manufacturer's instructions. After lysis of the bacterial suspension the DNA is isolated by anion exchange chromatography and resuspended in RNase free water. The concentration of the plasmid DNA solution was determined by UV/Vis spectrometer (NanoDrop®ND 1000, Thermo Scientific, Waltham, US, λ = 260 nm).

2.2.3 Sequencing

Sequencing primer pET11d-fw:	5′-TAA TAC GAC TCA CTA TAG G-3′
Sequencing primer pET11d-r:	5′-ATC ATG ACA TTA ACC TAT AAA-3′
Sequencing primer pMAL5X-fw:	5′-GGT CGT CAG ACT GTC GAT GAA GCC-3′
Sequencing primer pMAL5X-r:	5′-TGT CCT ACT CAG GAG AGC GTT CAC-3′

To evaluate if the plasmid DNA contains the correct insert, the plasmid was sequenced according to Sanger. For preparation of sequencing, 50–100 ng of DNA each was treated with 5 µM forward (SeqAT1f) or reverse primer (SeqAT1r) and brought to a final volume of 10 µL with Milli-Q water. Sequencing was performed by Eurofins Genomics.

2.2.4 Agarose gel electrophoresis

TAE buffer:	0.5 mM EDTA, 2.5 mM $NaCOOCH_3$,
	20 mM TRIS, pH 7.2

The separation by agarose gel electrophoresis is performed based on the size and/or charge of the macromolecules. DNA has a uniform m/z ratio and is therefore separated by its number of base pairs (size). In the electric field, the negatively charged DNA migrates to the positively charged anode. The 1% agarose gel was stained with Synergy Brands Inc. (SYBR) Safe, the contained SYBR green is only fluorescently active when bound to the DNA. The DNA samples were diluted 6:1 with loading buffer, before running the agarose gel (100 V, 30 min) in tris(hydroxymethyl)-aminomethane (TRIS)-acetate-ethylenediaminetetraacetic acid (EDTA) (TAE) buffer. Afterwards the bands were detected by using the SYBR green channel of the imaging system (Molecular Imager ® VersaDoc™, Bio-Rad, Hercules, US).

2.3 Expression and purification of ligands in *E. coli*

2.3.1 Recombinant expression and extraction

An individual colony was picked from the agar plates produced as described in section 2.2.1 and was transferred into 2 mL of LB_{Amp} medium containing additional 25 µg/mL chloramphenicol (Rosetta) or 50 µg/mL gentamycin (AE) and shaken (37 °C, 6 h, 200 rpm). Afterwards 50 µL of the turbid bacteria solution was added to 100 mL LB_{Amp} medium (containing the appropriate antibiotic) and incubated (37 °C, 16 h, 200 rpm). Then, about 50 ml of the overnight culture was added to 800 ml LB_{Amp} medium or until the OD_{600} was approx. 0.3 ± 0.1. The solution was incubated until an OD_{600} of 0.8 ± 0.1 (0.4 ± 0.1 in case of AE) and afterwards treated with isopropyl-β-D-thiogalactopyranosid (IPTG) to a concentration of 0.4 M (0.7 M in case of AE). The bacteria solution was shaken (37 °C, 3 h, 200 rpm or 4 °C, 16 h, 200 rpm (AE)) and afterwards centrifuged (4 °C, 20 min, 5000 × g).

The supernatant was discarded, and the pellet dissolved in 20 ml Dulbecco's Phosphate Buffered Saline (DPBS) and frozen until further needed for a minimum of 16 h. The different recombinant plasmids and the bacteria strains used for expression are listed in Table 4.

Table 4: Overview of the different recombinant expressions.

Ligand	Vector	*E. coli* strain
K-EGF^{RR}	pET11d	BL21(DE3) NiCo21(DE3) Rosetta(DE3) ArcticExpress(DE3) Lemo21(DE3)
LSP	pET11d pMAL-c5X	NiCo21(DE3)
C-preS1-K	pET11d pMAL-c5X	NiCo21(DE3)
K-preS1-C	pET11d pMAL-c5X	NiCo21(DE3)
C-ApoA1	pET11d pMAL-c5X	NiCo21(DE3)

Before purification of the ligands, the bacteria suspension was lysed via French Press (Thermo Scientific, Waltham, US) and afterwards centrifuged (4 °C, 30 min, 30,000 × g). K-EGF^{RR} was found to be in inclusion bodies and had to be recovered according to the procedure of Patra *et al.* [143] which will be described in the following section.

2.3.2 Recovery from inclusion bodies

Washing buffer A:	50 mM TRIS, 5 mM EDTA, 0.1% Tween-20, pH 8.5
Washing buffer B:	50 mM TRIS, pH 8.0
Solubilization buffer:	50 mM TRIS, 2 M urea, pH 12
Dialysis buffer:	20 mM TRIS, 1 mM EDTA, 1 mM reduced glutathione, 0.1 mM oxidized glutathione, 10 wt% sucrose, pH 8.5

For recovering K-EGF^{RR} from inclusion bodies the supernatant of the lysis was discarded, and the pellet was resuspended 2× in washing buffer A, 1× in washing buffer B and 1× in ultra-pure water. After each resuspension, the solution was centrifuged (4 °C, 20 min, 30,000 × g) and the supernatant was discarded. Afterwards the pellet was dissolved in 20 mL solubilization buffer, incubated (25 °C, 30 min) and dialyzed against dialysis buffer (4 °C, 72 h).

2.3.3 Purification

After lysis and recovery from the inclusion bodies, the ligands were purified using different affinity chromatography purification steps (Table 5). The specific methods are described in the following sections.

Table 5: Summary of purification steps for each ligand.
(IMAC = immobilized metal affinity chromatography; MBP = maltose binding protein)

Ligand	Vector	Purification steps
K-EGF^{RR}	pET11d	IMAC
LSP	pET11d	IMAC
	pMAL-c5X	IMAC, Amylose affinity chromatography
C-preS1-K	pET11d	IMAC
	pMAL-c5X	IMAC, Amylose affinity chromatography
K-preS1-C	pET11d	IMAC
	pMAL-c5X	IMAC, Amylose affinity chromatography
C-ApoA1	pET11d	IMAC
	pMAL-c5X	Amylose affinity chromatography MBP cleavage IMAC

2.3.3.1 Amylose affinity chromatography

Washing buffer:	20 mM TRIS HCl, 200 mM NaCl, 1 mM EDTA, pH 7.4
Elution buffer:	20 mM TRIS HCl, 200 mM NaCl, 1 mM EDTA, 10 mM Maltose, pH 7.4

The ligands that were expressed using the pMAL-c5X vector are resulting in a maltose binding protein (MBP)-fusion protein and were purified via amylose affinity chromatography. Here, the MBP is interacting with amylose attached to agarose beads and is eluted by maltose solution. In an empty gravity column 4 mL (2 mL bed volume) amylose agarose resin was added and equilibrated 4× with 10 mL washing buffer. The protein solution was added to the column and incubated inverted (4 °C, 1 h). The resin was washed 4× with 10 mL washing buffer and eluted 10× with 1 mL and 15× with 2 mL elution buffer.

2.3.3.2 MBP cleavage

To cleave off the MBP-tag Factor Xa protease was used. This protease is cutting at its specific cleavage site (Ile-(Glu or Asp)-Gly-Arg |) which is located in the pMAL-c5X vector between MBP and the protein of interest. The protein solution was treated with 0.02 eq. Factor Xa and incubated (25 °C, 24 h).

2.3.3.3 Immobilized metal affinity chromatography

Washing buffer:	50 mM $NaH_2PO_4 \times 2\ H_2O$, 300 mM NaCl, 20 mM imidazole, pH 8.0
Elution buffer E31 / 62 / 125 / 250 / 500:	50 mM $NaH_2PO_4 \times 2\ H_2O$, 300 mM NaCl, 31.25 / 62.5 / 125 / 250 / 500 mM imidazole, pH 8.0

This method is based on the interaction of nickel-nitriloacetic acid (Ni-NTA) on Sepharose resin with histidine (His) rich sequences of a protein. Therefore, it is possible to separate the ligands equipped with 6×His-tags from other proteins like bacteria proteins by eluting them via an imidazole gradient. In an empty gravity column 6 mL (3 mL bed volume) Ni-NTA Sepharose resin was added and washed 2× with 10 mL Milli-Q water and equilibrated 4× with 10 mL washing buffer. The protein solution was adjusted to 20 mM imidazole, added to the column, and incubated inverted (4 °C, 1 h). Afterwards the resin was washed 2 × 10 mL washing buffer and eluted with an imidazole gradient (5× E31, 5× E62, 5× E125, 5× E250 (1 mL each), 5× E250 (2 mL each)).

2.3.4 Sodium dodecyl sulphate-polyacrylamide gel electrophoresis

4× SDS Sample buffer:	Non-reducing: 0.25 mM Tris-HCl, 40% [v/v] glycerol, 8% [w/v] SDS, 0.04% [w/v] bromophenol blue, pH 6.8 Reducing: 4× non-reducing sample buffer, 8% [v/v] β-mercaptoethanol
SDS-PAGE gel	
Separating buffer:	1.5 M Tris-HCl, 0.4% [w/v] SDS, pH 8.8
Stacking buffer:	0.5 M Tris-HCl, 0.6% [w/v] SDS, pH 6.8
Running buffer:	20 mM TRIS, 192 mM glycine, 0.1% [w/v] SDS, pH 8.3
Tris-Tricine SDS-PAGE gel	
Separating/Stacking buffer:	3 M Tris-HCl, 0.6% [w/v] SDS, pH 8.45
Anode buffer:	0.2 M TRIS, pH 8.8
Tris-Tricine running buffer:	0.1 M TRIS, 0.1 M tricine, 0.1% [w/v] SDS, pH 8.3

This method enables the electrophoretic separation of proteins according to their molecular mass independent of their charge and shape. In this process, sodium dodecyl sulphate (SDS) denatures the protein and generates a net negative charge depending on the number of amino acid residues. This enables the size-dependent migration of the protein toward the anode. For this purpose, the C.B.S. horizontal electrophoresis system (80×85×0.75 mm) was used as the running chamber. For analysing smaller proteins like EGF the tris-tricine SDS-PAGE gel was used, whereas for the other ligands a 12% SDS-PAGE was used. The exact volumes used for gel preparation are listed in Table 6.

Table 6: Buffer composition of the SDS-PAGE gels.

SDS-PAGE gel (12%)	**Separating gel**	**Stacking gel**
MilliQ water	1.48 mL	0.72 mL
Separating buffer	1.06 mL	/
Stacking buffer	/	0.30 mL
30% acryl amide	1.70 mL	0.18 mL
10% ammonium persulfate	30.0 µL	10.0 µL
TEMED	3.00 µL	3.00 µL
Tris-Tricine SDS-PAGE gel	**Separating gel**	**Stacking gel**
MilliQ water	1.75 mL	1.95 mL
Separating/stacking buffer	2.50 mL	0.78 mL
glycerol	2.50 mL	/
30% acryl amide	0.75 µL	0.40 mL
10% ammonium persulfate	7.00 µL	7.00 µL
TEMED	7.00 µL	7.00 µL

The samples were denatured with 4× non-reducing or reducing sample buffers (96 °C, 5 min), 15 µL were applied to the stacking gel and the proteins were separated (200 V, 40 mA (1 gel) / 80 mA (2 gels), 40–90 min). In case of tris-tricine gels, the anode buffer was added on top of the chamber and the tris-tricine running buffer was added on the bottom. The SDS-PAGE gels were either stained with Coomassie brilliant blue or scanned with the imaging system (Molecular Imager ® VersaDoc™, Bio-Rad, Hercules, US) to detect the protein bands or further used for western blots (WB).

2.3.5 Coomassie staining

Staining solution:	0.1% [w/v] Coomassie brilliant blue R-250, 40% [v/v] ethanol,10% [v/v] acetic acid
Destaining solution:	20% [v/v] ethanol, 10% [v/v] acetic acid

Coomassie brilliant blue R-250 stains non-specifically aromatic as well as basic amino acids. This enables the visual detection of proteins within the SDS-PAGE gel. For this purpose, the gels were stained and incubated (25 °C, 16 h) on a rocker shaker (Rocky, Fröbel Labor Technik, Lindau, Germany). Afterwards the staining solution was discarded, and the gel washed with water and several times with destaining solution (25 °C, 30 min) until only the protein bands were visible.

2.3.6 Western blot

Blotting buffer:	25 mM TRIS, 192 mM glycine, 10% [v/v] ethanol
Blocking buffer:	5% skimmed milk
$PBSB_{0.2}$:	PBS with 0.2% [w/v] Brij 58, pH 7.4
Ponceau Rot	0.1% [w/v] Ponceau S, 5% [v/v] acetic acid
ECL solution A	100 mM TRIS HCl, 14.11 mM luminol, pH 8.6
ECL solution B	6 mM *p*-coumarin acid in DMSO
ECL solution C	30% [v/v] H_2O_2

Western blot is using the antigen-antibody-binding principle to enable the immune detection of proteins. The SDS-PAGE gel was transferred to a nitrocellulose membrane by an electrophoretic transfer (50 V, 50 min). The scheme in which order the compartments are arranged is shown in Figure 10.

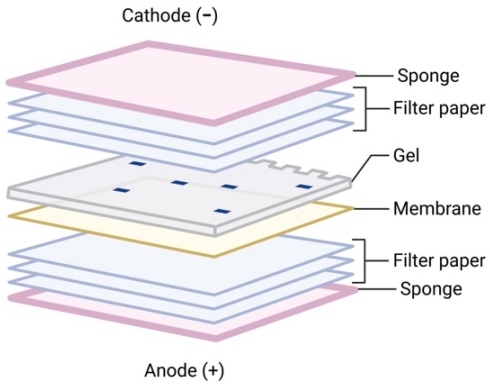

Figure 10: Schematic experimental structure of western blot.
Adapted from "Membrane Transfer Schematics", by BioRender.com (2023). Retrieved from https://app.biorender.com/biorender-templates.

The successful transfer was verified by ponceau S staining (5 min) and documented. Afterwards the membrane was washed several times with water. In case of EGF the membrane was treated with 0.1% glutaraldehyde (25 °C, 30 min) to fix the small protein before blocking free binding sites with 10 mL skimmed milk (25 °C, 30 min). The membrane was washed 2× with PBS and treated with 10 mL primary antibody in $PBSB_{0.2}$ (Table 7) and incubated (25 °C, 1 h or 4 °C, 16 h) on a rocker shaker (Rocky, Fröbel Labor Technik, Lindau, Germany). The next day the membrane was washed 4× with $PBSB_{0.2}$, treated with the respective secondary HRP antibody (Table 7) (25 °C, 30 min) and washed 3× with $PBSB_{0.2}$. All the solution was discarded, and the membrane dried with filter paper before adding the chemo luminescence solution (1000 µL ECL solution A, 100 µL solution B, 1 µL solution C). The bands were visually detected by using the ultra-sensitive blotting channel of the imaging system (Molecular Imager ® VersaDoc™, Bio-Rad, Hercules, US).

Table 7: Antibodies used for western blot.
(*) Horse raddish peroxidase (HRP) marked antibody

Primary AB	Dilution	Incubation	Secondary AB	Dilution	Incubation
anti-EGF	1:2500	4 °C, 16 h	GAR*	1:2000	25 °C, 30 min
anti-ApoA1	1:2000	25 °C, 1 h	RAM*	1:2000	25 °C, 30 min
anti-preS1	1:2500	4 °C, 16 h	RAM*	1:2000	25 °C, 30 min
anti-MBP	1:10.000	25 °C, 1 h	RAM*	1:2000	25 °C, 30 min

2.3.7 Dialysis

After purification of the proteins with affinity chromatography, they were dialysed against PBS for further storage. Based on the volume as well as size of the protein, a dialysis tube of appropriate size exclusion (1.0 MWCO (EGF); 3.5 MWCO (others)) was equilibrated in final buffer for 10 min and the protein was dialysed against 1–2 L of PBS with continuous stirring (4 °C, 16 h). In case of EGF, Amicon filtration leads to the loss of the whole product. Therefore, the final buffer was 0.2× PBS and the solution was concentrated to 1× PBS by rotary vacuum concentration (section 2.3.8). The concentration of the protein solution was determined via BCA (section 2.3.9) or UV/VIS photometer (section 2.4.4).

2.3.8 Rotary vacuum concentration

In this method, the solution is concentrated in vacuum while centrifuged. For this procedure, the reaction vial is placed open in the rotary vacuum concentrator (RVC 2-25, Martin Christ, Osterode am Harz, Germany) device and centrifuged (30 °C, 3 h, 20,000 rpm) or until the desired volume is obtained.

2.3.9 BCA

The concentration of the proteins was determined by a bicinchoninic acid (BCA) assay. This assay relies on the reduction of Cu^{2+} to Cu^{+} by the proteins. The Cu^{+} then forms a water soluble chelate complex with BCA, which shows an absorbance signal at 562 nm. A standard dilution series (15.13, 31.25, 61.5, 125, 250, 500, 1000, 2000 µg/mL) of bovine serum albumin (BSA) was used to calculate the concentration of the proteins. In a 96-well-plate stripe, 25 µL sample or standard or buffer (blank) was added as well as 200 µL BCA solution and incubated (37 °C, 30 min). The absorbance was measured at 562 nm and analysed by microplate reader (SpectraMax 340P, Molecular Devices, San Jose, US).

2.4 Chemical modification of ligands

2.4.1 Conjugation of cyanine-dyes or linkers

In this thesis two different functional groups of the ligands are addressed for conjugation of a dye (to track it *in vivo*) or a click-chemistry-linker (to conjugate it to the scaffold). One is the amine group of a lysine that is reacting with an N-hydroxysuccinimide (NHS)-ester and the other one is the thiol group of a cysteine that can undergo a thiol-ene Michael addition with maleimide. In a reaction vial 2 or 10 eq. of cyanine 3 or cyanine 5 dye or dibenzocyclooctyne (DBCO)- polyethylene glycol (PEG)-linker (in dimethyl sulfoxide (DMSO)) was added to the protein solution (in phosphate-buffered saline (PBS)) and incubated (25 °C, 16 h, 800 rpm) (Table 8).

Table 8: Summary of dyes and linkers used for modifying ligands.

K-EGF^{RR}		**C-ApoA1**	
Dye or linker	Eq.	Dye or linker	Eq.
Sulfo-Cy3-Mal	10	Cy3-NHS	2
Sulfo-Cy3-NHS	10	Sulfo-Cy3-Mal	10
Sulfo-Cy5-Mal	10	Sulfo-Cy3-NHS	2 or 10
Sulfo-Cy5-NHS	10	Sulfo-Cy5-Mal	10
		Sulfo-Cy5-NHS	10
		Sulfo-Cy5.5-NHS	2 or 10
DBCO-PEG$_{12}$-NHS	10	DBCO-PEG$_{12}$-Mal	10
DBCO-PEG$_3$-S-S-NHS	10	DBCO-PEG$_3$-hydrazon-Mal	10
		DBCO-PEG$_{12}$-NHS	10
		DBCO-PEG$_3$-S-S-NHS	10

2.4.2 Synthesis of SO1861-EGF

To obtain an EGFR-targeted endosomal escape enhancer (EEE), SO1861-N-ε-maleimidocaproic acid hydrazide (EMCH) was conjugated to EGF. Before the hydrazone group of the EMCH can react with the EGF, a thiol group has to be generated. Therefore, EGF was treated with 2 eq. 2-iminothiolane · HCl and incubated (25 °C, 1 h, 800 rpm). Afterwards 0.8 eq. SO1861-EMCH was added and again incubated (25 °C, 16 h, 800 rpm). The SO1861-hydrazon-EGF was used without any further purification for *in vitro* analysis (section 2.8).

2.4.3 Size exclusion chromatography

To separate the unconjugated dye or linker from the desired protein product, size exclusion chromatography (SEC) was used. This method allows the separation of the compounds based on the different sizes of the molecules. The mixture solution is added to a porous matrix of spherical beads. Smaller molecules can diffuse into the beads, whereas larger molecules are unable to enter and therefore are eluted first. The PD-10 column (Sephadex G-25) was equilibrated with the respective buffer (4× 5 mL). After the sample was applied to the column, the volume was adjusted to 2.5 mL with buffer. The sample was eluted with 3.5 mL DPBS and collected in constant fractions (7× 500 mL) or by visual control (when the dye-labelled ligand was visible on the column). The protein concentration of the fractions as well as the conjugation degree were analysed by UV/Vis photometer.

2.4.4 UV-Vis spectroscopy

UV-Vis measurements were performed on a NanoDrop®ND 1000 (Thermo Scientific, Waltham, US) spectrophotometer in the spectral range of 200–750 nm.

2.5 Characterization of ligand interactions

The interaction between the before expressed and purified ligands and targeted cells in which the respective receptor is overexpressed was explored by flow cytometry (section 2.5.1). To evaluate the interaction of the ligands and the receptor sandwich enzyme-linked immunosorbent assay (ELISA) (section 2.5.4) as well as surface plasmon resonance (SPR) (section 2.5.5) was performed.

2.5.1 Flow Cytometry

To evaluate the interaction of the target cells with the ligands, flow cytometry was used. The cells are single passaged in front of a laser, where they are detected, counted and/or sorted. The flow cytometry experiments were performed by Meike Kolster at the Freie Universität Berlin (FUB). For these experiments the human embryonal kidney cell line HEK293-FT, human breast cancer cell line MDA-MB 468, human squamous cell cancer cell line A431, human metastatic melanoma cell line A2058 and mouse liver cell line Hepa 1-6 were used.

After cultivation, 20,000 cells per well in 100 µL DMEM were seeded in a 96-well-plate and cultivated for 24 h. Then, the culture medium was completely exchanged against fresh culture medium supplemented with the compounds to be tested. For investigation of the concentration-dependent uptake, cells were incubated (37 °C, 5% CO_2, 95% humidity, 24 h) with ligand solutions of varying concentrations.

Time-dependent uptake was examined by adding a solution with a constant ligand concentration of 100 nM (Cy5-K-EGF^{RR}) or 500 nM (Cy5-C-ApoA1) to the cells at different time intervals and different wells before the end of the incubation period.

For the investigation of the competition between the ligand variants and their unlabelled counterparts, cells were incubated (37 °C, 5% CO_2, 95% humidity, 4 h) with the same constant ligand variant concentration (either 100 or 500 nM as above) and varying concentrations of EGF (0.1–10 µM) or ApoA1 (0.5–5 µM).

To analyse internalization, cells were washed twice with 150 µL Dulbecco's Phosphate Buffered Saline (DPBS) before 150 µL Trypsin/Versene solution was added to detach the cells. The resulting cell suspensions were transferred to microcentrifuge tubes and kept on ice until fluorescence cytometry analysis using a CytoFLEX flow cytometer (Beckmann Coulter, Indianapolis, US).

Blank cell suspensions were used to manually establish the gating of single cells based on their forward scatter (FSC-height vs. FSC-width). A minimum number of 10,000 single cells were included in the analysis of each condition. To assess the Cy5-related fluorescence signal, the signal of the cell in the allophycocyanin (APC)-channel (excitation: red laser, 638 nm, emission bandpass filter: 660/10 nm) was evaluated.

2.5.2 Primary hepatocyte spheroid culture

Primary hepatocytes were isolated from C57BL/6JOlaHsd male mice and seeded in a Petri dish in William's E spheroid medium supplemented with 10% FBS, 1% penicillin/streptomycin and 100 nM dexamethasone. The cells were incubated (37 °C, 5% CO_2, 95% humidity, 8 d), and the medium was changed every 2–3 days using William's E spheroid medium supplemented with 1% penicillin/streptomycin and 100 nM dexamethasone. Afterwards, 10 spheroids in 40 µL serum-free medium per well were added to the 384-well plate, incubated (37 °C, 5% CO_2, 95% humidity, 30 min) and aspirated to 30 µL serum-free William's medium. The spheroids were treated with 30 µL of C-ApoA1-Cy3 at increasing final concentrations (1 nM, 10 nM, 100 nM, 1 µM) or left untreated, and incubated (37 °C, 5% CO2, 95% humidity, 120 min). After the uptake, the cells were washed with PBS using a HydroSpeed™ plate washer (Tecan), fixed with 3.7% formaldehyde (40 µL, 35 min, RT), and stained with DAPI and Phalloidin-488. Images of spheroids were acquired using an automated spinning disk confocal microscope (CellVoyagerTM 7000; Yokogawa) equipped with three Andor Neo 5.5 sCMOS cameras. Briefly, plates were pre-scanned with a low-magnification objective (4x/0.16 ULPSAPO), and individual spheroids were automatically detected using the smart imaging capabilities of the microscope software (Cell Voyager Measurement system Release R1.17.05).

High-magnification images of automatically detected spheroids were acquired using a 60x ULPSAPO objective. CellMask blue and DAPI were imaged using laser excitation at 405 nm and an emission bandpass filter BP445/45, FITC and Alexa 488 with a 488 nm laser and BP525/50 filter, Alexa 594 with a 561 nm laser and BP600/37 filter, and Alexa 647 and Cy5 with a 640 nm laser and a BP676/29 filter.

2.5.3 Primary hepatocyte sandwich culture

Primary hepatocytes were isolated from BL6 male mice, and 200.000 cells/well were plated onto collagen (0.9 mg/mL) coated 24-well plates in Williams E medium (PAN Biotech, Aidenbach, Germany) supplemented with 10% FBS, 1% penicillin/streptomycin and 100 nM dexamethasone. The cells were incubated (37 °C, 5% CO_2, 95% humidity, 2 h), the medium was removed, and non-attached cells and debris were washed out with cold PBS.

Then, cells were incubated again on 950 µL of fresh medium (37 °C, 5% CO_2, 95% humidity, 3 h). Afterwards, the top collagen layer (0.6 mg/mL) was added and incubated (37 °C, 5% CO_2, 95% humidity, 1 h). After gelation, 1 mL of medium was added to the sandwich culture and the cells were incubated (37 °C, 5% CO_2, 95% humidity, 96 h) with continuous medium change every day. For uptake experiments, the cells were starved (2 h) in medium without serum and afterwards treated with 1 µM C-ApoA1-Cy3 and incubated (37 °C, 5% CO_2, 95% humidity) in full medium for different time points, followed by a cold wash with PBS. The cells were fixed with 4% paraformaldehyde and stained with DAPI and Phalloidin-488. Samples were analyzed using a Laser Scanning Confocal Microscope (Olympus Fluoview 3000, LMF facility, MPI-CBG, Dresden) equipped with an Olympus UPlanSApo 60×1.35 Oil immersion objective at a resolution of app. 0.207 µm/pixel and 500 nm step size.

2.5.4 Sandwich-ELISA

Wash buffer:	PBS, 0.05% Tween®-20 Detergent
Blocking solution:	Diluent A

To evaluate the interaction of the ligand with its respective receptor, an ELISA was performed. ELISA is an antibody-based assay, where the antigen (receptor + ligand) is immobilized to a surface and is afterwards treated with the detection antibody (HRP-antibody). By adding a substrate (TMB), HRP catalyses an enzymatic reaction. The wells of a streptavidin (SA) coated 96-well-plate were washed 3× with 200 µL wash buffer and afterwards treated with 100 µL of the respective biotinylated receptor (5 µg/mL; 500 ng/well; EGFR or SR-BI), covered with an adhesive plastic and shaken (4 °C, 16 h) on a rocker shaker (Rocky, Fröbel Labor Technik, Lindau, Germany). The coating solution was removed, and the wells washed 3× with 200 µL wash buffer.

Afterwards 200 µL blocking solution (2 h), 100 µL respective ligand (1 µg/mL; 100 ng/well; EGF or ApoA1, 1 h), 100 µL primary rabbit antibody (1:1000; anti-EGF (16 h) or mouse anti-ApoA1 (1 h)), 100 µL secondary antibody (1:1000; goat anti rabbit immunoglobulins or rabbit anti mouse immunoglobulins, 1 h) and 100 µL 3,3′,5,5′-tetramethylbenzidine (TMB) substrate (15 min) were added. After each step, the wells were washed 3× with 200 µL wash buffer.

The TMB reaction was stopped by adding 100 µL of 2 M sulfuric acid. The absorbance at 450 nm was determined by microplate reader (SpectraMax 340P, Molecular Devices, San Jose, US).

2.5.5 SPR

HBS-EP buffer:	10 mM HEPES pH 7.4, 150 mM NaCl, 3 mM EDTA, 0.005% v/v Surfactant P20

The interaction of the ligands with the corresponding receptor was studied by SPR with a Biacore X100 SPR device (Biacore X100, Cytavia, Marlborough, US) using SA sensor chips. Here, the binding of the ligand is measured as the changes of the resonance angle due to mass change on the sensor chip and quantified in resonance units (RU). The respective biotinylated receptor was immobilized on the SA chip to a level of 5000 RU (EGFR), or 3000 RU (SR-BI) dissolved in HBS-EP buffer on Flow cell 2 (Fc2). The reference flow cell (Fc1) was left untreated. For the binding studies the respective ligand (in HBS-EP buffer) was injected with a contact time of 180 s and a dissociation time of 600 s. For regeneration, the chip was treated with 10 mM sodium hydroxide (NaOH) with 30 s contact time and 60 s stability time. The equilibrium dissociation constant K_D was determined by using the Biacore X100 Evaluation Software (version 2.0.2) and applying the steady state fit.

2.6 Dendron synthesis

2.6.1 SPPS

The dendrons used in this thesis where synthesised via solid phase peptide synthesis (SPPS). This method is divided in four main steps: (1) swelling, (2) deprotection, (3) activation and conjugation of amino acid and (4) cleavage. Steps (2) and (3) are repeated until the desired length or generation of the peptide dendron has been reached.

2.6.1.1 Swelling

In a reaction syringe with membrane 50 mg Wang-resin was added and dissolved in 500 µL dimethyl formamide (DMF). The resin was then allowed to swell (25 °C, 15 min) and afterwards filtered and washed 2× with DMF.

2.6.1.2 Deprotection

Fmoc has been used as protecting group which can be cleaved under basic conditions. Piperidine (500 µL, 20% in DMF) was added to the resin and shaken (25 °C, 20–60 min, 600 rpm). The solution was discarded and fresh piperidine (500 µl, 20% in DMF) was added. Afterwards, the resin was filtered and washed 3× with DMF, 2× with dichloromethane (DCM) and 3× with DMF (500 µL each).

2.6.1.3 Activation of amino acid and conjugation

The amino acid (4 eq. per amino group at resin) that should be added was dissolved in DMF (0.250–1 mL), hexafluorophosphate azabenzotriazole tetramethyl uronium (HATU) (4 eq. per amino group at resin) and N,N-diisopropylethylamine (DIPEA) (4 eq. per amino group at resin) were added to the reaction vial. After shaking (25 °C, 5 min, 600 rpm) the solution was added to the resin. The reaction mixture was shaken (25 °C, 16 h, 600 rpm) and afterwards filtered and washed 3× with DMF, 2× with DCM and 3× with DMF (500 µL each). The completion of the coupling was determined via Kaiser test. If the Kaiser test was still positive, the whole step was repeated.

2.6.1.4 Kaiser Test

Solution A:	80% [w/v] phenol in ethanol
Solution B:	KCN in water/pyridine
Solution C:	6% [w/v] ninhydrin in ethanol

The Kaiser test, also known as ninhydrin test, is a sensitive test for detecting primary amines. In the presence of free amino groups and thus incomplete peptide coupling, a dye called Ruhemann's blue is formed and is visible by eye. After washing, a few resin beads were placed in a reaction vial and solution A, B and C (20 µL each) were added, mixed and heated (95 °C, 5 min). If the solution was blue (positive), the coupling was not complete and step 2.6.1.3 had to be repeated. If the solution was colourless or yellow the synthesis could be continued with a new amino acid in step 2.6.1.2 or terminated as described in step 2.6.1.5.

2.6.1.5 Cleavage

After the desired generation was obtained, the peptide dendron was cleaved off by using TFA. For this purpose, TFA (500 µL, 80% in DCM) or in case of unprotected cysteines TFA (500 µL, 95%, 2.5% TIS, 2.5% water) was added to the resin and incubated (25 °C, 4 h, 600 rpm). The solution was filtered and washed 1× with TFA and 2× with DCM (250 µL each). The fractions were collected and precipitated in 10 mL cold diethyl ether (4 °C, 16 h).

The solution was centrifuged (4 °C, 15 min, 4000 rpm), the diethyl ether was discarded, and the precipitate was dissolved in 500 µL MilliQ water and afterwards lyophilised. The amounts of the compounds used to synthesize different dendrons (D1, D2, D3, D4) and generations are listed in Table 9.

Table 9: Amount and order of amino acids and coupling reagents to synthesize D1–D4.

	Substance	M (g/mol)	G	m (mg) / V (µL)	n (mmol)	eq.
	Fmoc-Lys-Boc Wang resin	100–200 mesh 0.4–1.0 mmol/g ~ 0.7 mmol/g		50 mg	0.035	1
D1	Fmoc-Lys-Fmoc	590.70 g/mol	G0	82.7 mg	0.14	4
			G1	165.4 mg	0.28	8
			G2	330.8 mg	0.56	16
			G3	661.6 mg	1.12	32
D2	Fmoc-Lys-N_3	394.42 g/mol		55.2 mg	0.14	4
	Fmoc-Lys-Fmoc	590.70 g/mol	G0	82.7 mg	0.14	4
			G1	165.4 mg	0.28	8
			G2	330.8 mg	0.56	16
			G3	661.6 mg	1.12	32
D3	Fmoc-Lys-Fmoc	590.70 g/mol	G0	82.7 mg	0.14	4
			G1	165.4 mg	0.28	8
	Fmoc-Cys-S(tBu)	431.57 g/mol	G2	241.7 mg	0.56	16
	Fmoc-Lys-Fmoc	590.70 g/mol	G3	330.8 mg	0.56	16
D4	Fmoc-Lys-Fmoc	590.70 g/mol	G0	82.7 mg	0.14	4
	Fmoc-Cys-S(tBu)	431.57 g/mol	G1	120.8 mg	0.28	8
	Fmoc-Lys-Fmoc	590.70 g/mol	G2	165.4 mg	0.28	8
			G3	330.8 mg	0.56	16
	HATU	380.28 g/mol		53.2 mg	0.14	4
				106.5 mg	0.28	8
				212.9 mg	0.56	16
				425.9 mg	1.12	32
	DIPEA	129.25 g/mol		24.4 µL	0.14	4
				48.8 µL	0.28	8
				97.6 µL	0.56	16
				195.1 µL	1.12	32

2.6.2 Lyophilization

Freeze-drying was performed on an Alpha 1-2 LD plus lyophiliser (Martin Christ Gefriertrocknungsanlagen GmbH). The samples were frozen with liquid nitrogen and placed into the freeze-dryer at high vacuum for 24 h.

2.6.3 HPLC

The previously synthesized dendrons were purified using high-performance liquid chromatography (HPLC). The separation principle of HPLC is based on the different interaction of the sample components with the adsorbent material (stationary phase) while passing through in a solvent (mobile phase). The purification was performed on an 1100 series HPLC (Agilent, Santa Clara, US) and a C18 column (Luna® 5 µM C18(2) 100 Å 250×10 mm). As mobile phase a gradient from 20% to 80% acetonitrile (ACN) with 0.1% TFA was used eluting the components over a period of 40 min. The different observed peaks were collected in separated fractions and afterwards analysed by matrix-assisted laser desorption/ionization-time of flight mass spectrometry (MALDI-TOF-MS).

2.6.4 MALDI-TOF-MS

The crude as well as the purified dendrons were analysed by MALDI-TOF-MS. The spectra were recorded on a MALDI-Mass Spectrometer (Ultraflex III, Bruker, Billerica, US). Typically, the sample was dissolved in MilliQ water in nanomolar to micromolar concentrations and was spotted on the target plate (MTP 384 target plate ground steel T F, Bruker Daltons) using either super 2,5-dihydroxybenzoic acid (SDHB) (99%, Fluka) or p-chloro-α-cyanocinnamic acid (CICCA) as the matrix via the dried-droplet-method. PepMix (Peptide Calibration Standard) or ProteMass (Protein Calibration Standard) served as calibration standards.

2.7 Polyplex formation

2.7.1 General procedure

Polyplex formation is based on the electrostatic interaction between the negatively charged phosphate backbone of the DNA plasmid and the positively charged amine groups of the dendron. For 20 µL polyplex, 7.5 µL plasmid (0.2 mg/mL, in 10 mM HEPES) coding for either enhanced green fluorescence protein (eGFP) or luciferase was added to 12.5 µL dendron solution (in 10 mM 4-(2-hydroxyethyl)-1-piperazineethanesulfonic acid (HEPES)), vortexed and incubated (25 °C, 1 h). Charge ratios (N/P) were calculated based on the number of phosphate groups of the DNA and the number of terminal amine groups on the dendron. The concentration of the dendron stock solution was calculated and prepared for N/P 16. Solutions for the lower N/Ps were obtained by serial dilution (N/P 8, 4, 2, 1, 0.5).

2.7.2 Addition of K-EGF^{RR}

K-EGF^{RR} was either added without a DBCO-linker to electrostatically interact with the positively charged dendron or with a DBCO-linker (section 2.4.1) to be covalently attached to the dendron bearing an azide-group (dendron D2). The polyplex is either formed before adding the K-EGF^{RR} as described in 2.7.1 or after the ligand is attached to the dendron. After adding the ligand (in PBS), the mixture is pipetted up and down (5×) and incubated (25 °C, 16 h). The amount of EGF was calculated according to the weight/weight ratio of EGF to DNA and varies from 10–0.1.

2.7.3 Pico488 assay

In this assay the DNA-binding benzothiazole dye Pico488 is used. It is a double stranded DNA specific fluorescent sensor and can be detected by using a fluorometer. The Pico488 solution was diluted 1:400 and 200 µL were added to each well of a 96-well-plate (black, clear bottom) and 5 µL blank, control or sample was added. The plate was then incubated under exclusion of light (25 °C, 5 min) and the fluorescence was measured using the fluorometer (Fluoroscan Ascent FL, Thermo Scientific, Waltham, US).

2.7.4 Dynamic light scattering (DLS)

The size of the polyplexes in suspension was determined via dynamic light scattering (DLS). In a cuvette, 60 µL HEPES (10 mM) were placed and 10 µL polyplex solution were added and mixed by pipetting up and down (5×). The solution was allowed to find back into the equilibrium state for 10 min before measuring the samples with DLS device (Zetasizer Ultra, Malvern Panalytical, Malvern, UK) at 25 °C. Afterwards, 70 µL sodium chloride (NaCl) solution (300 mM) was added to the solution, mixed (5×), incubated (25 °C, 10 min) and measured again. The parameters were calculated using the ZS Xplorer software (Version. 2.3.0.62).

2.8 *In vitro* evaluation

The human embryonal kidney cancer cell line HEK293-FT, human breast cancer cell line MDA-MB 468, human squamous cell cancer cell line A431, human lung cancer cell line PC-9, and human colon cancer cell line HCT-116 were used for *in vitro* experiments.

2.8.1 General culture methods

The cells were cultured under constant conditions in the incubator (37 °C, 5% CO_2, 95% humidity) and all cell biology work was always performed under sterile conditions (laminar air flow workbench). The cell lines were cultivated in medium (Table 10) supplemented with 10% fetal bovine serum (FBS) and 1% penicillin/streptomycin.

Table 10: Medium used for each cell line.

Medium	Cell line
DMEM	HEK293-FT, MDA-MB-468, A431
RPMI 1640	PC-9
McCoy's 5A	HCT-116

To cultivate the cells from the stock in the −173 °C nitrogen tank, the cell line was thawed in a water bath (37 °C, 5 min), transferred in 5 mL medium and centrifuged (25 °C, 5 min, 1200×g). The supernatant was discarded, the pellet resuspended in 5 mL of medium and transferred to a T25 tissue culture flask and incubated. The medium was exchanged after 24 h.

For splitting the cells, the old medium was aspirated, and the cells washed with DPBS and detached from the cell culture flask with 250 µL trypsin (0.25%, 37 °C, 5 min). To neutralize the trypsin the cells were dissolved in 5 mL medium, centrifuged (25 °C, 5 min, 1200 rpm) and the pellet was resuspended in 1 mL medium. The cells were cultivated in a new T25 culture flask containing 5 mL medium to obtain a final confluency of 20–40%. For seeding the cells into a 96-well-plate, 10 µL from the cell suspension was treated with 10 µL trypan blue and the number of cells was measured via cell counter device (Luna™, logos biosystems, Annandale, US). The respective amount was added to the wells. For the following assays 80 µL cell suspension was added into a 96-well-plate containing 4000 (HEK293-FT), 6000 (A431, A2058) and 10,000 cells per well (MDA-MB 468).

2.8.2 GFP assay

To evaluate the transfection efficiency, the dendrons were polyplexed with eGFP plasmid DNA (section 2.7.1), which will lead to the expression of eGFP in case of successful transfection and translation of the DNA. This green fluorescence as well as the confluency was live imaged and detected via the live-cell analysis system (Incucyte® S3 Sartorius, Göttingen, Germany).

After the cells were seeded (section 2.8.1) in a 96-well-plate and incubated (37 °C, 24 h), 40 µL fresh medium was added to each well. Afterwards 15 µL DMEM, lipofectamine control (prepared according to manufacturer) or sample (75 ng DNA per well) was added as well as additional 15 µl SO1861 (4 or 0.4 µM in well) or PBS. The plate was placed in the Incucyte® S3 and an image was taken every 2 h over a period of 96 h and 10× objective. The cell confluency as well as the green fluorescence was determined via the Incucyte® S3 software.

2.8.3 Luciferase reporter assay

Another assay to investigate the transfection efficiency is the luciferase reporter assay. This assay was performed in the same way as the GFP assay described above (section 2.8.2) with one important change: the polyplexes used here were containing plasmids which are encoding for luciferase instead of eGFP (section 2.7.1). The cells were also monitored via live cell imaging by the Incucyte® S3 and afterwards treated with 100 µL Steady-Glo® luciferase assay solution. After incubation (25 °C, 5 min) the luminescence was determined via luminometer (Fluoroscan Ascent FL, Thermo Scientific, Waltham, US).

2.8.4 Cell viability assay (MTS assay)

The cell viability was determined by using 3-(4,5-dimethylthiazol-2-yl)-5-(3-carboxymethoxy-phenyl)-2-(4- sulfophenyl)-2H-tetrazolium (MTS) that is reduced to water-soluble formazan. After transfection (37 °C, 96 h), 15 µL MTS solution was added to the wells and incubated (37 °C, 2 h). The absorbance was measured via microplate reader (SpectraMax 340P, Molecular Devices, San Jose, US) at 490 nm. The absorbance of the blank (MTS in DMEM without cells) was subtracted from the absorbance of the samples.

3 Results

3.1 Design of plasmids and variants

One part of this thesis is focusing on the expression and purification of targeting ligands. As described before, two different cell types, namely cancer and liver, should be addressed to demonstrate the diverse applicability of the ENDOSCAPE prototype. For cancer cells the epidermal growth factor (EGF) was the ligand of choice as many cancer cells are overexpressing the EGF receptor (EGFR), whereas for liver there were several options. On one hand there were protein ligands from the hepatitis B virus, which are causing a liver disease. The large surface protein (LSP) of this virus was chosen, as it contains the liver binding region, the so called preS1 domain. Additionally, this domain was also chosen with either lysine at the N-terminus and cysteine at the C-terminus or *vice versa*. On the other hand, we evaluated the apolipoproteinA1 (ApoA1) as a liver ligand, which is part of the high-density lipoprotein (HDL) and is involved in cholesterol transport to the liver. When designing the ligands, we wanted to answer the question of how to avoid cross-linking and aggregation of ligands or ligand conjugates. This typically occurs when the components contain multiple conjugation sites that can interact inter- and intramolecularly to form aggregates. In order to avoid this, the targeting ligand must be specifically designed in such a way that it contains only a single conjugation site that is used to bind to a cargo like the non-viral vector or a drug (Figure 11). In case of EGF, the natural occurring lysines at position 32 and 52 were replaced by arginine, as it is known from previous studies that this does not have an effect on the functionality [144]. Additionally, one or two artificial lysines were added near the N-terminus, which serve as single conjugation sites. Even though, KK-EGF^{RR} contains two lysines, it is unlikely that conjugations occur at both lysines due to steric hindrance. For the preS1 domains and ApoA1 the design was straight forward, as they do not contain any natural cysteines (both) and lysines (preS1). Therefore, the preS1 domains were either equipped with a single lysine at the N-terminus and a single cysteine at the C-terminus or the other way around. In case of ApoA1 only a single cysteine was added close to the N-terminus. For purification purposes a 6×His-tag was added and in case of the preS1 domains a tobacco etch virus (TEV) cleavage site was inserted between the 6×His-tag and the modified ligand. The reason is that the preS1 domain is rather small (35 amino acids (aa)) and therefore the 6×His-tag could have a higher impact on the binding to the receptor than for the other ligands (EGF^{RR}: 59 aa, ApoA1: 247 aa, LS protein: 405 aa).

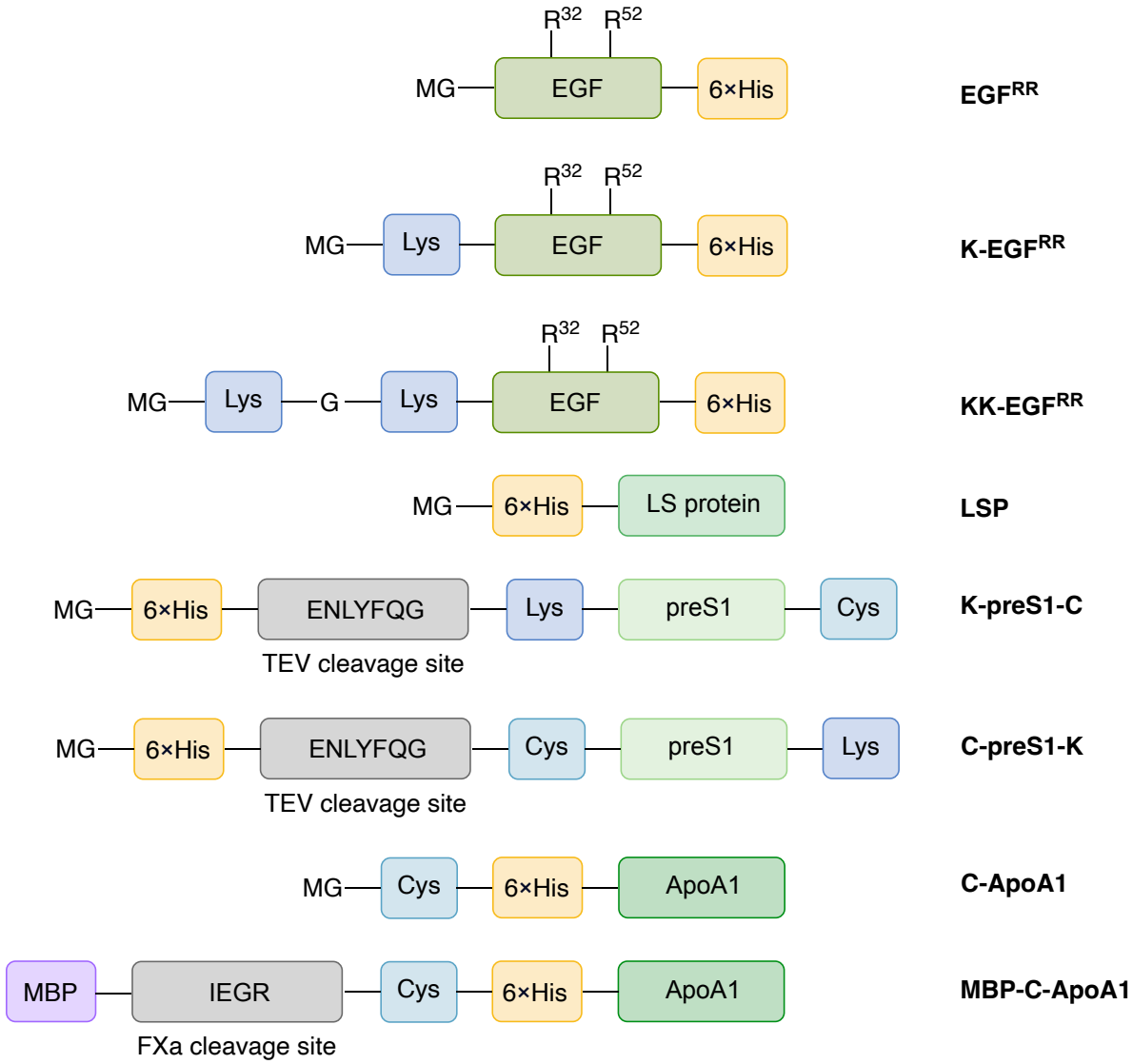

Figure 11: Design of ligand variants for targeted therapy.
Cancer targeting: EGF^{RR}, K-EGF^{RR}, KK-EGF^{RR}; liver targeting: LSP, K-preS1-C, C-preS1-K, C-ApoA1. The artificially inserted amino acids are indicated in blue, the ligands in green, the 6×His-tag in yellow, the MBP-tag in purple and the protease cleavage sites in grey.

The before described ligand sequences were produced by BioCat and cloned by the company into a pET11d vector by the restriction enzymes NcoI and EcoRI. Additionally, as part of this thesis, the C-ApoA1 sequence was also inserted into a pMAL-c5X vector. In this case, the expression results in a maltose binding protein (MBP) fusion protein with ApoA1 and a FXa cleavage site to cleave off the MBP afterwards. The hepatitis B derived LSP was cloned from pET11d-OTC-spacer-LSP formerly obtained from BioCat, where OTC stands for ornithine transcarbamylase. Restriction enzyme digestion was used to obtain the desired plasmid. First, the plasmid was digested with NheI and SpeI to cut off the OTC and afterwards digested with SmaI and SnaBI to generate the desired pET11d-LSP (Appendix Figure S1). Before using the ordered and cloned plasmids, they were amplified by plasmid preparation and analysed via Sanger sequencing and agarose gel electrophoresis.

3.2 Recombinant expression and purification of ligands

3.2.1 Cancer targeting ligand

The previous described and designed plasmids pET11d-EGF^{RR}-6×-His, pET11d-K-EGF^{RR}-6×-His, and pET11d-KK-EGF^{RR}-6×-His were first transformed into the *E. coli* strain ArcticExpress DE3 (AE(DE3)). Here, the expression and purification was only successful for EGF^{RR} and K-EGF^{RR} with a yield of 100–250 µg per 1 L approach while for KK-EGF^{RR} no band was observed in the anti-EGF western blot. For further experiments we decided to go with K-EGF^{RR} as it has a single conjugation site. To improve the yield pET11d-K-EGF^{RR}-6×-His was additionally transformed into the different *E. coli* strains BL21(DE3), NiCo21(DE3), and Rosetta(DE3). The expression was induced by 0.4 mM (BL21(DE3), NiCo21(DE3), and Rosetta(DE3)) or 0.7 mM (AE(DE3)) IPTG and according to western blot (Figure 12 A) the highest expression level was observed in Rosetta. However, K-EGF^{RR} was detected in the pellet and not in the supernatant after lysis. This indicates that the variant was encapsulated in inclusion bodies. For this reason, the ligand had to be released from the inclusion bodies and refolded before purification using 2 M urea. Because of the 6×His-tag, the desired product could be purified via NiNTA and be eluted by an imidazole gradient. Nevertheless, the desired and pure product was only obtained in case of Rosetta(DE3) and AE(DE3), where only the expected band at approximately 7.6 kDa on the SDS-PAGE (Figure 12 B) was observed. In case of NiCo21(DE3) no pure product was obtained after NiNTA.

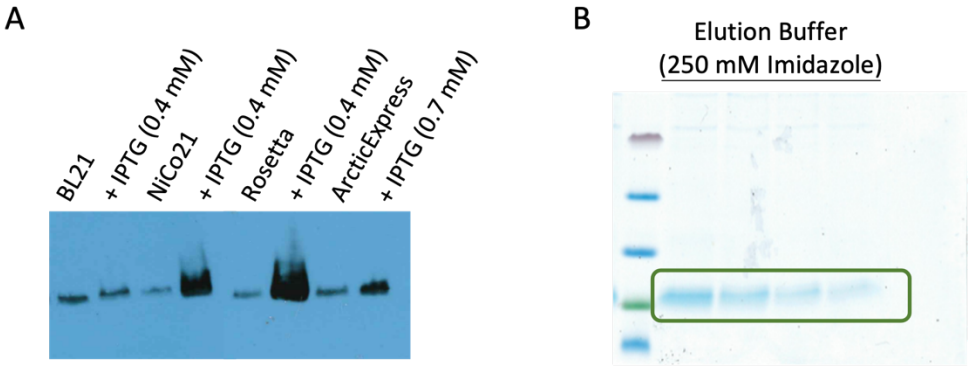

Figure 12: Expression and purification of K-EGF^{RR}.
(A) Expression of K-EGF^{RR} in different E. coli *strains. (B) Elution of K-EGF^{RR} expressed in Rosetta(DE3) after NiNTA affinity chromatography. Green indicates the band of the pure K-EGF^{RR}.*

Due to its small size, K-EGF^{RR} was dialyzed against PBS using low binding dialysis tubes to prevent interaction of the protein with the dialysis membrane, which would lead to the loss of the product. We successfully increased the yield of pure K-EGF^{RR} from 250 µg in AE to 5–6 mg per 1 L expression approach using Rosetta *E. coli* strain.

3.2.2 Liver targeting ligands

For the hepatitis B derived ligands, LS protein and preS1 domains, which were inserted into the pET11d vector, were expressed by using the NiCo21(DE3) *E. coli* strain. Unfortunately, neither after purification with NiNTA using the 6×-His-tag, nor after purification with chitin affinity chromatography, which could trap the bacterial proteins containing a chitin-binding domain (CBD)-tag when using NiCo21(DE3) strain, the desired products were obtained. For this reason, the DNA sequences were cloned into a pMAL-c5X vector, but also this approach did not lead to a successful expression and purification of the hepatitis derived ligands.

As mentioned before, the 6×-His-C-ApoA1 was cloned into two different vectors, namely pET11d and pMAL-c5X. The expression in NiCo21(DE3) was not successful by using the pET11d, but with the pMAL-c5X vector, which led to the expression of a MBP-C-6×His-ApoA1 fusion protein. This protein was purified via amylose affinity chromatography taking advantage of the MBP-tag. Two bands were observed after elution with 10 mM maltose (Figure 13 A). The band at 72 kDa (yellow box in Figure 13 A) that belongs to the MBP-ApoA1 fusion protein as well as a band at 42 kDa (orange box) that represents the MBP alone is observed in SDS-PAGE. All fractions containing both the fusion protein itself (pure fraction) or additional free MBP (impure fraction) were collected as the protein mixture was later purified with NiNTA exploiting the 6×His-tag on ApoA1. In this purification step, the free MBP is found in the flow through, whereas the 6×His-C-ApoA1 was afterwards eluted with imidazole. To receive the pure ApoA1 (30 kDa), the MBP-tag was cleaved off using the factor Xa protease. This protease acts at its preferred cleavage site Ile-(Glu or Asp)-Gly-Arg which is located between the MBP and the artificially inserted cysteine of the C-ApoA1 leading to the desired product. In order to find the optimal reaction time, the fusion protein was incubated for different time points (Figure 13 B). According to this western blot, a reaction time of minimal 24 h can be considered as optimal and was therefore used in further experiments. After the cleavage of MBP, the protein solution was purified via NiNTA taking advantage of the 6×His-tag. The purification was successful and yielded the desired C-ApoA1 (30 kDa) with a yield of 4–6 mg of pure fraction per 1 L expression approach (Figure 13 C, D). The different outcomes of the expression conditions for the ligand variants and their outcome are summarized in Figure S2.

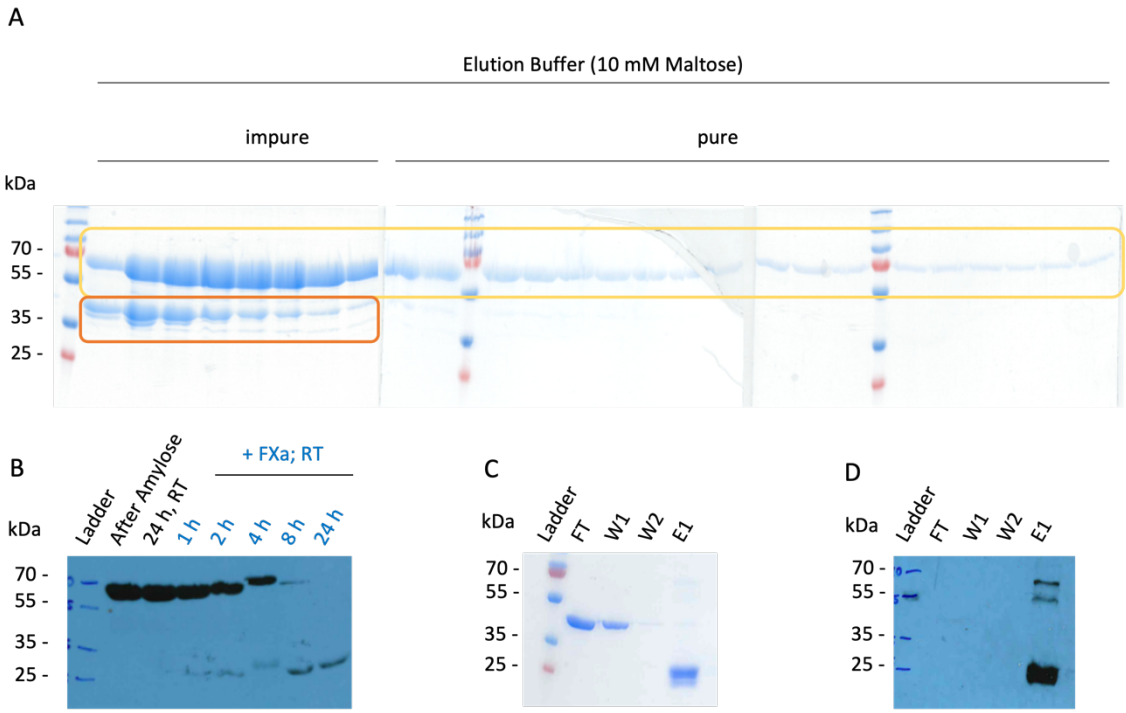

Figure 13: Expression and purification of MBP-C-ApoA1.
(A) Elution of MBP-C-ApoA1 expressed in NiCo21 E. coli *after amylose affinity chromatography. The pure fractions only contained the fusion protein MBP-C-ApoA1 (yellow box) whereas the impure fractions contained additional MBP (orange box). (B) Anti-ApoA1 western blot of MBP-C-ApoA1 incubation with factor Xa. (C) SDS-PAGE and (D) anti-ApoA1 western blot after Ni-NTA purification.*

3.3 Equipment of ligands

After successful expression and purification of the ligand variants K-EGF^{RR} and C-ApoA1, the reactivity and accessibility of the functional groups were investigated by treating the ligands with dyes bearing the complementary functional group. To address the amino group of the lysines, a cyanine-3 dye with an *N*-hydroxy succinimide (NHS) ester (Cy3-NHS) was used to form an amide bond with the amine of the side chain (Figure 14 A). On the other hand, the thiol groups of the eight cysteines were treated with a maleimide cyanine-3 dye (Cy3-Mal) to undergo a thiol-ene-Michael addition (Figure 14 B). The same reactions will also be used to introduce the cleavable and non-cleavable linker, which will be discussed afterwards.

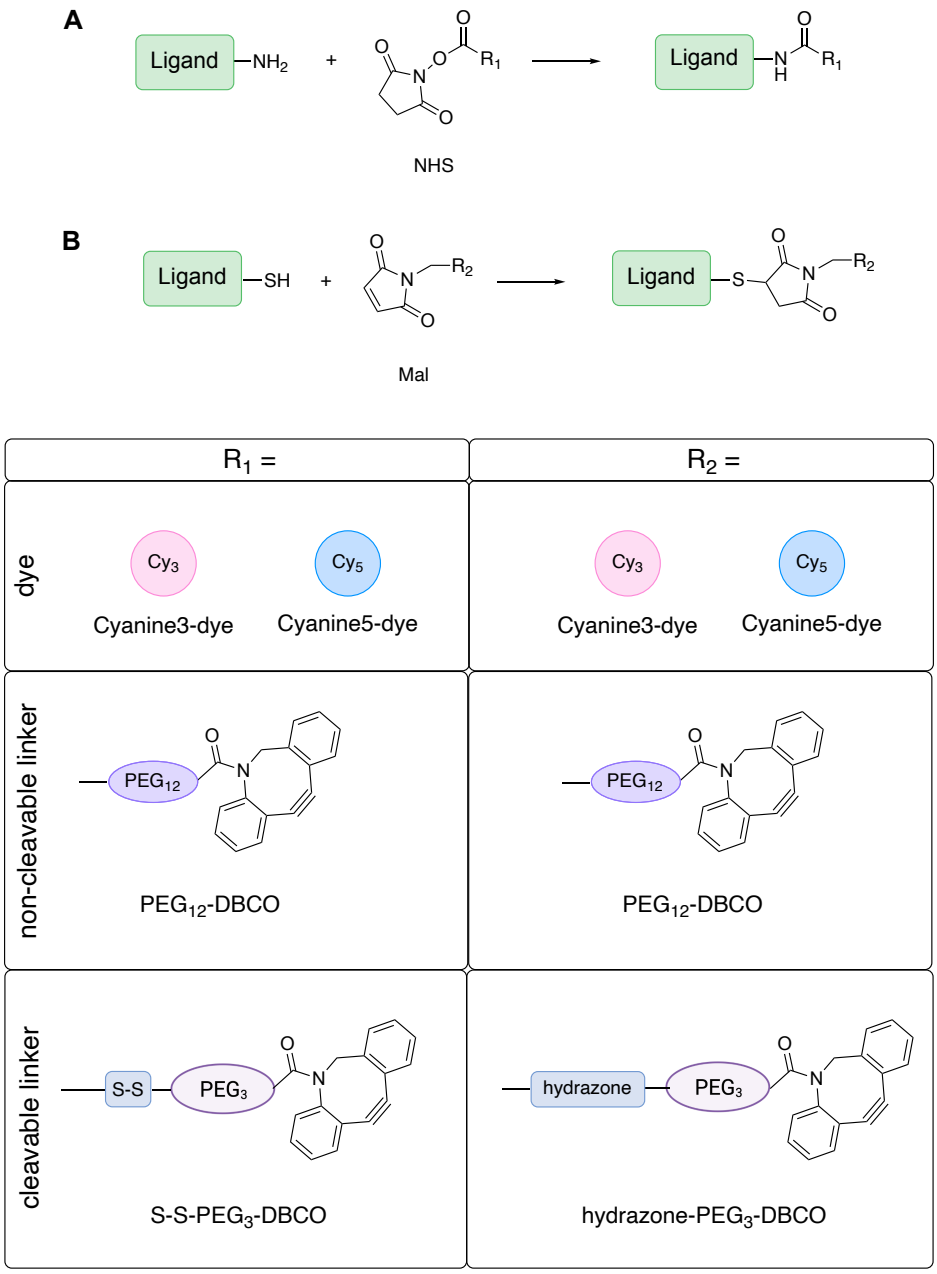

Figure 14: Conjugation of dyes at the ligand.
(A) Conjugation at the lysine of ligands via amide binding. (B) Conjugation at the cysteine of the ligand by thiol-ene Michael addition.

To exclude non-specific interaction of the Cy3 dye with the proteins, they were also treated with Cy3-COOH. Due to its low reactivity, the carboxyl group should not be able to react with the functional groups of the ligand. The accessibility and reactivity were confirmed by SDS-PAGE. The desired bands were observed at the expected height in the Cy3-channel of a molecular imager (VersaDoc™) in case of the ligands treated with Cy3-Mal or Cy3-NHS, but not in case of Cy3-COOH (Figure S3). The band of the Cy3-NHS treated C-ApoA1 was brighter than the one of the Cy3-Mal, which is not surprising as C-ApoA1 contains only one cysteine but 21 lysines. The appearance of a band when treating K-EGF^{RR} with Cy3-Mal indicates that not all natural disulphide bridges within the EGF are closed in each molecule.

After the accessibility of the functional groups was confirmed, the ligands were now equipped with dyes for the follow-up *in vitro* studies and determination of the conjugation rate. In addition, they were also conjugated to non-cleavable and cleavable linkers (Figure 14). For labelling, cyanine-NHS dyes were used to address the lysines of the ligands. For C-ApoA1 this means to address multiple lysines (21) whereas for the K-EGF^{RR}, it is only a single conjugation site. Multiple conjugation sites for labelling were chosen in case of C-ApoA1 to retain the single cysteine for conjugation of the click-adapter. For the conjugation at K-EGF^{RR} there is only one lysine available, which means that the EGF variant can be either equipped with a dye or a linker. The cysteines were not addressed in case of K-EGF^{RR} to not destroy the integrity of the ligand.

After treating the ligands with the dyes, the amount of dye per ligand was determined by UV/Vis-spectroscopy by dividing the amount of dye by the amount of ligand. For the first experiments Cy3-NHS (2 eq.) was conjugated at C-ApoA1 and the number of dye molecules per ligand after size exclusion chromatography was determined to be 0.89 (Table 11). However, free dye was detected in the purified Cy3-C-ApoA1 by SDS-PAGE, which is leading to incorrect high dye loading values. For this reason, sulfo-cyanine-dyes were used instead. These dyes are much less susceptible for aggregation under aqueous conditions, due to their hydrophilicity and resulting water solubility. When using the same amount of sulfo-Cy3-NHS the dye loading is reduced to 0.39 (vs. 0.89 Cy3-NHS) but no free dye was detected via SDS-PAGE. Therefore, the amount of dye was increased to 10 eq., whereupon the ratio of dye per ligand increased to 0.87 (sulfo-Cy3-NHS) or even 0.99 (sulfo-Cy5-NHS). These conditions were also applied to the conjugation experiments with K-EGF^{RR}, leading to a dye loading of 0.65 (Table 11).

Table 11: Summary of dyes used for labelling of the ligands and their conjugation rate.
(*) this value also includes free dye

Ligand	Conjugation reagent	equivalents	Dye per ligand
C-ApoA1	Cy3-NHS	2	0.89*
	Sulfo-Cy3-NHS	2	0.39
	Sulfo-Cy3-NHS	10	0.87
	Sulfo-Cy5-NHS	10	0.99
K-EGF^{RR}	Sulfo-Cy5-NHS	10	0.65

To create a conjugation site at the ligands for click chemistry to couple them either to a drug or to a scaffold used to polyplex the gene delivery vector, in our case the strain-promoted azide-alkyne cycloaddition (SPAAC), a dibenzo cyclooctyne (DBCO) group was introduced using a heterobifunctional polyethylene glycol (PEG) linker.

The PEG linker provided either a maleimide group for conjugation with cysteines or an NHS ester for conjugation with lysines. In addition, linkers were chosen to introduce cleavable bonds that allow separation of the cargo and the ligand after internalization. The non-cleavable linkers consist of DBCO, PEG and Mal/NHS (DBCO-PEG_{12}-Mal/NHS), whereas the cleavable ones possess an additional hydrazone (DBCO-PEG_3-hydrazone-Mal) or disulphide bond (DBCO-PEG_3-S-S-NHS). The hydrazone bond is pH sensitive and is cleaved under acidic conditions, whereas the redox labile disulphide bond can be cleaved under reducing conditions. The linkers were either conjugated to the single cysteine (Figure 15 A, B) or to multiple lysines (Figure 15 C, D) of the pre-labelled Cy3-C-ApoA1 using different equivalents of the linkers. As the determination of the amount of linker per ligand was not possible by UV/Vis-spectroscopy due to low concentrations, the successful conjugation was confirmed by SDS-PAGE. Therefore, Cy5-azide was added to the samples, as the azide will react selectively with the DBCO of the linker. A band at about 30 kDa was observed in the Cy3-channel for every sample treated with different equivalents of linker (Figure S4). In the Cy5-channel, the intensity of this band increased with the number of linker equivalents used in the conjugation step. Additionally, no band for the negative control (0 eq.) – where no linker was added to the Cy3-C-ApoA1 – is observed in the Cy5-channel as expected (Figure 15). These results are indicating that the conjugation of the linker at Cy3-C-ApoA1 was successful.

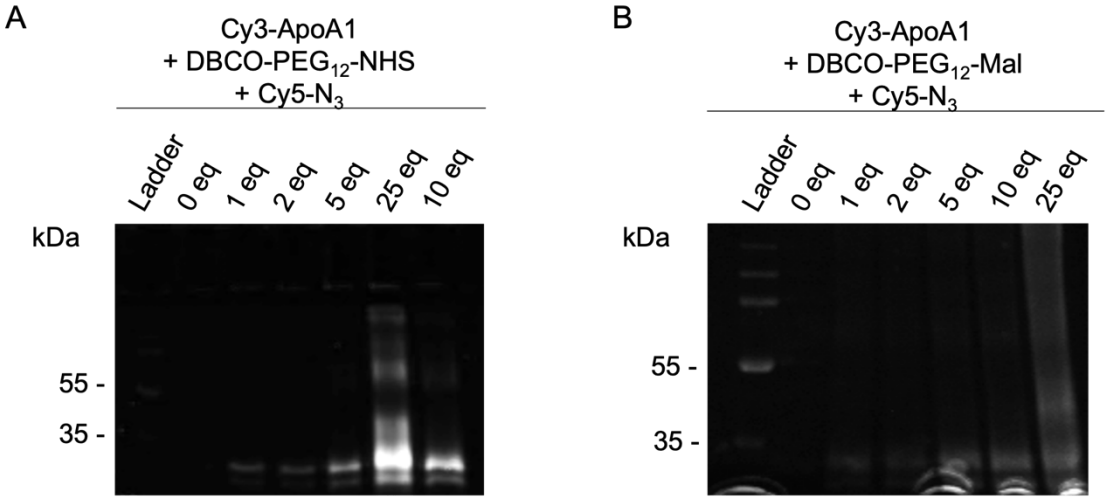

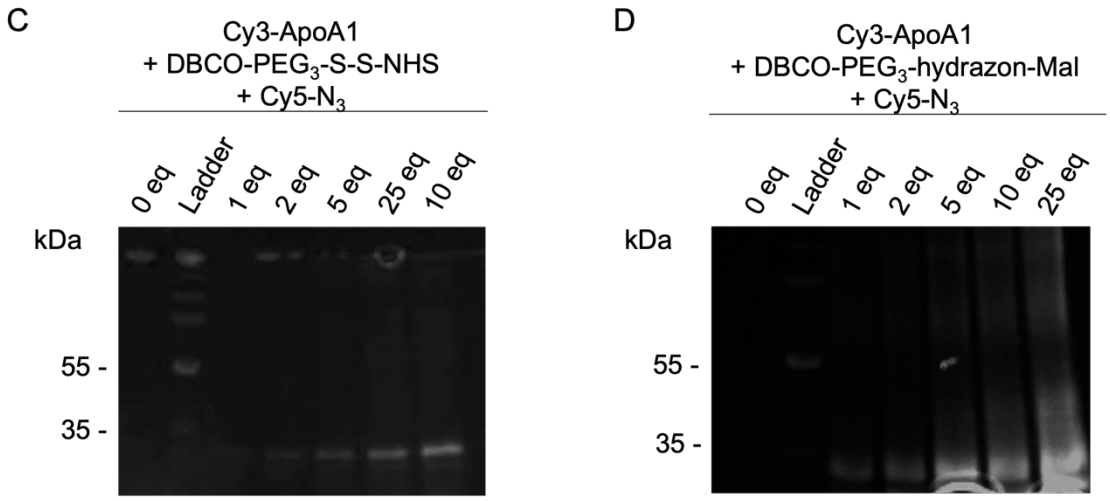

Figure 15: Verification of the successful conjugation of the linker to Cy3-C-ApoA1.
Conjugation of (A) non-cleavable and (B) cleavable DBCO-PEG-Mal linker at Cy3-C-ApoA1 with different equivalents of linker (previous page). Conjugation of (C) non-cleavable and (D) cleavable DBCO-PEG-NHS linker at Cy3-C-ApoA1 with different equivalents of linker. Afterwards the Cy3-C-ApoA1-Linker conjugates were incubated with Cy5-N_3, to check if the conjugation of the linker was successful. The images were obtained by using the Cy5-channel or Cy3-channell (Figure S4) of a VersaDoc device.

The same experiment was repeated with K-EGF^{RR}, but only the NHS-linkers were used, due to the single lysine conjugation site. The analysis of the SDS-PAGE reveals that Cy5-intensity of the band also increased by using more equivalents of linker (Figure 16). These observations correlate with the results seen for the conjugation of linkers to C-ApoA1.

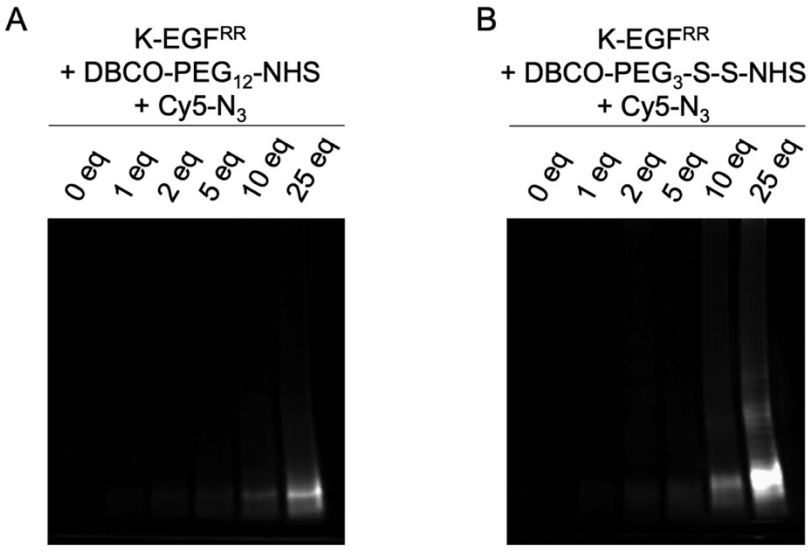

Figure 16: Verification of the successful conjugation of the linker to K-EGF^{RR}.
Conjugation of (A) non-cleavable and (B) cleavable DBCO-PEG-NHS linker at K-EGF^{RR} with different equivalents of linker. Afterwards the K-EGF^{RR}-linker conjugates were incubated with Cy5-N3, to check if the conjugation of the linker was successful. The images were obtained by using the Cy5-channel of a VersaDoc device.

Additionally, the K-EGF^{RR} was also equipped with the EEE SO1861 to create a targeted SO1861. As described before, the SO1861 was functionalized with an EMCH linker and therefore contains an acid labile hydrazone bond as well as a maleimide group which can react with a thiol. For this reason, the amine group of the single lysine at the N-terminus had to be converted into a thiol group. This was achieved by treating K-EGF^{RR} with 2-iminothiolane, which reacts with the primary amine to introduce the thiol group after ring opening. This functional group can then undergo a thiol-ene Michael addition with SO1861-EMCH (Figure 17).

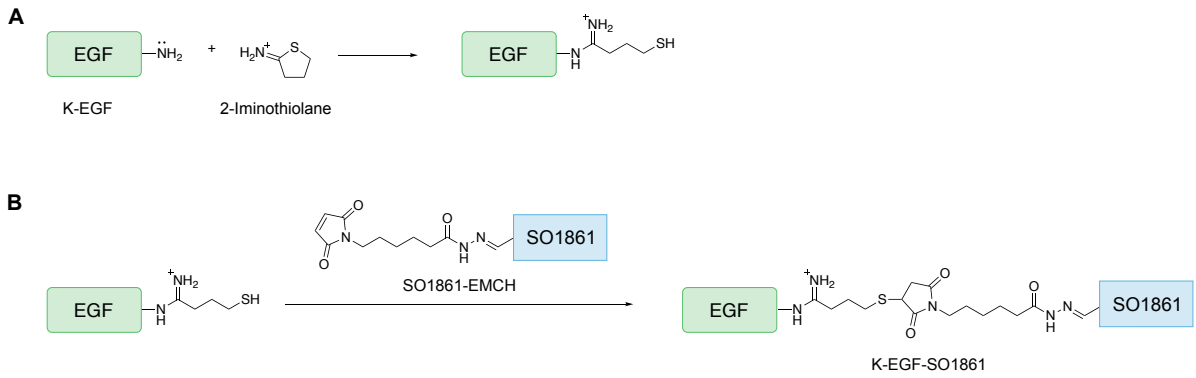

Figure 17: Conjugation of K-EGF^{RR} to SO1861-EMCH.

The successful reaction was confirmed by MALD-TOF-MS where an additional peak was detected at 9656 m/z which refers to SO1861-EGF (Figure 18 C, blue box). This peak is not observed for K-EGF^{RR} (Figure 18 A) or only rarely visible for K-EGF^{RR} only treated with SO1861-EMCH but not with 2-iminothiolane (Figure 18 B), where the amine group of the K-EGF^{RR} was not converted into a thiol group. The small peak observed could be due to non-specific interactions of SO1861-EMCH with the amino group of the lysine or the N-terminus of K-EGF^{RR}. Nevertheless, the peak of SO1861-EGF is more detectable when K-EGF^{RR} was treated with 2-iminothiolane, indicating that the conversion of the amino to a thiol group was successful, leading to the desired product. However, the peak of K-EGF^{RR} at about 7500 m/z (green box) is visible in all cases, indicating that the conversion of the amine to the thiol group was not complete. The SO1861-EGF was used without further purification *in vitro*.

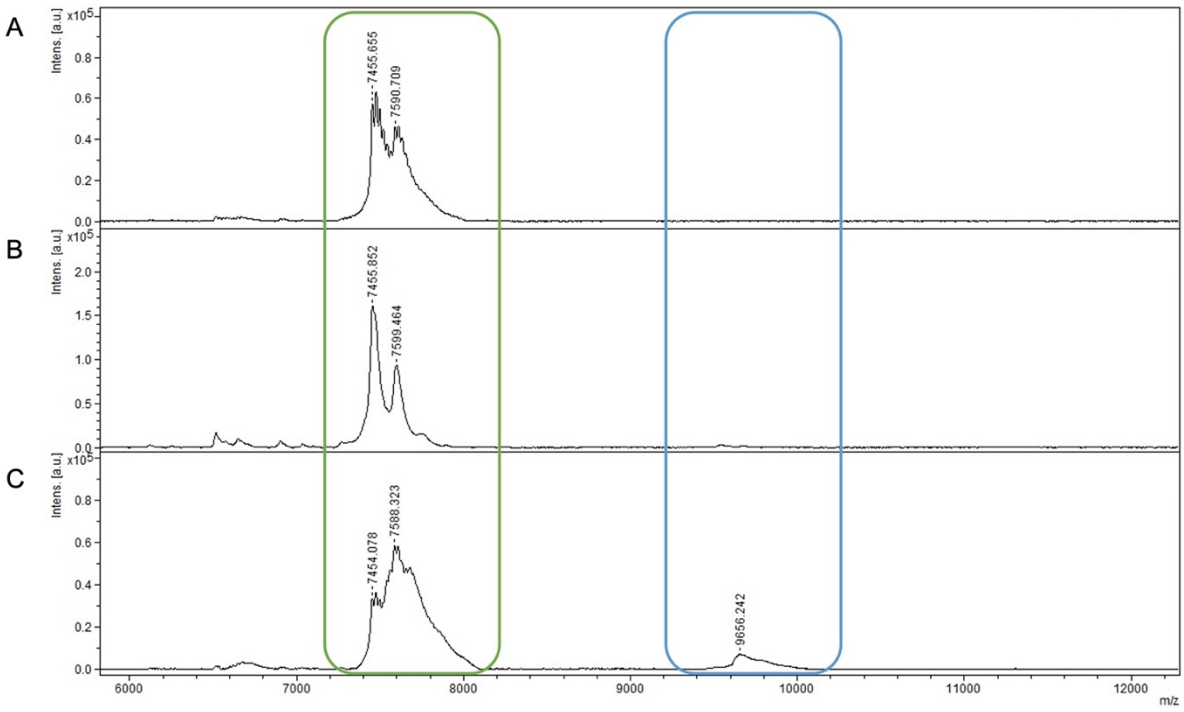

Figure 18: MALDI-TOF-MS to verify the synthesis of SO1861-EGF.
(A) K-EGF^{RR}, (B) K-EGF^{RR} (without 2-iminothiolane) + SO1861-EMCH, (C) K-EGF^{RR} + 2-iminothiolane + SO1861-EMCH. Green indicates K-EGF^{RR}, whereas blue indicates SO1861-EGF.

3.4 Evaluation of ligand interactions

3.4.1 Ligand-cell interaction

The interaction of the two ligands with target or off-target cells were evaluated by flow cytometry, which was performed by Meike Kolster (FUB). The cells were treated with different concentrations of Cy5-labelled ligands and for different time ranges. As K-EGF^{RR} is addressing the EGF receptor (EGFR), the following cell lines were chosen based on their normalized transcripts per million (nTPM) of EGFR. As EGFR positive cell lines A431 (5282.1 nTPM) and MDA-MB 468 (613.3 nTPM) where chosen for EGF and A2058 (0.2 nTPM) as EGFR negative cell line. A time- and concentration-dependent interaction with target and off-target cell lines was detected (Figure 19 A, C). The intensity of the Cy5-fluorescence signal of the cells and thereby the ligand-cell interaction correlates with the EGF-receptor (EGFR) expression [145]. To exclude that the fluorescence signal is due to free dye or the interaction of the dye with the cells, the cells were incubated with equivalent concentrations of Cy5. The free dye exhibited lower fluorescence intensities. Cy5-C-ApoA1 also showed a time and concentration-dependent uptake, in contrast to K-EGF^{RR} this uptake seems to be unspecific, as the fluorescence intensity is higher in the off-target cells (HEK293-FT) compared to cells that have a higher level of SR-BI receptors (Hepa 1-6) (Figure 19 B, D).

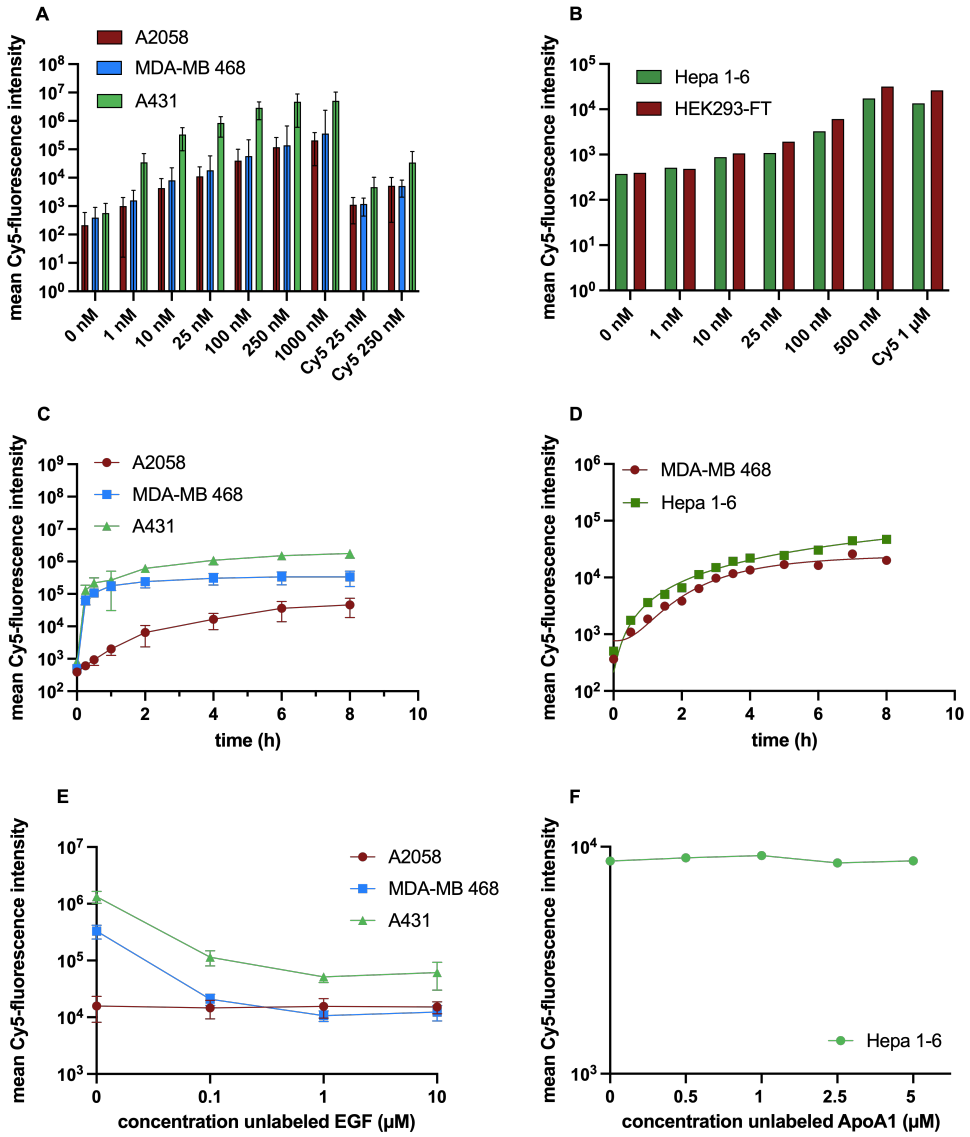

Figure 19*: In vitro* cell-ligand interaction of Cy5-labelled ligand variants by flow cytometry.
K-EGF^{RR} was evaluated in cell lines A2058 (EGFR–), MDA-MB 468 (EGFR+) and A431 (EGFR++) (0.25 Cy5/EGF). C-ApoA1 (0.39 Cy5/ApoA1) in cell lines Hepa 1-6 (HDL+), HEK293-FT or MDA-MB 468 (HDL–). Concentration and time dependent uptake of (A, C) Cy5-labelled K-EGF^{RR} and (B, D) C-ApoA1 incubated for 24 h. Competitive inhibition of internalization of Cy5-labelled K-EGF^{RR} or (F) C-ApoA1 by unlabelled K-EGF^{RR} or unlabelled C-ApoA1 in varying concentrations. The mean value ± SEM is shown (biological replicates (N) = 3, technical replicates (n) = 2).

To determine if the interaction between cell and ligand is due to ligand-receptor interaction, competitive inhibition assays were performed. In these experiments 100 nM Cy5-K-EGF^{RR} or 500 nM Cy5-C-ApoA1 and different concentrations of unlabelled ligand were simultaneously added to the cells for 4 h. For EGF, a decrease of the target cell fluorescence intensity to the level of off-target cells was observed when increasing the concentration of the competitive non-labelled EGF (Figure 19 E) indicating a receptor dependent uptake. However, for ApoA1 no change was detected (Figure 19 F), which correlated with the unspecific uptake observed in the off-target cell line.

Additional *in vitro* internalization experiments were performed by Max Planck Institute (MPI, Dresden). In the case of EGF, Hela cells were used (26.4 nTPM) and treated with EGFR siRNA to knock down the EGFR or Mock transfected with medium. Afterwards the cells were treated with 9 nM commercial wild-type EGF labelled with 2–3 eq. Alexa-647 or the K-EGF^{RR} labelled with 0.25 eq. of sulfo-Cy5-NHS per ligand or treated with PBS. The fluorescence was measured at different timepoints. The cells were additionally treated with 4',6-diamidino-2-phenylindol (DAPI) to stain the cell nucleus indicated in grey in the high-content pictures whereas the labelled EGF is indicated in green (Figure 20 A). According to the pictures the fluorescence intensity was substantially lower in EGFR knock-down cells. Furthermore, the number of EGF-positive cells is increasing over time (Figure 20 B) for either knock-down or Mock transfected cells. The signal of the wild-type EGF is higher compared to the mutant. However, it is important to note, that only 0.25 K-EGF^{RR} ligands were labelled with dye compared to 2–3 Alexa-647 per wild-type EGF. Additionally, the fluorescence excitation/emission are different for both dyes and therefore absolute intensities are not comparable. Nevertheless, these results also indicate a receptor mediated uptake of EGF, which correlates with the flow cytometry results.

For ApoA1 two different mouse primary hepatocyte cultures were used, namely hepatocyte spheroids and collagen sandwich cultures. In case of spheroids, Phalloidin-488 staining was used to highlight cell boundaries and the spheroids were treated with different amounts of Cy3-labelled C-ApoA1. Fluorescent signals were detected for 100 nM and 1 µM C-ApoA1-Cy3 but not at lower concentrations (Figure 21 A). Due to the inherent three-dimensional nature of spheroid cultures, detailed subcellular analysis beyond the initial cell layer was challenging. Therefore, experiments were carried out using collagen sandwich cultures of mouse hepatocytes, where the hepatocytes were properly polarized. This was visualized by the actin-rich apical membrane forming bile canaliculi between hepatocytes. In this setup, hepatocytes grow as a monolayer, allowing easier access to subcellular structures. However, a drawback was encountered in the form of thick collagen matrix surrounding hepatocytes, hindering the interaction of different ligands with the cell surface. To address this issue, holes were pinched into the collagen matrix to facilitate the penetration of ligands and their access to the cells. In collagen sandwich hepatocytes, the MPI performed pulse and chase experiments with Cys-ApoA1-Cy3 (Figure 21 B), revealing that cytosolic fluorescence became apparent within hepatocytes after just 5 min. However, the presence of fluorescence within endosomal structures was rarely visible. Furthermore, some hepatotoxic effects were observed, and bright fluorescent aggregates were present outside the cells.

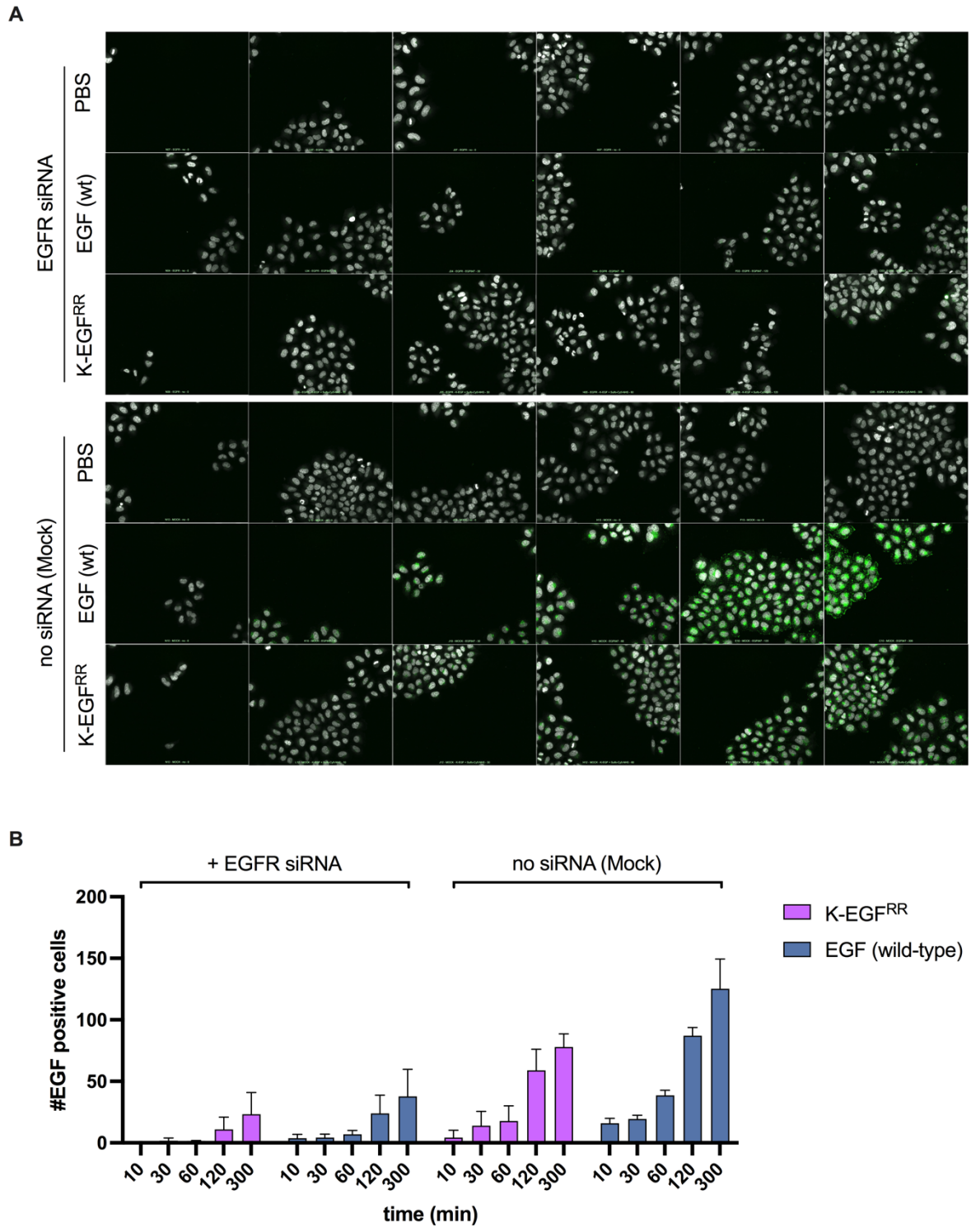

Figure 20: Uptake of EGF.
(A) High-throughput imaging of HeLa Kyoto cells either mock transfected or with siRNA against EGFR. Cells were treated with commercial EGF labelled with Alexa-647 (EGF (wild-type), 9 nM), (sulfo-Cy5-NHS)$_{0.25}$-K-EGF^{RR} (K-EGF^{RR}, 9 nM) or treated with PBS for 0, 10, 30, 60, 120 and 300 min (green). Cells were stained with a mix of DAPI and CellMask (grey). (B) Plot of the mean number of EGF positive cells for EGF (wild-type) and K-EGF^{RR} for different timepoints and on cells treated with EGFR siRNA and no siRNA (Mock). The mean value ± SEM is shown (N = 3, n = 4).

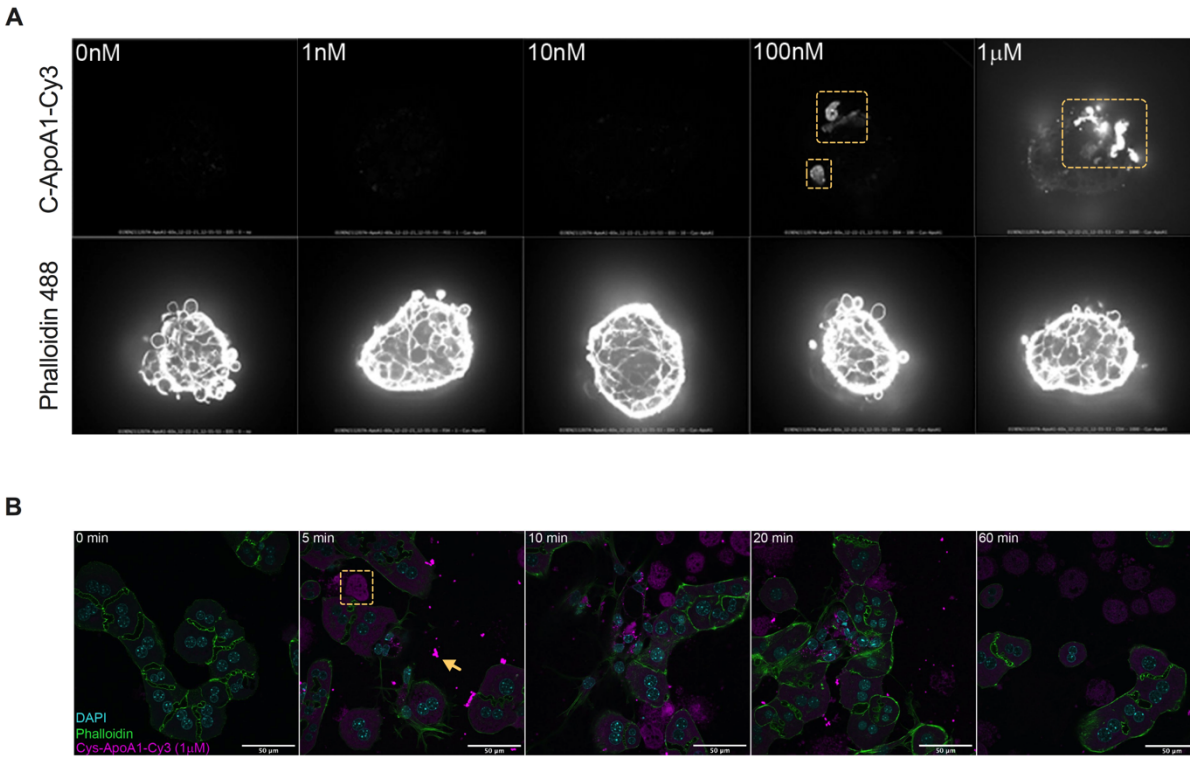

Figure 21: Uptake of ApoA1.
(A) High-magnification images of individual spheroids imaged by automated smart-image microscopy. Uptake of C-ApoA1-Cy3 was performed during 2 h at the indicated concentrations (upper panels). The yellow boxes indicate the fluorescence of C-ApoA1-Cy3. Spheroids were stained with Phalloidin-488 to visualize the cell borders (lower panels). (B) Representative images of adult primary hepatocytes growth in collagen sandwich cultures after a 10 min pulse with C-ApoA1-Cy3 (magenta) and tracked for 0, 5, 10, 20, and 60 min. Cells were fixed and stained with Phalloidin-488 (green) and DAPI (cyan). The yellow box indicates representatively the fluorescence of C-ApoA1-Cy3 in the cytosol and the yellow arrow the fluorescent aggregates.

3.4.2 Ligand-receptor interaction

To further evaluate the binding of the ligand variants to its respective receptor, enzyme-linked immunosorbent assay (ELISA) (Figure 22) and surface plasmon resonance (SPR) studies (Figure 23) were performed. For ELISA, the biotinylated receptors were immobilized to plates with streptavidin-coated wells and treated with PBS, the respective ligand variants, or the wild-type ligands. For K-EGF^{RR}, the absorbance at 450 nm was even higher than for wild-type EGF (Figure 22 A), whereas, for the ApoA1, no absorbance was detected, neither for the C-ApoA1 nor the wild-type ApoA1 (Figure 22 B). These findings suggest that EGF effectively binds to EGFR, while ApoA1 does not demonstrate an interaction the SR-BI receptor.

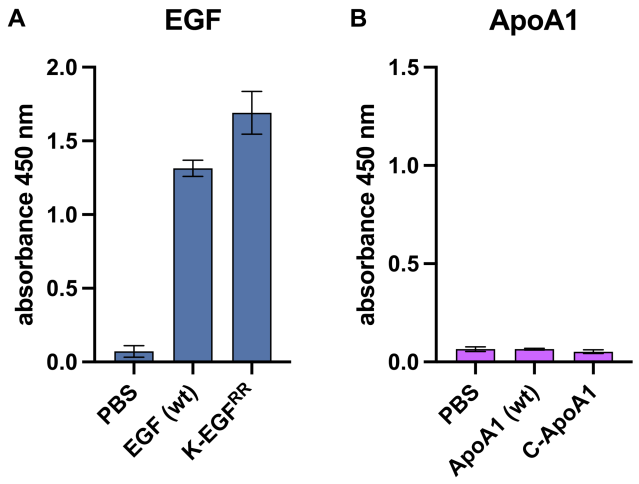

Figure 22: Comparison of ligand-receptor interaction of ligand variants and commercially available ligands determined by ELISA.
Biotinylated (A) EGFR or (B) SR-BI was immobilized on streptavidin coated well plates and treated with K-EGF^{RR}/EGF or C-ApoA1/ApoA1. Absorbance was measured at 450 nm. The mean value ± SEM is shown (N = 3, n = 3).

Another method to evaluate the ligand-receptor interaction is SPR. Here, the biotinylated receptors, EGFR and SR-B1 respectively, were immobilized on streptavidin coated SPR sensor chips. For comparison, not only the self-expressed ligands were used, but also the commercially available wild-type proteins. The curves revealed a moderate to fast association, leading to an equilibrium state, and dissociation for the EGF ligands. The equilibrium dissociation constant K_D was calculated using the steady state affinity fit. For K-EGF^{RR}, the K_D was comparable with the commercially available EGF (5.9×10^{-9} vs. 7.3×10^{-9} M) (Figure 23) pointing to comparable interaction of the variant and the wild-type protein with the receptor. For ApoA1, no binding at SR-BI was observed. In summary, the results of ELISA and SPR are complementary and yielded comparable results, which are also in line with the results observed *in vitro*.

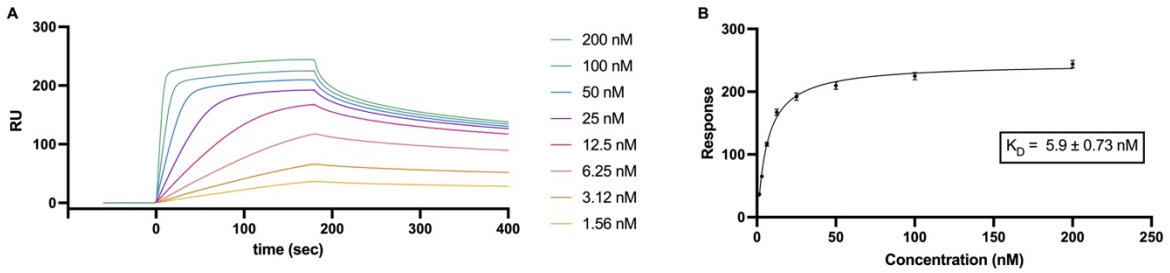

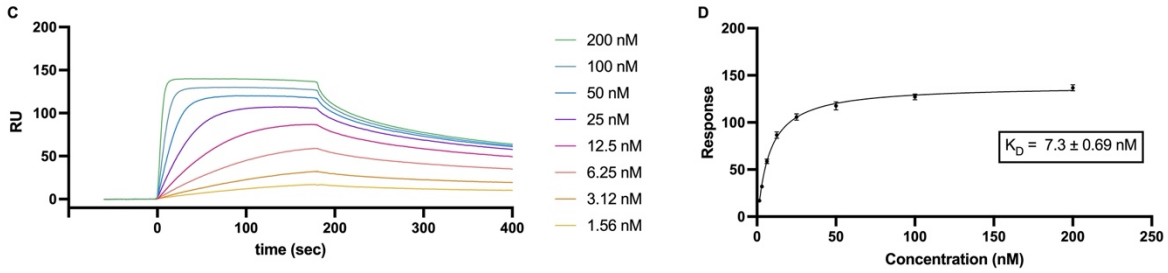

Figure 23: Comparison of ligand-receptor interaction of ligand variants and commercially available ligands determined by SPR.
Biotinylated EGFR or SR-BI was immobilized on streptavidin coated SPR chip and treated with different amounts of (A) K-EGF^{RR} or (C) commercially available wild-type EGF. (B, D) The KD constant was determined by using the steady state affinity fit. The mean value ± SEM is shown (N = 1, n = 2).

3.5 Synthesis and purification of multivalent dendrons

The second part of this thesis was focusing on the synthesis of dendrons with a defined number of functional groups. The synthesis should allow us to control the number of ligands or EEEs attached to each dendron but is also expected to increase homogeneity of the polyplexes. SPPS was used to build the dendrons, as it is a simple, well established, and effective approach without complex purification steps in between reactions. As described in section 1.2, SPPS is divided in four main steps: (1) deprotection, (2) activation and (3) coupling of the new amino acid and (4) cleavage, whereas steps (1) to (3) are repeated until the desired length is achieved. As the attachment of the first amino acid to the resin is a critical step, we chose to use the Fmoc-Lys-Boc Wang resin, where the first lysine is already coupled to the solid support, for the synthesis of dendrons D1–D4. Here, the initial amino acid was orthogonally protected by Fmoc and Boc. As in this thesis the Fmoc strategy was chosen, the amino acids attached to the resin were deprotected by cleavage of Fmoc under basic conditions using piperidine. The Boc-protected amino group is stable under these conditions. Afterwards the amino acid we wanted to attach was activated and coupled by using N,N-diisopropylethylamine (DIPEA) and O-(7-azabenzotriazol-1-yl)-N,N,N′,N′-tetramethyluronium-hexafluorphosphat (HATU). After treatment with the base DIPEA, a carboxylate anion is generated, which attacks HATU and results in the formation of a 1-hydroxy-7-azabenzotriazole (HOAt)-active ester and tetramethyl urea. The activated amino acid can then react with the amine attached to the resin to form an amide bond. The completion of the coupling was monitored by using the Kaiser test, also known as ninhydrin test. The ninhydrin forms in the presence of free amino groups, indicating incomplete coupling, Ruhemann's blue that is a dye visible by eye. When the test revealed a positive result (blue), the activation and coupling step had to be repeated until a negative result (yellow or colourless) was observed. This test can also be used to monitor the successful deprotection of the amines by piperidine.

Since the number of amino groups increases with the number of generations, and the Kaiser test is sensitive and will give a positive result even if only a few amino groups are deprotected, the Kaiser test was not performed after the deprotection step. This was done in order not to reduce the yield by irreversibly removing the resin beads needed for this test. Instead, the incubation time and the amount of piperidine was increased with higher generations. Depending on the specific amino acid (Fmoc-Lys-Fmoc or Fmoc-Lys-N_3 or Fmoc-Cys(StBu)) and the order in which they were used, four different dendrons (D1–D4) were obtained (Figure 24). The bis-Fmoc protected lysines served as branching points, whereas Fmoc-Lys-N_3 or Fmoc-Cys(StBu) were providing the functional groups azide and thiol. Dendron 1 (D1) is built from only lysines, whereas dendron 2 (D2) contains a single additional azide group for conjugation of the ligand equipped with a DBCO-linker. This single conjugation site allows us to form a more homogenous gene delivery vector, as it reduces crosslinking and aggregation. Dendrons 3 (D3) and 4 (D4) have additional thiol groups for conjugation of SO1861-EMCH. Here we choose to go with two and four thiol groups, to have the chance to conjugate different amounts of the EEE. After the desired third generation (G3) was achieved, TFA was used to cleave off the dendron from the resin and simultaneously the Boc protected amine was deprotected. With this procedure, different dendrons containing different numbers of amino groups and conjugation sites (Figure 24) were synthesised.

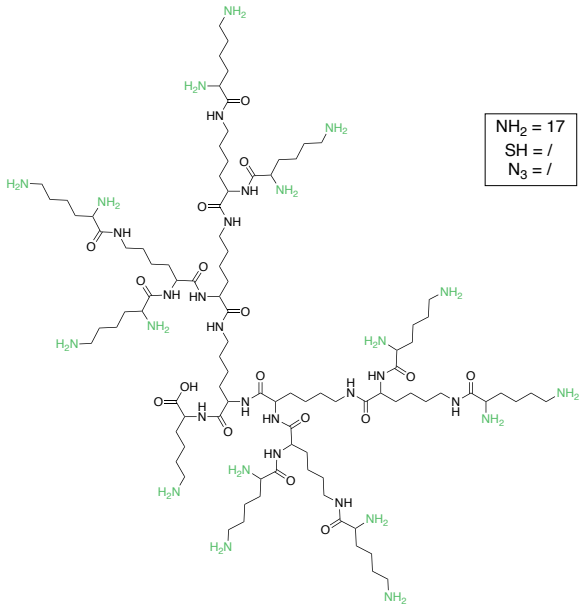

D1 (G3)

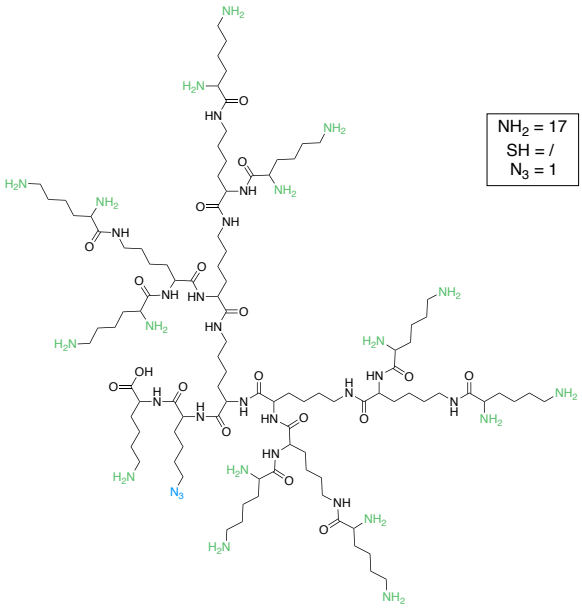

D2 (G3)

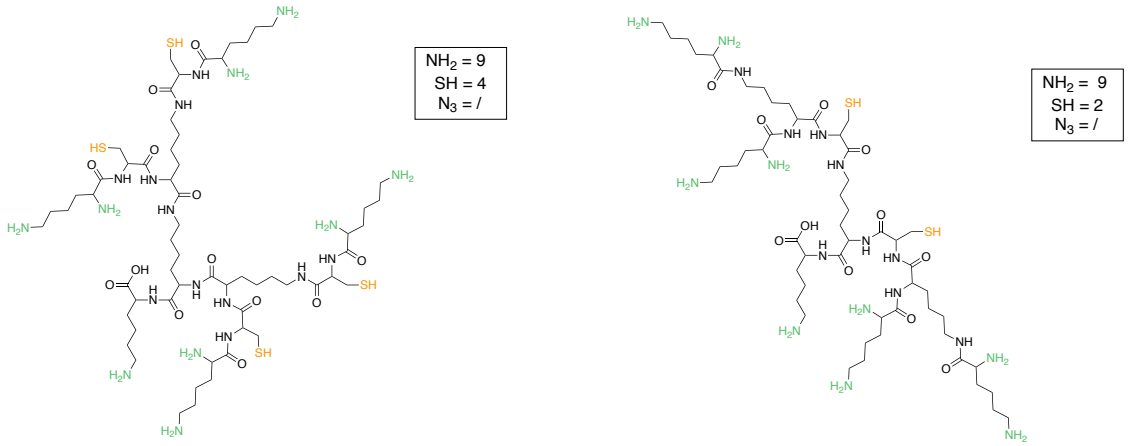

D3 (G3) D4 (G3)

Figure 24: Overview of dendrons synthesized by SPPS.
The dendrons structures are for generation 3 (G3), their respective number of functional groups are described in the boxes. Green indicates the terminal amine groups, blue the terminal azide groups, yellow the terminal thiol groups.

Successful SPPS of the dendrons was confirmed by MALDI-TOF MS. We detected the expected masses for all dendrons in the spectra (Figure S5–Figure S8). Afterwards the dendrons were purified via preparative HPLC using a reverse phase C18 column as stationary phase and water/ACN gradient as mobile phase. Different methods were used, where the gradient times as well as the flow rates differed (Table 12). In method 6 and 7, the ion-pairing reagent TFA (0.1%) was added to the solvent.

Table 12: Methods used for purification of dendritic peptides via preparative HPLC.

Method	Solvents	ACN Gradient	Flow (ml/min)	V (injection)
1	Water, ACN	20-40-60-80*	0.75	50 µL
2	Water, ACN	20-80**	0.75	50 µL
3	Water, ACN	20-80**	1	50 µL
4	Water, ACN	20-80**	2	50 µL
5	Water, ACN	20-80**	3	50 µL
6	Water, ACN + 0.1% TFA	20-80**	0.75	50 µL
7	Water, ACN + 0.1% TFA	20-80**	2	50 µL

* (20–40–60–80): 20–40: 5 min; 40–60: 20 min; 60–80: 5 min; 80–20: 5 min; 20: 5 min
** (20–80): 20–80: 30 min; 80–20: 5 min; 20: 5 min

The fractions were collected manually and afterwards analysed by MALDI-TOF MS. The fractions containing the desired product were analysed by analytical HPLC. Highest purity of the dendrons was reached by method 6 and was therefore used for subsequent experiments. The pure fractions were pooled, lyophilized, and used for the formation of polyplexes described in the next section.

3.6 Creation and evaluation of polyplexes

3.6.1 Polyplex formation

The purified dendrons were mixed with DNA plasmids encoding for enhanced green fluorescence protein (eGFP) or luciferase to form the polyplexes. Here, the positively charged amines of the dendrons are interacting electrostatically with the negatively charged phosphate backbone of the DNA. For the evaluation of the gene loading capacity, we determined the N/P ratios needed to complex the whole amount of DNA. Here, N is referring to the amines of the dendron, whereas P is referring to the phosphates of the DNA. The polyplexes were formed by mixing DNA and dendrons (D1–D4) in HEPES according to 2.7.1 using N/P ratios 0.5, 1, 2, 4, 8 and 16 where the amount of DNA was constant for all ratios and all four dendrons. As described before D1 and D2 contained 17 amines, whereas D3 and D4 only contained 9 amines.

To investigate if the DNA was fully complexed a Pico488 double-stranded DNA quantification kit was used. Here, the fluorophore Pico488 intercalates into free double stranded DNA, which leads to an increase of the fluorescence signal that can be detected by a fluorometer. In order to quantify the amount of free DNA the fluorescence signals were normalized to the control, where only DNA without dendron was used. For all dendrons N/P 16 revealed a reduced fluorescence signal dependent on the dendron to 4–13% of the initial value, whereas for N/P 8 this was only observed for D1, D2 and D4 but not for D3 (Figure 25). An additional method we used to determine the optimal N/P ratio was an agarose gel retardation assay. In an electric field, the free DNA that is negatively charged moves to the anode (+), whereas the polyplexed DNA is stuck in the pockets. The results (Figure S9) are consistent with those of the Pico488 assay.

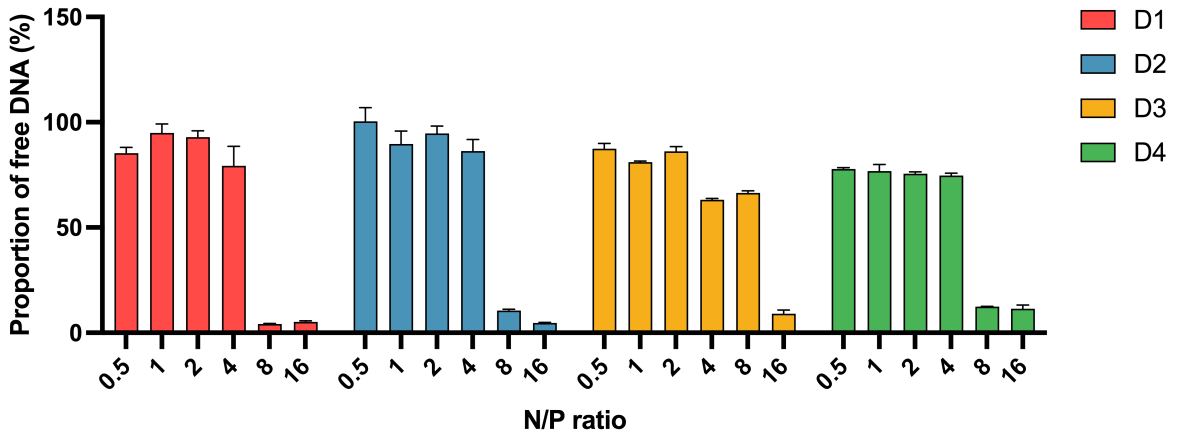

Figure 25: Determination of free DNA for D1–D4 polyplexes.
Plot of the Pico488 assay showing the percentage of free DNA of polyplexes consisting of eGFP plasmid and D1–D4 at different N/P ratios (0.5–16). The mean value ± SEM is shown (N = 1, n = 3).

It is known that the size of the polyplexes plays a crucial role in successful uptake in drug delivery, with an optimal size being not more than 100–200 nm. Therefore, we determined this parameter by using dynamic light scattering (DLS). The particles were measured in HEPES alone and after addition of NaCl (150 mM) to mimic physiological conditions. The polydispersity index (PDI) indicates how heterogenous a sample is based on its size. The PDI differs from 0–1, whereby the smaller the PDI the more homogenous is the distribution of the particle size. If we compare the polyplexes D1–D4 [N/P 8], the PDI was lower for D3/D4 [N/P 8] without the addition of NaCl compared to D1/D2 [N/P 8], whereas when we compare the values for D1–D4 [N/P 16] it was the other way around (Figure 26). For both cases the PDI was increasing when adding NaCl. Considering the size of the polyplexes (Peak 1 (nm)), D1–D4 [N/P 16] reveals smaller particle sizes compared to D1–D4 [N/P 8]. Together with the results from the Pico488 assay, N/P 16 was used for the further experiments.

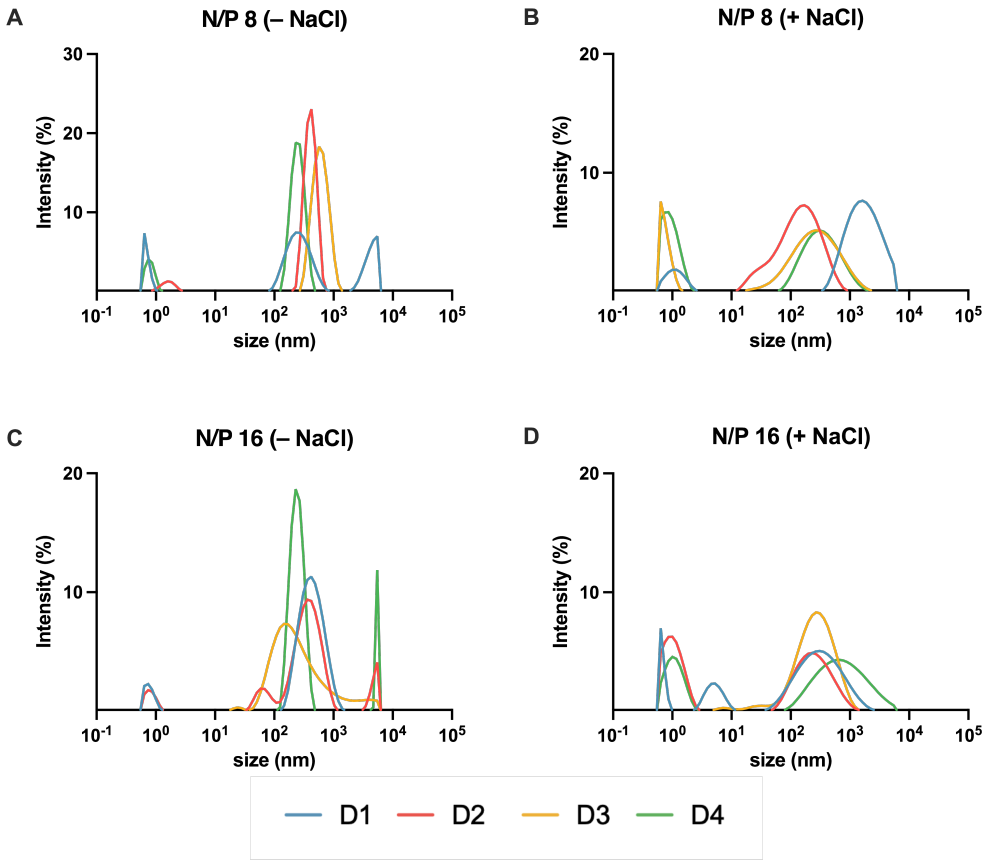

E

	Dendron	D1		D2		D3		D4	
	NaCl	–	+	–	+	–	+	–	+
N/P 8	PDI	0.62	0.83	0.60	0.50	0.26	0.92	0.35	1.00
	Peak 1 mean (nm)	243	1987	452	443	608	686	250	417
	Peak 1 area (%)	54	88	95	83	98	82	83	67
	Peak 2 mean (nm)	4403	1	2615	2053	61	1	1	1
	Peak 2 area (%)	29	12	5	17	2	18	17	33
N/P 16	PDI	0.27	0.72	0.46	0.89	0.37	0.53	0.75	0.75
	Peak 1 mean (nm)	416	369	350	509	276	309	211	1071
	Peak 1 area (%)	95	68	83	65	95	92	83	72
	Peak 2 mean (nm)	1	2	40	1643	2753	9	3543	1
	Peak 2 area (%)	5	22	7	35	5	8	17	28

Figure 26: DLS particle size determination of D1–D4 [N/P 8] and D1–D4 [N/P 16] polyplexes. *Exemplary one representative experiment is shown in (A)–(D). D1–D4 [N/P 8] polyplexes (A) before and (B) after NaCl addition. D1–D4 [N/P 16] polyplexes (C) before and (D) after NaCl addition. (E) Summary of particle sizes and PDI.*

3.6.2 Addition of EGF to polyplexes

After evaluating the optimal N/P ratio for polyplex formation, we added purified K-EGF^{RR} to the polyplex in order to produce a targeted gene delivery platform. According to Li *et al.* [146], it is possible to incorporate EGF also by electrostatic interactions to the polyplex, as EGF is negatively charged at pH 7.4, due to its isoelectric point of 5.87. Therefore, all synthesised dendrons can complex EGF as they all contain positively charged amino groups. Additionally, D2 offers with its azide group the possibility to covalently couple EGF.

It can react via SPAAC with EGF equipped with a DBCO-linker. In this way we have three different methods for D2 to form EGF-polyplexes. The first one is the electrostatically polyplexed version (D2 [N/P 16, EGF (pp)]), which also works for the other dendrons (Figure 27 A). In method two and three the EGF-DBCO is covalently attached to D2. The dendron can either be first polyplexed with the DNA and afterwards treated with EGF-DBCO (D2 [N/P 16, EGF (after)], Figure 27 B) or the ligand can be bound via click chemistry to D2 before being polyplexed with the plasmid (D2 [N/P 16, EGF (before)], Figure 27 C). We treated the dendron or polyplexes with different quantities of EGF (10, 1, 0.1), where the numbers refer to the wt/wt ratio of EGF to DNA. In case of D1–D4 [N/P 16, EGF 0] no EGF was added to the polyplexes, instead DPBS was added since EGF is dissolved in this buffer.

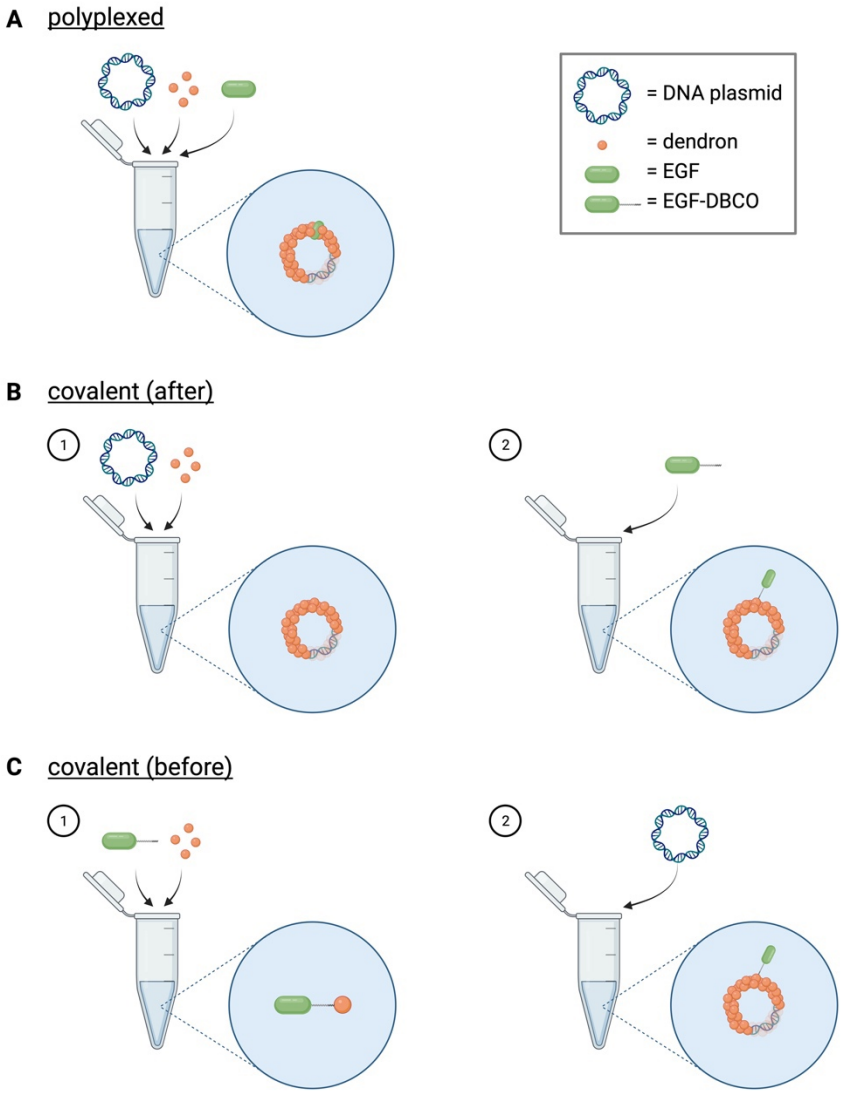

Figure 27: Different methods performed to obtain D2 [EGF] polyplexes.
The EGF can be either (A) polyplexed or covalently bound (B) after or (C) before plasmid was added. Created with BioRender.com.

After creating the different polyplexes, the amount of free DNA was determined with the Pico488 assay, to evaluate if the EGF disturbs the interaction between the genetic material and the dendron. EGF did not have any significant effect on the polyplex formation of the plasmid in case of D1 [N/P 16, EGF 0.1–10 (pp)] and D2 [N/P 16, EGF 0.1–10 (pp)] (Figure 28 A). In contrast, the amount of free DNA increased when the amount of EGF was increased for D3 and D4, especially when comparing D3/4 [N/P 16, EGF 1 (pp)] with D3/4 [N/P 16, EGF 10 (pp)]. This observation was not surprising, as D3 and D4 only have 9 amines in comparison to D1 and D2 bearing 17 amines. For the polyplex formation of D2 polyplexes neither the amount of EGF nor the method had an impact on the DNA condensation (Figure 28 B).

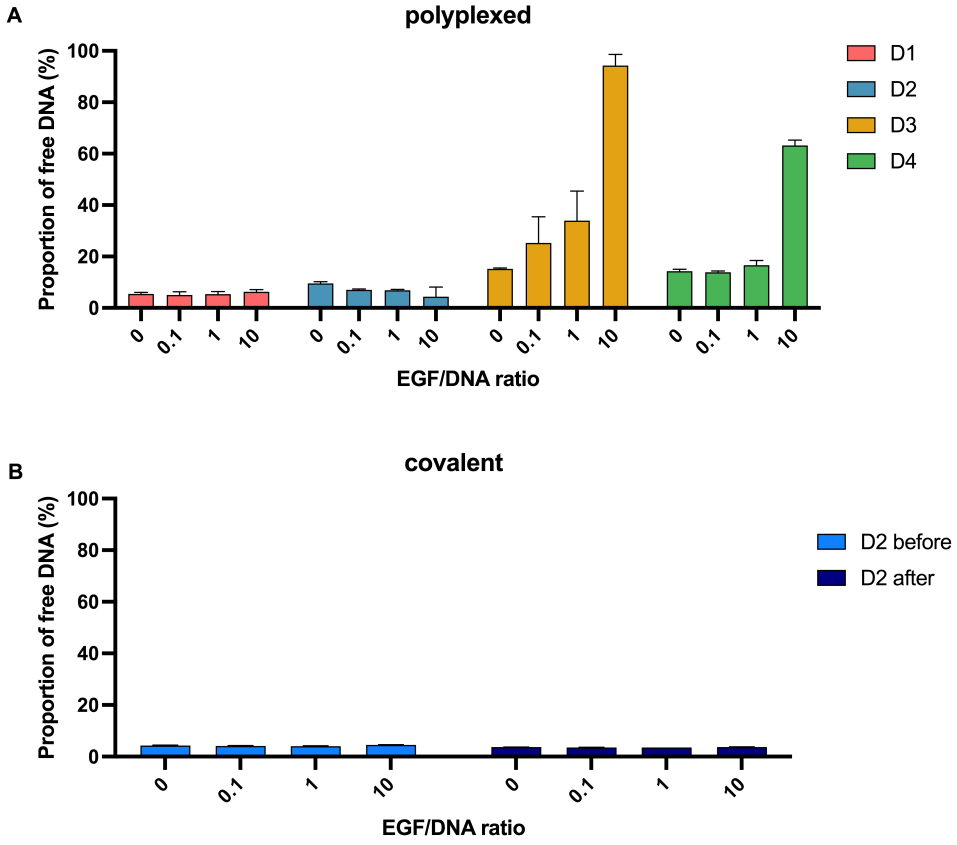

Figure 28: Determination of free DNA for D1–D4 [N/P 16, EGF 0–10] polyplexes.
Plot of the Pico488 assay showing the percentage of free DNA of polyplexes consisting of eGFP plasmid and D1–D4 with different amounts of EGF/DNA wt/wt ratio (0, 0.1, 1, 10). EGF was either (A) polyplexed to D1–D4 or (B) covalently bound to D2. The mean value ± SEM is shown (N1 = 1, n = 3).

The effect of EGF on the particle size was evaluated by DLS measurements. For D2 [N/P 16, EGF 0–10 (pp)] the size decreased when increasing the EGF amount. Especially the size of D2 [N/P 16, EGF 0] could not be determined, as the particles were not in the cut-off of the DLS.

In contrast, D3 [N/P 16, EGF 0–10 (pp)] polyplexes are getting bigger when more EGF was involved and after adding NaCl, whereas for D1/D4 [N/P 16, EGF 0–10 (pp)] no significant trends were observed. It must be noticed, that for D3/D4 [N/P 16, EGF 10 (pp)] the polyplex formation was not complete according to Pico488 assay. Surprisingly, the size of D1–D4 [N/P 16, EGF 0] differed from the polyplexes without EGF (D1–D4 [N/P 16], Figure 26), even though no EGF is involved in the polyplex. The only differences were the concentration of the polyplexes in solution and the buffer. D1–D4 [N/P 16] were dissolved in HEPES only, whereas D1–D4 [N/P 16, EGF 0–10] were dissolved in HEPES and additional DPBS.

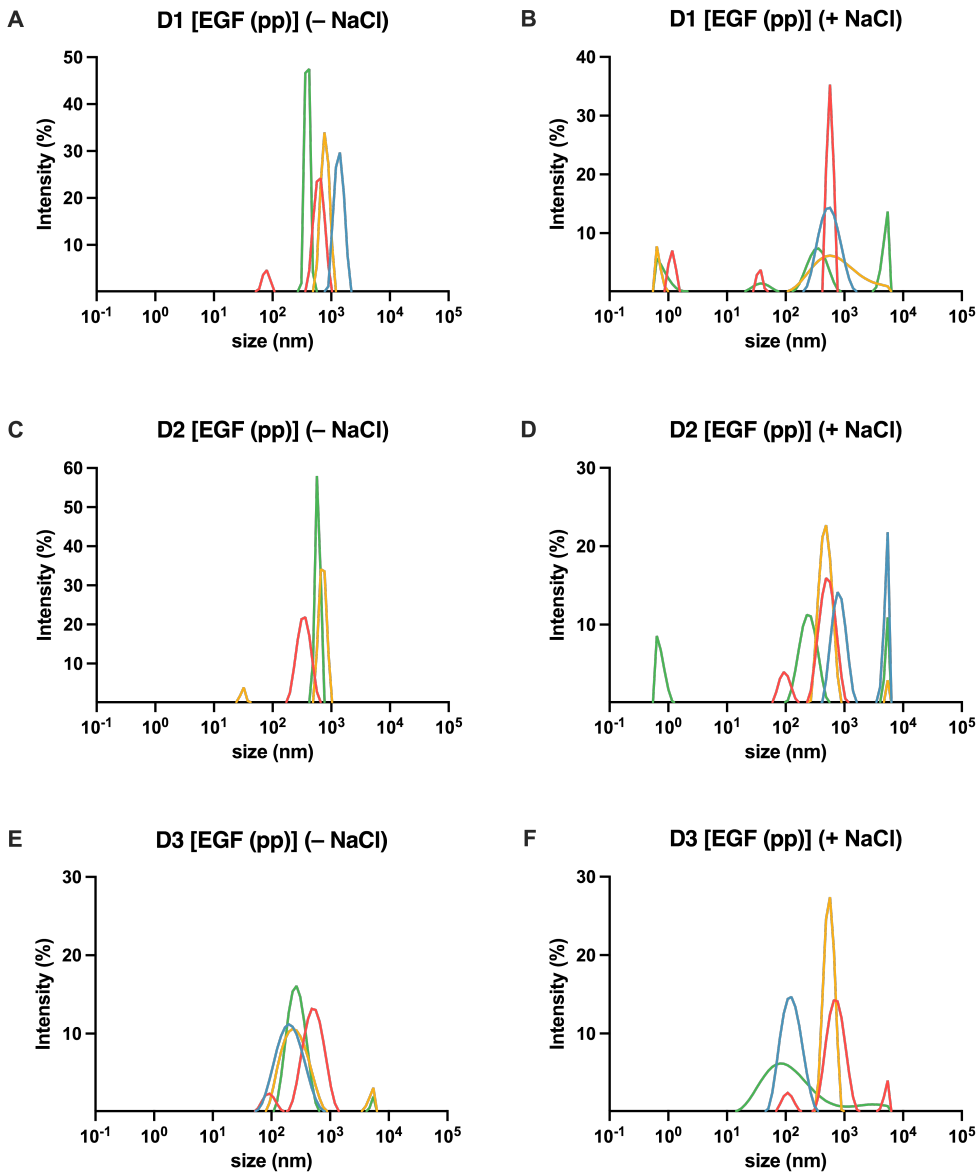

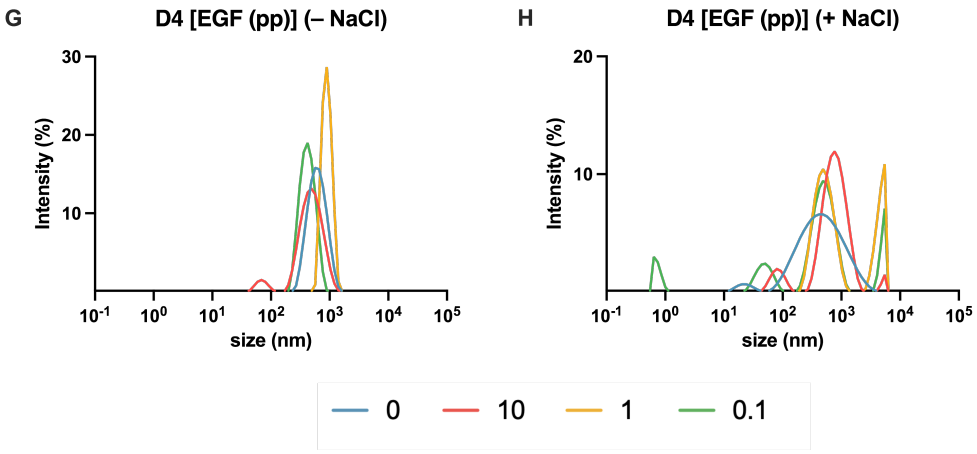

I

	EGF:DNA	0		0.1		1		10	
	NaCl	–	+	–	+	–	+	–	+
D1	PDI	0.21	0.13	0.99	0.56	0.66	0.52	0.63	0.67
	Peak 1 mean (nm)	1412	581	393	366	788	805	616	621
	Peak 1 area (%)	100	98	100	79	100	84	75	83
	Peak 2 mean (nm)		1		3273		2	100	583
	Peak 2 area (%)		2		21		16	25	17
D2	PDI	n. d.	0.79	0.94	0.62	0.68	0.57	0.40	0.42
	Peak 1 mean (nm)	n. d.	1550	690	286	745	591	383	501
	Peak 1 area (%)	n. d.	40	100	66	90	97	97	93
	Peak 2 mean (nm)	n. d.	5134		1629	46	2734	2759	82
	Peak 2 area (%)	n. d.	60		34	10	3	3	7
D3	PDI	0.31	0.16	0.33	0.68	0.39	0.48	0.41	0.51
	Peak 1 mean (nm)	270	130	308	630	288	589	603	739
	Peak 1 area (%)	99	99	95	87	94	99	89	91
	Peak 2 mean (nm)	4651	4939	5131	1414	4847	5294	105	107
	Peak 2 area (%)	1	1	5	13	6	1	11	9
D4	PDI	0.22	0.67	0.42	0.48	0.13	0.48	0.32	0.48
	Peak 1 mean (nm)	616	617	427	440	920	785	514	806
	Peak 1 area (%)	100	94	97	66	100	72	94	92
	Peak 2 mean (nm)		9	1	63		4503	79	78
	Peak 2 area (%)		6	3	16		28	6	8

Figure 29: DLS particle size determination of D1–D4 [N/P 16, EGF 0–10 (pp)].
One representative experiment is shown exemplarily in (A)–(H). D1–4 [N/P 16, EGF 0–10 (pp)] polyplexes (A, C, E, G) before) and (B, D, F, H) after NaCl addition. (I) Summary of particle sizes and PDI. n.d = the size was out of range and could not be determined in DLS.

Considering the polyplexes where EGF was covalently attached, it is observed that they were smaller than D2 [N/P 16, EGF 0–10 (pp)] where the EGF was only incorporated into the polyplex by electrostatic interactions. Furthermore, opposite trends are observed: the size for D2 [N/P 16, EGF 0–10 (before)] was increasing when more EGF-DBCO is involved, whereas for D2 [N/P 16, EGF 0–10 (after)] the size decreases. When increasing the NaCl concentration the size was increasing, leading to the lack of detection for D2 [N/P 16, EGF 0.1 (after)] as it exceeded the cut-off of the device. We demonstrated that EGF only affects the DNA loading capacity for D3 and D4 containing less amino groups than D1 and D2. Additionally, it also effected the size, whereby no significant correlation between the number of amino groups and the size, nor the EGF amount was observed.

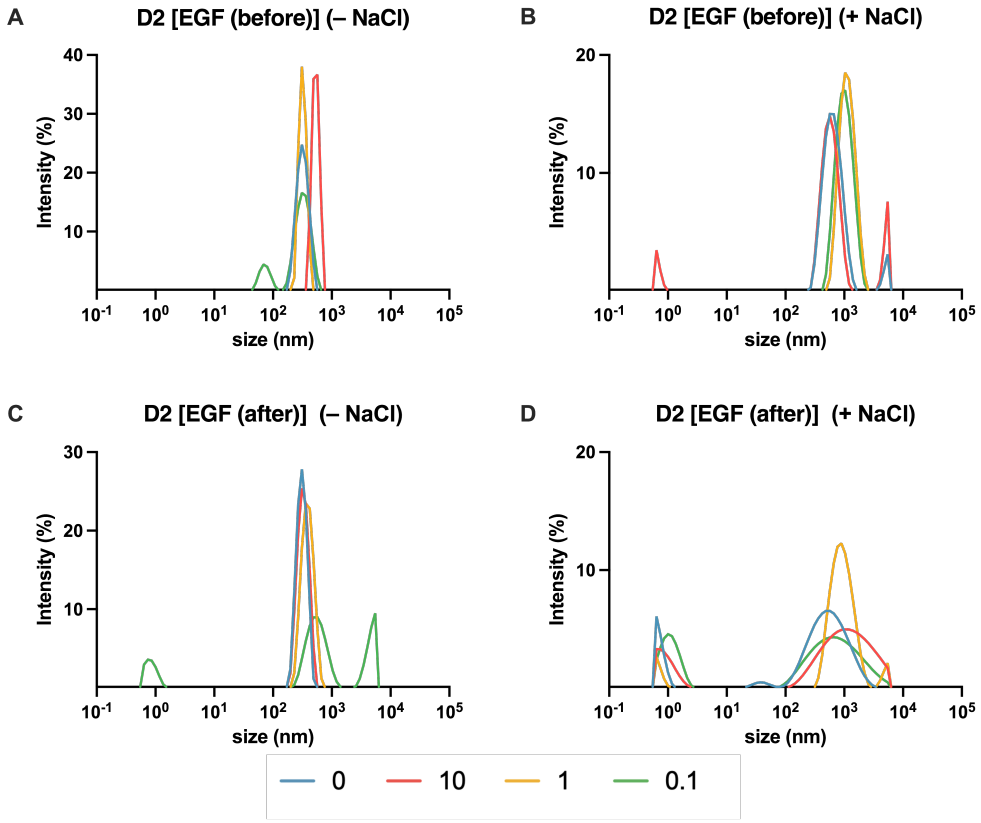

E

	EGF:DNA	0		0.1		1		10	
	NaCl	–	+	–	+	–	+	–	+
D2 (before)	PDI	0.39	0.36	0.50	0.33	0.53	0.30	0.57	0.50
	Peak 1 mean (nm)	354	620	376	1040	395	830	495	760
	Peak 1 area (%)	100	96	82	100	100	96	95	79
	Peak 2 mean (nm)		5196	83			4975	1	3407
	Peak 2 area (%)		4	18			4	5	21
D2 (after)	PDI	0.51	0.52	0.32	n. d.	0.36	0.45	0.48	0.90
	Peak 1 mean (nm)	346	897	621	n. d.	395	850	345	949
	Peak 1 area (%)	98	85	80	n. d.	100	90	95	62
	Peak 2 mean (nm)	1	3141	4807	n. d.	5468	1	72	1064
	Peak 2 area (%)	2	15	20	n. d.	1	10	5	38

Figure 30: DLS particle size determination of D2 [N/P 16, EGF0–10 (before)] and D2 [N/P 16, EGF 0–10 (after)] polyplexes.
One representative experiment is shown exemplarily in (A)–(D). D2 [EGF 0–10 (before)] polyplexes (A) before and (B) after NaCl addition. D2 [EGF 0–10 (after)] polyplexes (C) before and (D) after NaCl addition. (E) Summary of particle sizes and PDI. n.d = the size was out of range and could not be determined in DLS.

3.6.3 D1+D5 polyplexes

Further studies were performed to also investigate polyplexes containing not only one kind of dendrons but two. This approach was investigated in the Master thesis of Elisabeth Marzec [147], supervised by myself, using D1 and the commercially available polylysine dendron D5 (Figure S10). This dendron comprises eight amino groups and one thiol group.

Before starting to combine both dendrons in a polyplex, the DNA loading capacity of D1 and D5 was determined by agarose gel retardation assay. As seen in Figure S11, DNA was completely complexed for D1 [N/P 8] and D1 [N/P 16]. In contrast, only for D5 [N/P 16] no free DNA was detected. This correlates with the results from the Pico488 assay seen for D3 [N/P 16] (Figure 25), where also only eight amino groups are present. Based on these results, D5 [N/P 16] was either complexed with D1 [N/P 8] or D1 [N/P 16] in the following experiments. In addition, we also varied the ratio of dendrons (D1/D5) within these polyplexes. D1 and D5 were applied in the ratios of 4:1, 2:1, 1:1, 1:2, 1:4 with the eGFP plasmid. All ratios were able to complex the DNA (Figure S12) but led to the formation of different particle sizes. We observed that the size of polyplexes increased with decreasing amounts of amines. Therefore, the smallest size was detected for the polyplex D1+D5 [N/P 16+16, 4:1], where the amount of amine groups was the highest (17 (D1) vs. 8 (D5)). This correlates with the results seen for D1–D4 [N/P 16] (Figure 26). For this reason, N/P 16 and D1/D5 4:1 have been chosen as preferred conditions for the follow-up experiments.

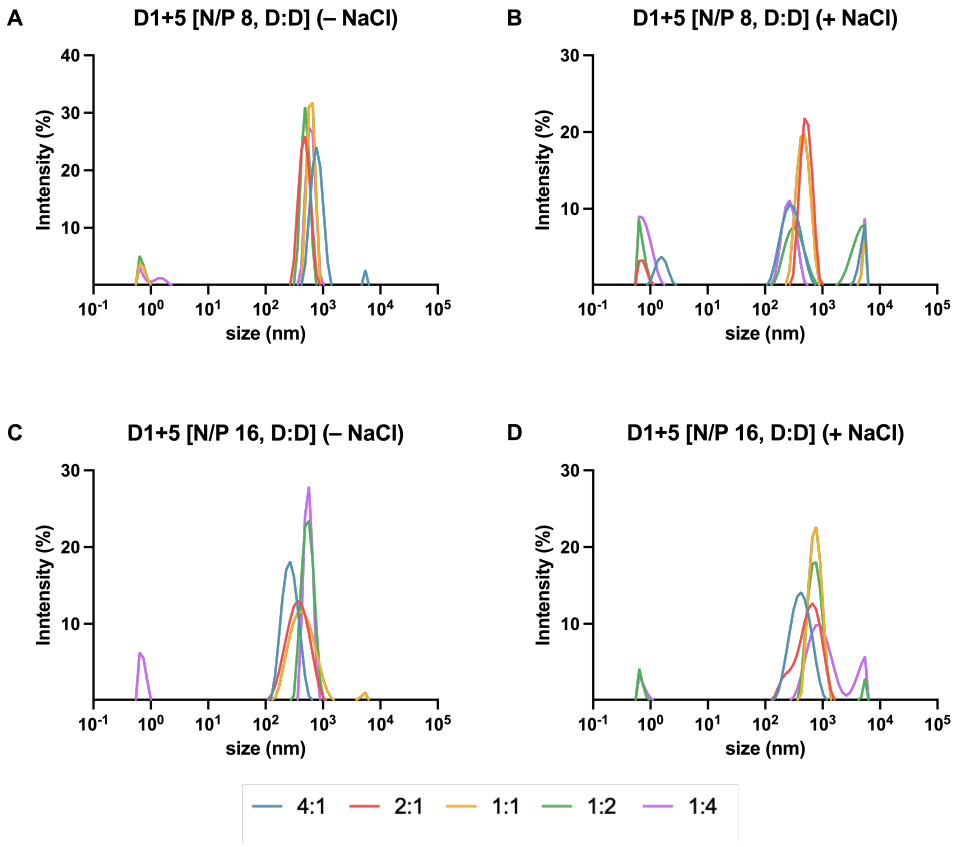

E

	D:D ratio	4:1		2:1		1:1		1:2		1:4	
	NaCl	–	+	–	+	–	+	–	+	–	+
N/P 8	PDI	0.46	0.39	0.45	0.52	0.58	0.57	0.85	0.75	0.65	0.72
	Peak 1 mean (nm)	707	538	449	895	611	577	435	272	621	384
	Peak 1 area (%)	91	82	100	89	86	84	88	47	80	72
	Peak 2 mean (nm)	5180	4829		2328	1	3433	1	4504	1	16
	Peak 2 area (%)	9	8		11	14	16	12	33	20	23
N/P 16	PDI	0.10	0.23	0.17	0.27	0.20	0.08	0.39	0.48	0.81	0.42
	Peak 1 mean (nm)	278	473	381	642	481	770	561	644	403	942
	Peak 1 area (%)	100	100	100	100	99	100	100	84	78	78
	Peak 2 mean (nm)					5145			1757	1	3206
	Peak 2 area (%)					1			16	22	12

Figure 31: DLS particle size determination of D1+D5 [N/P 8+16, D1/D5 4:1–1:4] and D1+5 [N/P 16+16, D1/D5 4:1–1:4].
One representative experiment is shown exemplarily in (A)–(D). D1+D5 [N/P 8+16, D1/D5 4:1–1:4] and D1+5 [N/P 16+16, D1/D5 4:1–1:4] polyplexes (A, C) before and (B, D) after NaCl addition. (E) Summary of particle sizes and PDI.

In the next experiments, we wanted to investigate if the polyplex procedure as well as the order of the different components have an impact on the loading capacity and the size. Four different methods of producing these polyplexes were performed (Figure 32). The first method (M1) is to polyplex both dendrons simultaneously with the DNA plasmid. In the second method (M2) D1 was first polyplexed with the DNA and after 1 h D5 was added, whereas the order of the dendrons was switched in method 3 (M3). The last method (M4) was to form both polyplexes individually and then mix them. For all methods the combination of the solutions in the first polyplex formation step was either done by pipetting up and down (mixed) or by vortexing the solution (vortexed).

The amount of free DNA was determined by agarose gel retardation assay and disclosed no difference between the methods, in all cases no free DNA was detected (Figure S13). In addition, we determined the particle sizes where no significant differences depending on the mixing procedure was observed (Figure 33). Therefore, M1 (vortexed) was used for further experiments.

Additionally, the D1+D5 [N/P 16+16, D1/D5 4:1, M1 (vortexed)] were also treated with EGF to form the targeted polyplexes. Here, the EGF was polyplexed like D1–D4 [N/P 16, EGF 0–10 (pp)] through electrostatic interactions as neither D1 nor D5 contains an azide group to conjugate EGF via DBCO-click adapter. The agarose retardation assay indicated that the EGF was also not affecting the complexation of the DNA plasmid (Figure S14). The same trend as for D2 [N/P 16, EGF 0–10 (pp)] was observed: the size decreased with an increasing amount of EGF, but in comparison to the mono polyplexes the measured particle sizes were bigger (Figure 34).

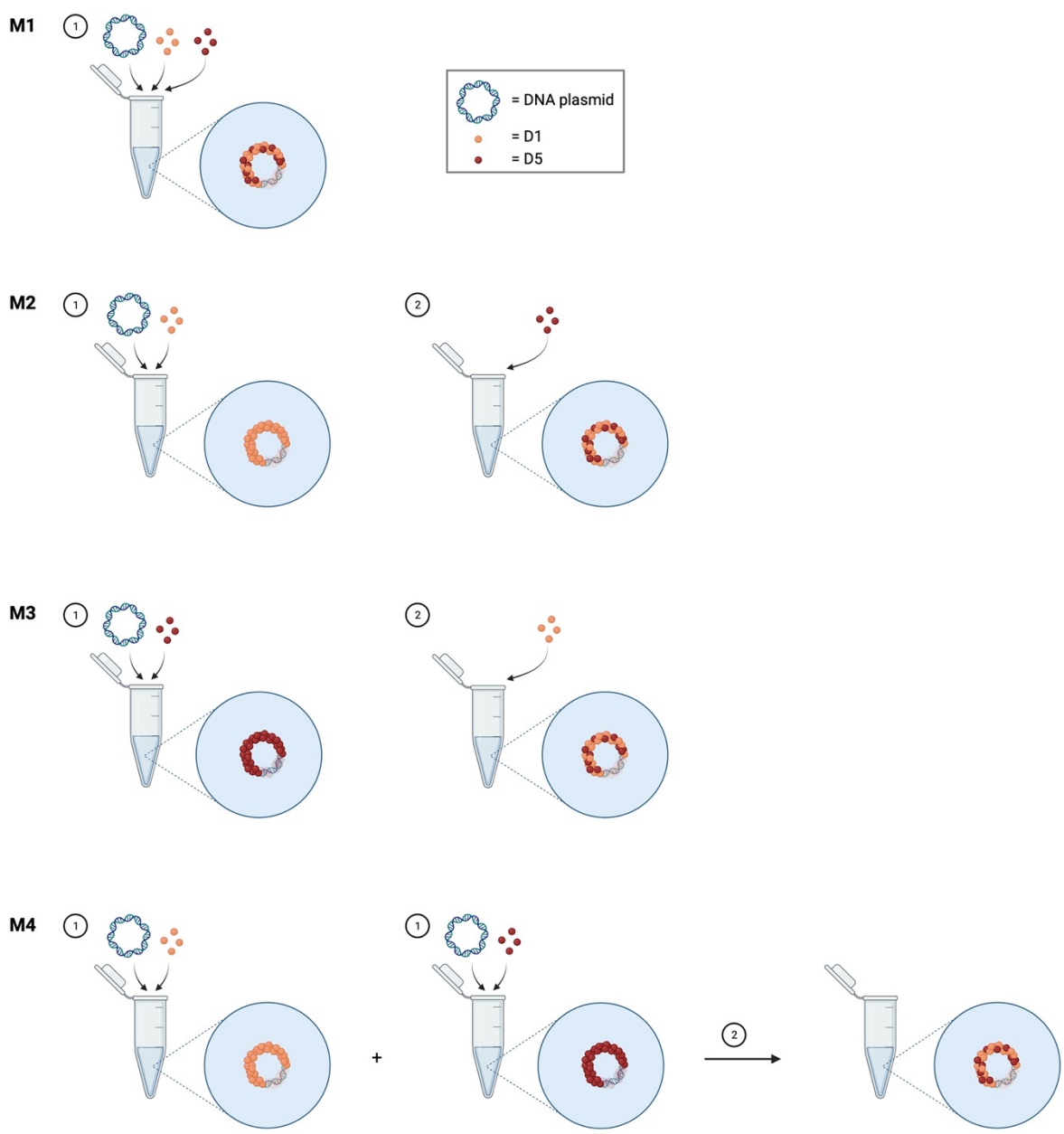

Figure 32: Different methods used to complex D1 and D5 with eGFP plasmid.
In method 1 (M1) D1 and D5 are polyplexed simultaneously with eGFP plasmid. In method 2 (M2) D1 is first polyplexed with plasmid and afterwards D5 is added, method 3 (M3) is the other way around. In method 4 (M4) D1 and D5 are complexed with DNA separately and then combined. Created with BioRender.com.

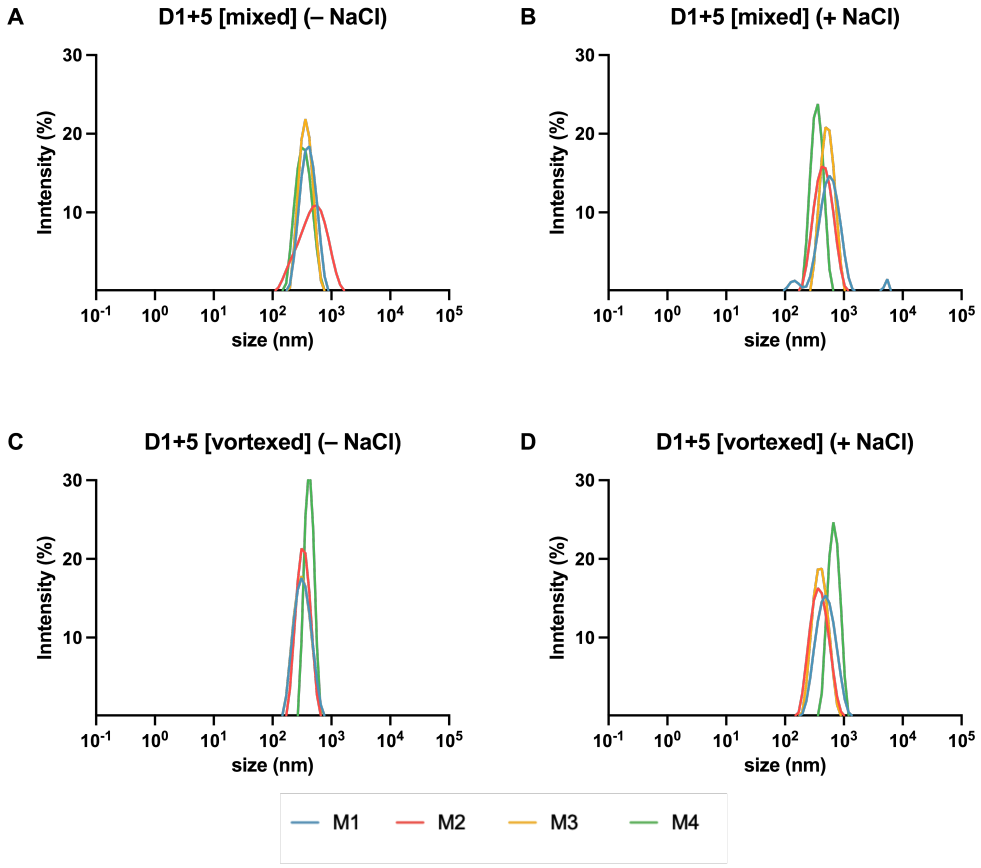

E

	EGF:DNA	M1		M2		M3		M4	
	NaCl	–	+	–	+	–	+	–	+
mixed	PDI	0.31	0.24	0.29	0.22	0.40	0.12	0.17	0.30
	Peak 1 mean (nm)	397	595	462	472	350	577	346	394
	Peak 1 area (%)	100	97	100	100	100	100	100	100
	Peak 2 mean (nm)		156						
	Peak 2 area (%)		3						
vortexed	PDI	0.15	0.19	0.40	0.19	0.17	0.18	0.50	0.27
	Peak 1 mean (nm)	335	527	328	404	367	427	419	664
	Peak 1 area (%)	100	100	100	100	100	100	100	100
	Peak 2 mean (nm)								
	Peak 2 area (%)								

Figure 33: DLS particle size determination of D1+D5 [N/P 16+16, D1/D5 4:1, M1–4 (mixed)] and D1+D5 [N/P 16+16, D1/D5 4:1, M1–4 (vortexed)].
One representative experiment is shown exemplarily in (A)–(D). D1+5 [N/P 16+16, D1/D5 4:1, M1–4] polyplexes (A, C) before and (B, D) after NaCl addition. (E) Summary of particle sizes and PDI.

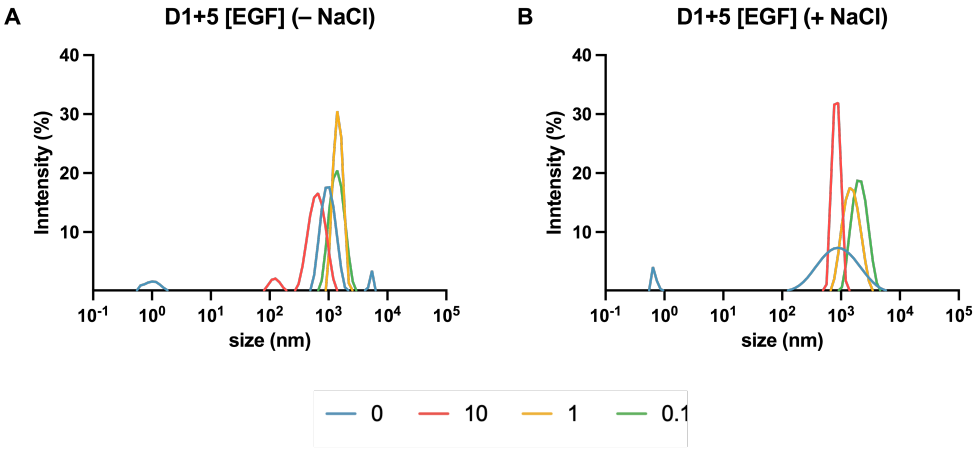

C

	EGF:DNA	0		0.1		1		10	
	NaCl	–	+	–	+	–	+	–	+
D1 + D5	PDI	0.36	0.50	0.50	0.67	0.30	0.66	0.38	0.38
	Peak 1 mean (nm)	1023	1081	981	1020	888	923	565	968
	Peak 1 area (%)	94	83	98	72	100	91	97	98
	Peak 2 mean (nm)	635	1	1	479		628	1738	5468
	Peak 2 area (%)	6	17	2	28		9	3	2

Figure 34: DLS particle size determination of D1+D5 [N/P 16+16, D1/D5 4:1, M1 (vortexed), EGF 0–10 (pp)].
One representative experiment is shown exemplarily in (A) and (B). D1+D5 [N/P 16+16, D1/D5 4:1, M1, vortexed, EGF 0–10 (pp)]. Polyplexes (A) before and (B) after NaCl addition. (C) Summary of particle sizes and PDI.

3.6.4 *In vitro* evaluation

3.6.4.1 Cell growth determination

After the polyplex formation was successful, the polyplexes D1–D4 [N/P 16, EGF 0–10] were selected for further *in vitro* evaluation regarding targeted gene delivery to the EGFR. The following cell lines were chosen based on their normalized transcripts per million (nTPM) of the EGFR. As target cell lines we chose A431 (5282.1 nTPM), MDA-MB 468 (613.3 nTPM) and PC-9 (180.3 nTPM), as they have higher expression levels of EGFR. HEK293-FT (3.6 nTPM) served as off-target cell line. Before starting with the actual evaluation, we had to determine the optimal cell number for the following assays. For this reason, different amounts of cells (2000–30,000) were seeded and incubated in DMEM or RPMI (PC-9) medium for 96 h. The live cell imaging as well as the analysis was performed using an Incucyte device. The cell growth was determined based on the confluency in each well. It is important to ensure that the cells will be still in the growth phase and will not reach a growth plateau before the end of the experiments (96 h). Based on the cell growth curves (Figure 35) a cell count of 4000 for HEK293-FT, 6000 for A431, 8000 for PC-9 and 10,000 for MDA-MB 468 were considered as optimal for further experiments where an incubation time of 96 h was used.

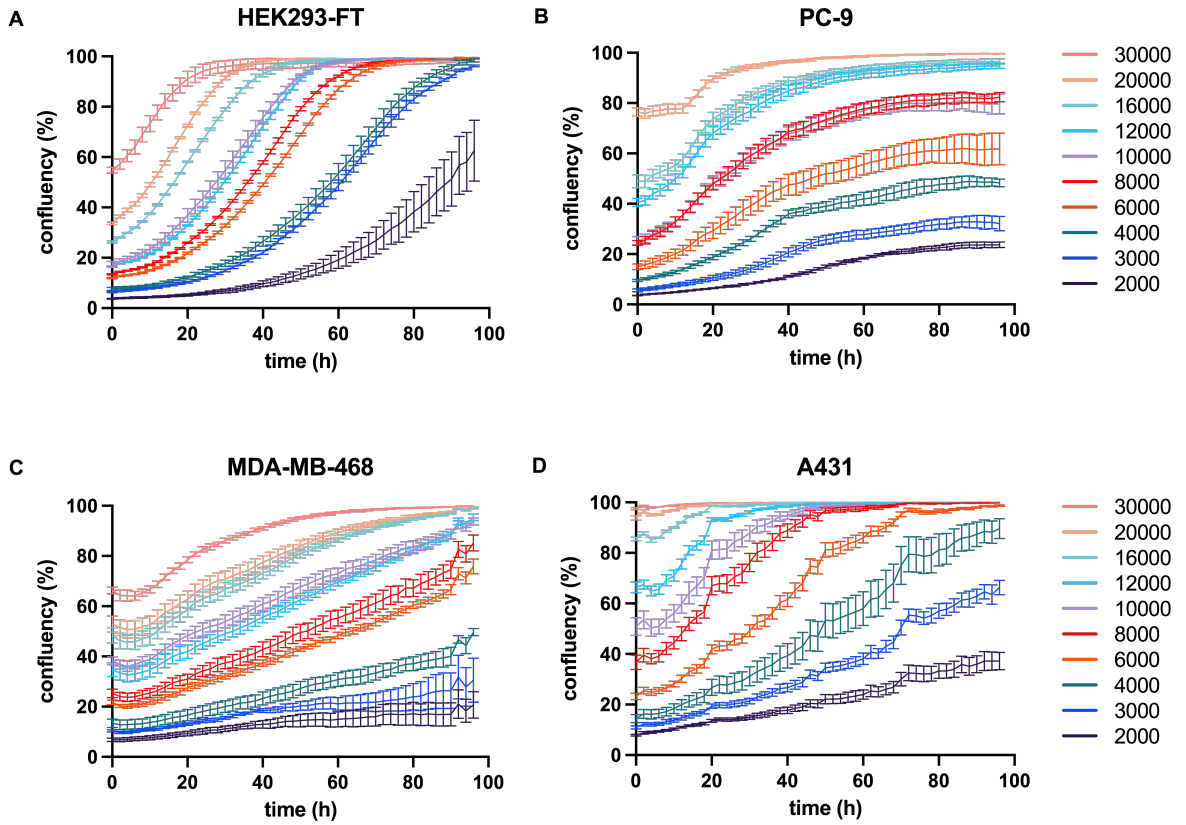

Figure 35: Cell number optimisation for *in vitro* assays.
Different cell numbers (2000–30,000) of (A) HEK293-FT, (B) PC-9, (C) MDA-MB 468 and (D) A431 in 80 µL cell medium. Each were seeded into a 96-well-plate and proliferation was detected microscopically (10 × magnification) for 96 h using an Incucyte device. The mean value ± SEM is shown (N = 1, n = 3).

3.6.4.2 Evaluation of transfection efficiency and cytotoxicity

To evaluate the transfection efficiency of the dendron polyplexes, the polyplexes were prepared according to 2.7.1 using a plasmid encoding for the enhanced green fluorescence protein (eGFP). This allows the detection of green fluorescence when the transfection was successful. For this purpose, D1 was polyplexed with eGFP plasmid and different amounts of EGF, and added to A431, MDA-MB 468, and HEK293-FT cells. Additionally, the cells were treated with different amounts (4 or 0.4 µM) of SO1861-EMCH or the before prepared SO1861-EGF. The confluency as well as the fluorescence were monitored via live cell imaging using an Incucyte device. At the end point (96 h) the cells were treated with MTS to detect the metabolic activity of the cells. Viable cells reduce the MTS tetrazolium compound to the coloured formazan dye, which is soluble in the medium. The cell viability was measured by the formazan signal at 490 nm and normalized to the wells treated only with DMEM (Figure 36 D). Applying the Incucyte software, the green area confluency (Figure 36 A), the fluorescence intensity (Figure 36 B) and the confluency (Figure 36 C) were determined.

We observed that the green area confluency as well as the fluorescence intensity are increasing with an increasing amount of EGF (D1 [N/P 16, EGF 10 (pp)], D1 [N/P 16, EGF 1 (pp)]). Furthermore, the fluorescence seems to be higher when adding SO1861-EGF. This effect is only seen in the EGFR positive cell lines (A431, MDA-MB 468) but not in the negative control cell line (HEK293-FT). In the off-target cell line only the cells treated with the transfection reagent lipofectamine and eGFP plasmid revealed a fluorescence signal. Interestingly, the confluency decreased significantly for the ones with higher fluorescence in the EGFR positive cell lines, but this trend was not observed that strong in the MTS assay. The experiment was repeated with D2 [N/P 16, EGF 0–10 (pp)], D2 [N/P 16, EGF 0–10 (after)] and D2 [N/P 16, EGF 0–10 (before)] as well as for D1+D5 [N/P 16+16, EGF 0–10 (pp)]. The results shown in Figure S15–Figure S18 disclosed the same trends as described before, except that the results from the MTS assay and the confluency determination are also consistent.

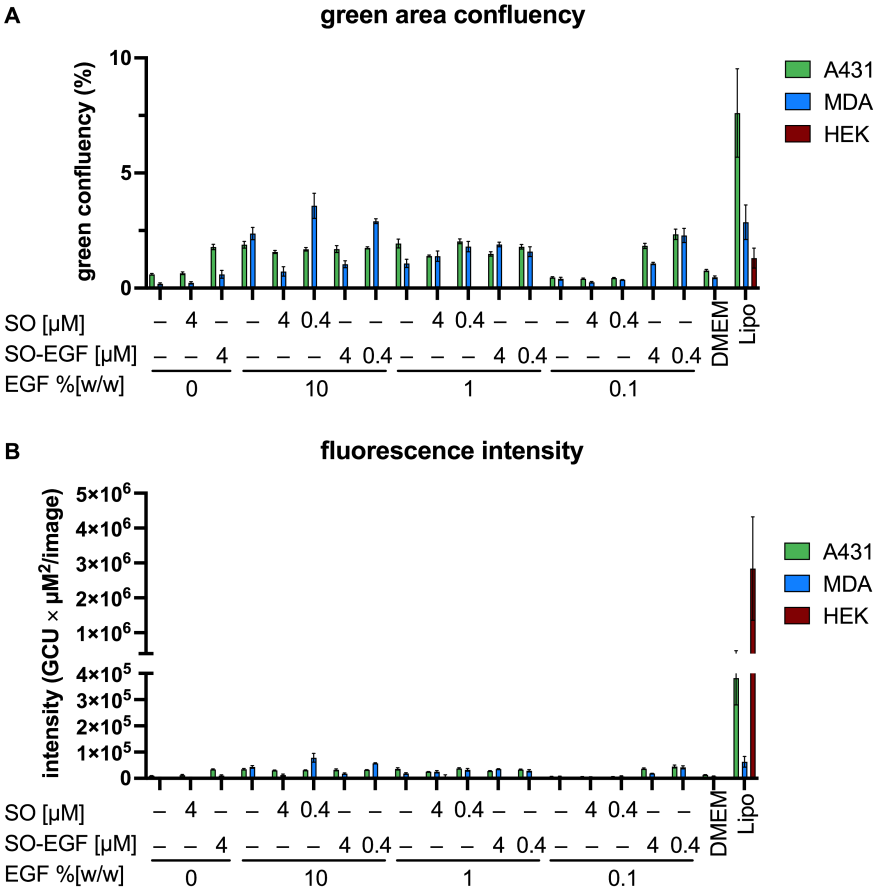

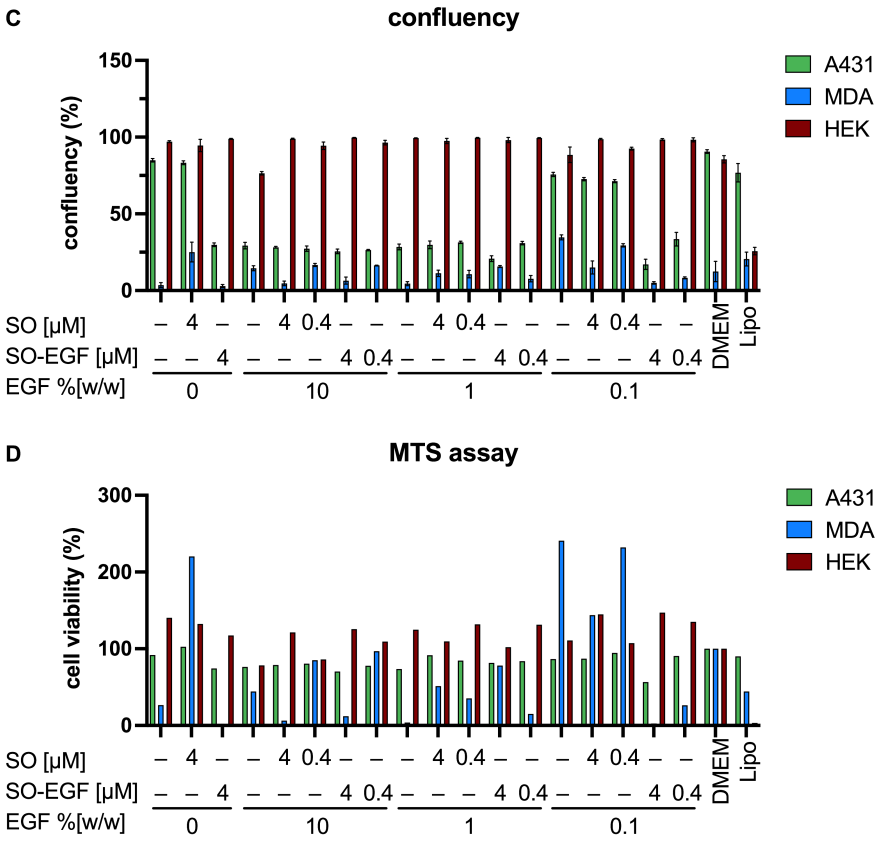

Figure 36: Transfection efficiency of eGFP plasmid and cytotoxicity of D1 [N/P 16, EGF 0–10 (pp)] with and without additional SO1861 or SO1861-EGF.
The assay was performed on EGFR positive cell lines A431 (green) and MDA-MB 468 (blue) as well as on EGFR negative cell line HEK293-FT (red). Analysis of (A) green area confluency, (B) fluorescence intensity and (C) confluency were performed by Incucyte measurements. (D) The absorbance of MTS proliferation assay was determined by SpectraMax 340. The mean value ± SEM is shown (N = 1, n = 3).

Because we observed the opposite trend of fluorescence signal and cell viability, we evaluated the cytotoxic effect of the EGF itself on the cells. For this purpose, the cells were treated with different amounts of EGF and SO1861-EGF and incubated for 96 h. In the EGFR positive cell lines A431 and MDA-MB 468 IC_{50} values of 4.91 nM and 5.82 nM were measured for EGF and 3.42 nM and 7.17 nM for SO1861-EGF (Figure 37). If we compare these IC_{50} values with the concentrations of EGF in previous experiments like 625 nM (D1/D2 [N/P 16, EGF 10]), 62.5 nM (D1/D2 [N/P 16, EGF 1]) or 6.25 nM (D1/D2 [EGF 0.1]) and 0.4 or 4 µM of SO1861-EGF, it could explain the low confluency and cell viability. For HEK293-FT and PC-9 cells no toxic effect was determined.

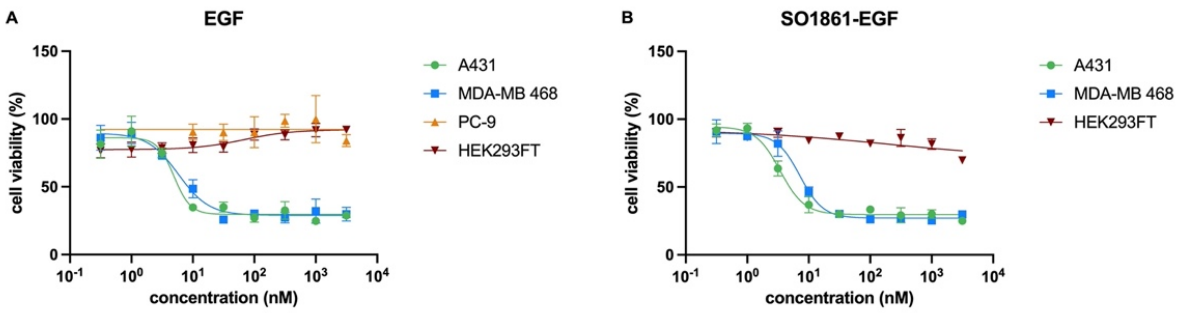

C

	IC50			
	A431	MDA-MB 468	PC-9	HEK293FT
EGF	4.91 nM	5.82 nM	/	/
SO1861-EGF	3.42 nM	7.17 nM	n.d.	/

Figure 37: Cytotoxicity of EGF and SO1861-EGF.
EGFR positive cells A431, MDA-MB 468 and PC-9 as well as EGFR negative cell line HEK293-FT were treated with different amounts of (A) EGF and (B) SO1861-EGF. The cytotoxicity was determined by MTS assay using a SpectraMax 340 device. (C) IC_{50} value was determined using Prism 9 software. The mean value ± SEM is shown (N = 1, n = 3).

3.6.4.3 Luciferase reporter assay

To exclude that the green fluorescence is not only occurring because of the autofluorescence but also to a certain extend due to successful transfection, a luciferase assay was performed. In these experiments D2 was polyplexed with a plasmid encoding for luciferase instead of eGFP and the EGF was either polyplexed or covalently bound with an amount of 10 and 0.1. The cells were also additionally treated with SO1861 and SO1861-EGF, incubated, and imaged every 2 h for 96 h in the Incucyte. Afterwards the cells were treated with the firefly luciferase substrate 5´-fluoroluciferin and the luminescence was measured. The data confirmed the trend that higher amount of EGF lead to an increase of both green area confluency and fluorescence intensity while it decreased the confluency of the cells. This observation was the same as seen for the experiments where eGFP plasmid was used (Figure 38). This indicates that the fluorescence detected before was not resulting from the transfection of eGFP plasmid but from the autofluorescence of the dead cells. This hypothesis is supported by the fact that there is no luciferase activity detectable for the cells treated with the polyplexes. Only the lipofectamine control showed a 50-fold increase of the luminescence signal compared to the negative control where the cells were only incubated in DMEM.

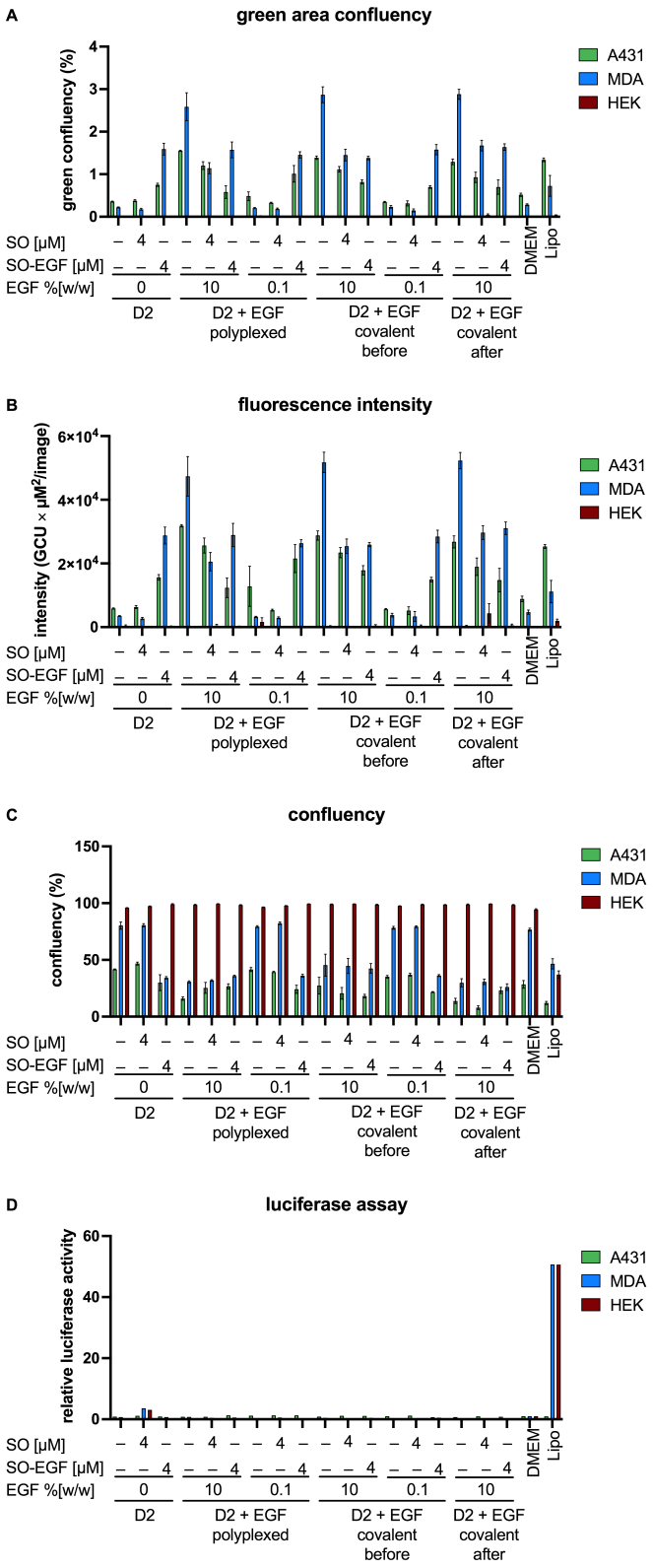

Figure 38: Transfection efficiency of luciferase and cytotoxicity of D2 [N/P 16, EGF 0–10 (pp or before or after)] with and without additional SO1861 or SO1861-EGF.
The assay was performed on EGFR positive cell lines A431 (green) and MDA-MB 468 (blue) as well as on EGFR negative cell line HEK293-FT (red). Analysis of (A) green area confluency, (B) fluorescence intensity and (C) confluency were performed by Incucyte measurements. (D) The luminescence of luciferase assay was determined by SpectraMax 340. The mean value ± SEM is shown (N = 1, n = 3).

After D2 did not show successful transfection of the luciferase plasmid, the luciferase assay was repeated with D1/D3/D4 [N/P 16, EGF 0–10 (pp)]. As EGF is toxic for A431 and MDA-MB 468, the assays were performed with PC-9 cells as target cell line, where EGFR is still overexpressed, but EGF did not show any cytotoxic effect (Figure 37). HEK293-FT remains as negative control cell line in these experiments. Unfortunately, neither for D1 [N/P 16, EGF 0–10 (pp)] nor for D3 [N/P 16, EGF 0–10 (pp)] and D4 [N/P 16, EGF 0–10 (pp)] luciferase transfection was detected. Only lipofectamine was able to transfect the luciferase plasmid successfully.

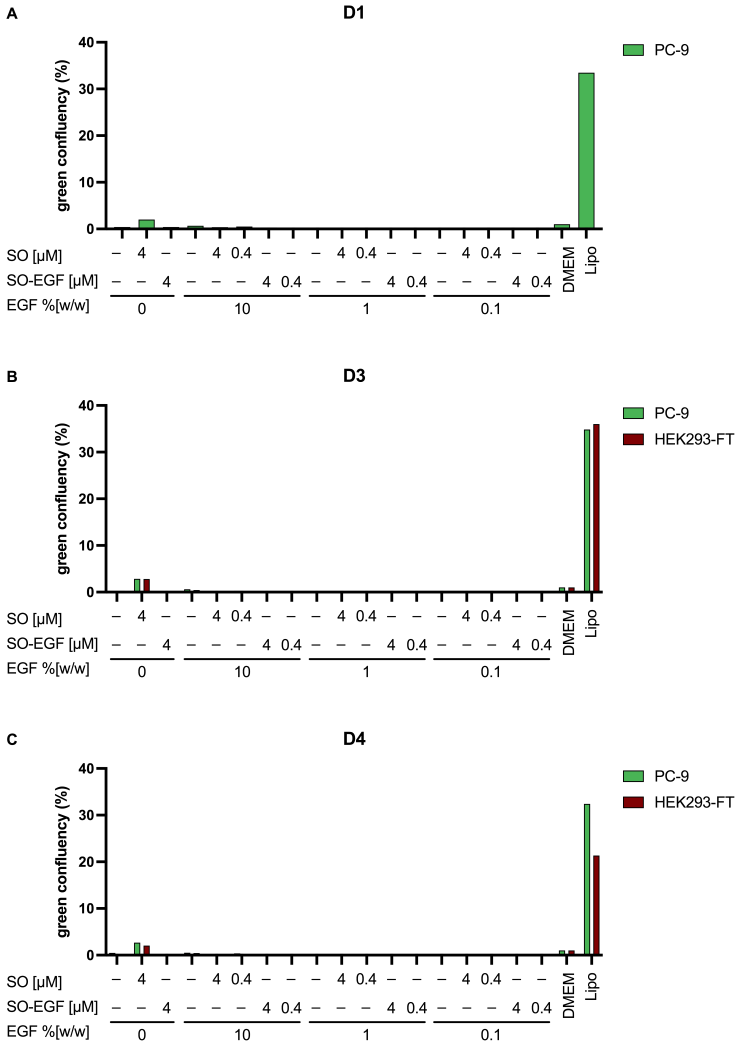

Figure 39: Transfection efficiency of luciferase and cytotoxicity of D1/D3/D4 [N/P 16, EGF 0–10 (pp)] with and without additional SO1861 or SO1861-EGF.
The assay was performed on EGFR positive cell line PC-9 (green) as well as on EGFR negative cell line HEK293-FT (red). Analysis of (A) green area confluency, (B) fluorescence intensity and (C) confluency were performed by Incucyte measurements. (D) The luminescence of luciferase assay was determined by SpectraMax 340. The mean value ± SEM is shown (N = 1, n = 3).

3.7 Proof of concept – targeted PAMAM polyplexes

As neither the polyplexes consisting of the self-synthesized dendrons D1–D4, nor the ones consisting of D1 and D5, can successfully transfect the genetic material, the ligand as well as the targeted SO1861-EGF were tested with PAMAM polyplexes. PAMAM is the commercial dendrimer selected in the ENDOSCAPE project as non-viral dendritic gene delivery vector. For the following experiments, PAMAM with a generation of 5 was used and was equipped with a PEG-azide linker (PAMAM G5-(PEG-N_3)$_5$). This dendrimer construct was afterwards polyplexed with eGFP plasmid using N/P 8, as this was the optimal N/P ratio identified in previous experiments and also used for the PAMAM prototypes in the ENDOSCAPE project. Furthermore, EGF was polyplexed using an EGF/DNA ratio from 0–10. The size of PAMAM [N/P 8, EGF 0–10 (pp)] was determined by DLS measurements (Figure 40). We observed that the polyplexes without EGF (PAMAM [N/P 8, EGF 0 (pp)]) are smaller compared to D1–D4 [N/P 16, EGF 0 (pp)]. When EGF is involved in the polyplexes, the size increased compared to PAMAM [N/P 8, EGF 0 (pp)], even though PAMAM [N/P 8, EGF 10 (pp)] is smaller than PAMAM [N/P 8, EGF 0.1 (pp)] and PAMAM [N/P 8, EGF 1 (pp)].

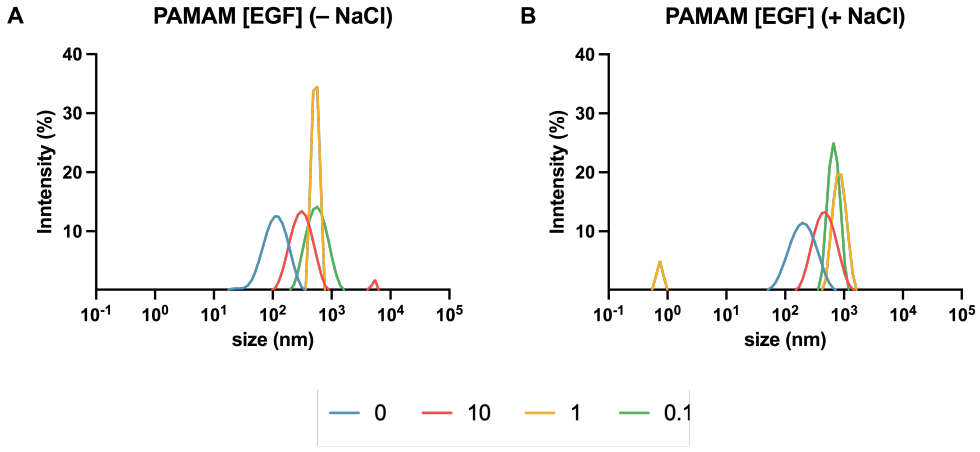

C

	EGF:DNA	0		0.1		1		10	
	NaCl	–	+	–	+	–	+	–	+
PAMAM	PDI	0.17	0.21	0.40	0.47	0.42	0.28	0.30	0.38
	Peak 1 mean (nm)	121	235	555	664	572	1017	364	471
	Peak 1 area (%)	100	100	100	100	100	89	95	96
	Peak 2 mean (nm)						1	1774	2622
	Peak 2 area (%)						11	5	4

Figure 40: DLS particle size determination of PAMAM [N/P 8, EGF 0–10].
One representative experiment is shown exemplarily in (A) and (B). PAMAM [N/P 8, EGF 0–10] polyplexes (A) before and (B) after NaCl addition. (C) Summary of particle sizes and PDI.

In another experiment polyplexes were formed with (PAMAM G5-(PEG-N_3)$_5$) where EGF was not only electrostatically bound but also covalently connected before and after eGFP plasmid was complexed. The PAMAM [N/P 8, EGF 10 (pp or before or after)] polyplexes were added to HCT-116 (EGFR positive cell line) and HEK293-FT (EGFR negative cell line) and the cells were treated with different additional amounts of SO1861 and SO1861-EGF. The transfection efficiency as well as the confluency was monitored over a period of 96 h via Incucyte measurements. The highest transfection efficiency (green confluency) was observed in HEK293-FT for PAMAM [N/P 8, EGF 10 (pp)] with additional SO1861-EGF in a concentration of 4 µM. For HCT-116 cells the green confluency was the same for PAMAM [N/P 8, EGF 10 (pp)] treated with additional 4 µM SO1861-EGF and SO1861. However, for the polyplexes where EGF was covalently bound to the dendrimer (PAMAM [N/P 8, EGF 10 (before and after)]) only low transfection was determined (Figure 41 A). Furthermore, no cytotoxicity was observed for all constructs (Figure 41 B). When monitoring the green fluorescence confluency over time for PAMAM [N/P 8, EGF 10 (pp)] (Figure 41 C, D) it is observed, that the cells treated with additional 4 µM SO1861-EGF are transfected earlier compared to the ones with 4 µM SO1861, which indicates that the targeted EEE is internalized faster that the non-targeted.

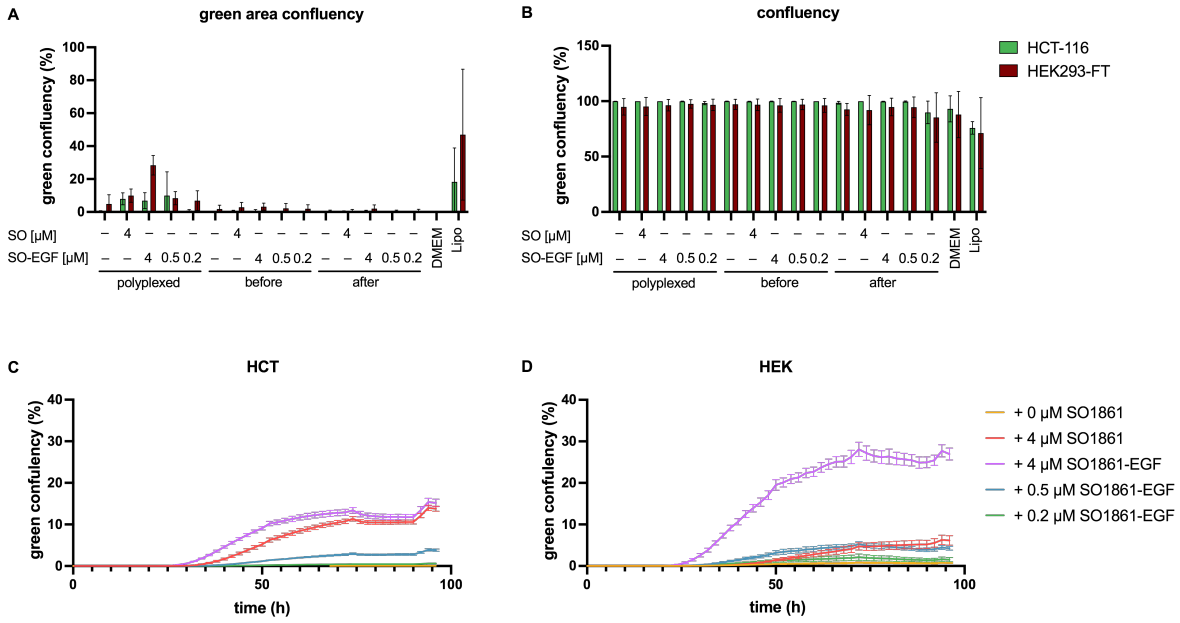

Figure 41: Transfection efficiency of eGFP plasmid and cytotoxicity of PAMAM [N/P 8, EGF 10 (pp or before or after)] with and without additional SO1861 or SO1861-EGF.
The assay was performed on EGFR positive cell lines HCT-116 (green) and EGFR negative cell line HEK293-FT (red). Analysis of (A) green area confluency and (B) confluency at the end point of 96 h and (C, D) over time for PAMAM [N/P 8, EGF 10 (pp)] were performed using an Incucyte device. The mean value ± SEM is shown (N = 1, n = 3).

The goal of developing a gene delivery system comprising a specific dendron and a targeting ligand was partially achieved. We successfully expressed the targeting ligands, evaluated their binding ability, and synthesized dendrons which are defined in terms of the number of functional groups. Furthermore, we generated polyplexes that incorporate both the K-EGF^{RR} and the dendrons, their size was evaluated, and *in vitro* experiments were performed. Although we did not achieve successful gene delivery using the dendron polyplexes, we did demonstrate a favourable effect of SO1861-EGF on the gene delivery when using PAMAM polyplexes.

4 Discussion

4.1 Do the mutations within the ligands influence their receptor-interaction?

As part of this thesis, we have investigated several options for liver targeting including Hepatitis B virus-derived large surface protein (LSP) and preS1 binding domain. In addition, the high-density lipoprotein (HDL) component apolipoprotein A1 (ApoA1) was selected as ligand. Successful expression of the preS1 domain in *E. coli* has been reported in several studies [148-150]. Deng *et al.* [151] used different tags to express the complete preS domain (preS1 + preS2) including the His- and maltose binding protein (MBP)-tags. However, only the thio and chitin-binding domain (CBD) preS were successfully expressed in their case. The His-preS was insoluble, while the MBP-preS1 was degraded. In our experiments, the expression of the Hepatitis B virus-derived ligands was neither successful using the pET11d vector nor the pMAL-c5X vector. Increased expression was not detected using SDS-PAGE. Furthermore, the western blot showed unspecific staining due to the primary-antibody (anti-preS1) and the bands belonging to the preS1 domain or the LSP were not identified. For this reason, the focus was on ApoA1 as a target for liver cells.

The pMAL-c5X vector used in this study to express the C-ApoA1 variant is commonly used for high-level expression [152, 153]. An additional advantage of this vector is the expression of the MBP fusion protein, which has an additional tag (in addition to the 6×His-tag) which allows the purification by amylose affinity chromatography (Figure 13). Using Factor Xa, the MBP tag was successfully cleaved from the MBP-C-ApoA1 fusion protein. However, evaluation of the interaction of C-ApoA1 with cells and with the scavenger BI receptor revealed no binding. In flow cytometry, the observed results indicate unspecific uptake of C-ApoA1 (Figure 19). The fluorescence images (Figure 21) revealed that C-ApoA1 enters the cell. However, it was not found in the endosomal compartments, suggesting that there is no receptor-mediated internalization. Furthermore, ELISA and SPR results supported the finding that cell interaction is unrelated to SR-BI binding (Figure 22, Figure 23). Similar results were observed with commercially available wild-type ApoA1. This could be due to the fact that the binding of ApoA1 has commonly been described when it is bound to HDL. Beer *et al*. [154] showed that the size and conformation of ApoA1 when attached to HDL also has an effect on the binding affinity of HDL to SR-BI. Here, larger HDLs (with the same amount of ApoA1 attached) had 50-fold greater binding than the smaller HDL. Therefore, it is possible that the C-ApoA1 is either not in the correct conformation or too small, when not incorporated into the HDL, for the intended binding. However, Xu *et al*. [86] also reported ApoA1 binding to the SR-BI receptor when it is “lipid free” *in vitro* and not bound to HDL. However, they have evaluated the binding only by measuring the concentration of unbound ApoA1.

They did not confirm the actual binding of ApoA1 to the SR-BI receptor by ELISA or SPR, neither the internalization by flow cytometry, or fluorescence microscopy. Finally, it remains unclear why ApoA1 did not bind under the applied conditions.

The second target of our studies is the EGF receptor (EGFR) which is overexpressed in many cancer cells. Therefore, EGF has been the ligand of choice for targeting cancer. So far, EGF has been expressed in eukaryotic systems as well as in *E. coli*. [155-157]. Due to its small size and three disulphide bonds, the expression of a correctly folded and soluble product is reported to be challenging. Su *et al.* [158] and Ma *et al.* [159] have attempted to overcome this problem by introducing a small ubiquitin-related modifier (SUMO). However, this strategy has the disadvantage of requiring an additional cleavage step using a protease to remove the SUMO moiety. Recombinant expression of an active and soluble EGF variant (K-EGF^{RR}) was achieved by inserting a 6×His-tag and using the ArcticExpress *E. coli* strain. Slow and controlled expression, which prevents misfolding, is achieved by expressing the protein at 16°C. We were successful in improving the yield from 250 µg to 5–6 mg when the EGF variant was expressed in Rosetta(DE3). This effect was also described by Tegel *et al.* when they compared the yields of proteins expressed in BL21(DE3) or Rosetta(DE3) [160]. However, the expressed K-EGF^{RR} was encapsulated in inclusion bodies when expressed in Rosetta(DE3). Inclusion bodies consist largely of aggregates of an overexpressed foreign protein, which often have a native-like secondary structure [161, 162]. During refolding and recovery of the expression product, this secondary structure is reported to be advantageous [163]. The procedure of Patra *et al.* [143] using 2 M urea for solubilization at pH 12, has been applied to recover the protein from the inclusion bodies. These conditions may be favourable due to the reduction of hydrophobic interactions by urea [164]. However, misfolding and inactive proteins are known to occur in the recovery of expression products from inclusion bodies. Fortunately, this was not observed in our experiments with the EGF variant K-EGF^{RR}, as proven in the binding studies.

K-EGF^{RR} was not only able to interact with cells as shown in flow cytometry experiments (Figure 19) and high-throughput imaging (Figure 20), but also to bind to the EGFR. In particular, the flow cytometry data revealed that the fluorescence signal of the Cy5-labelled EGF variant is more intense in cells in which the EGFR is overexpressed, especially in A431 cells. Furthermore, when EGFR was silenced by siRNA, there was a reduction in the number of EGF-positive cells. These results suggest that internalization is due to receptor interaction. In addition, receptor-mediated binding was confirmed by a competitive inhibition assay. Increasing the concentration of unlabelled EGF led to a significant decrease in the fluorescence signal in the target cell lines, but not in the off-target cells. The actual receptor-ligand interaction was determined by ELISA and SPR (Figure 22, Figure 23).

Compared to wild-type EGF, K-EGF^{RR} had a comparable or even slightly higher binding affinity. This also confirms that the replacement of the arginines by lysines and the artificially introduced lysine and 6×His-tag do not affect the biological activity of the variant. Replacement of lysines in EGF has been investigated in other studies. Bach *et al.* [165] for example developed a phage display system in which both lysines and arginines were replaced (K28Q, R45S, K48S and R53S). They even changed the basic character of EGF by replacing lysines and arginines with neutral amino acids such as serine or glutamine. By replacing lysines and arginines, they claimed that the EGF variant has the same binding affinity to the EGF receptor as wild-type EGF, which is consistent with the results presented in this thesis. In another recent study, Zhang *et al.* [166] replaced the same lysines as we did, however, they decided to replace them not only with two arginines (RR), but also serin and arginine (RS, SR). They observed a comparable level of extracellular signal-regulated kinase (ERK) phosphorylation for the RS and SR variants and a similar KD value compared to the wild-type EGF by *in situ* ELISA using A431 cells, whereas the RR variant showed a lower level of ERK phosphorylation compared to the wild-type. However, this mutation did not affect the binding ability or internalization of EGF (RR) when expressed as a fusion protein with the ribosome-inactivating protein saporin as demonstrated in previous studies performed by our group. [144]. In other former studies the wild type EGF was also recombinantly expressed as fusion protein containing either the toxins saporin or dianthin [167, 168].

Another reason for creating a fusion protein of EGF variant and saporin was to avoid heterogeneity and cross-linking during chemical conjugation. Homogeneity is a critical factor in clinical studies, as heterogeneity has some major drawbacks such as different pharmacokinetics, reproducibility, and consequently necessary adjustment of doses [169, 170]. Although heterogeneity is an accepted feature of antibody-drug conjugates for clinical trial approval, current research is exploring methods to obtain more homogeneous products. One method is to insert unnatural amino acids to the mAB backbone, another one glycosyl remodelling [171, 172]. As mentioned above, in the case of natural ligands such as EGF, the potentially multiple conjugation sites of the amino acids are often replaced by other amino acids to create a single conjugation site. For this purpose, Levashova *et al.* [173] modified the wild-type EGF by adding an artificial cysteine to the N-terminus to conjugate DOTA. A similar approach has been taken in this work by replacing the naturally occurring lysines with arginines and by the addition of an artificial lysine at the N-terminus. This provides a single and defined conjugation site that allows the EGF variant to be conjugated to any effector or carrier system. As a proof of concept, heterobifunctional PEG linkers were introduced. These linkers have NHS-esters on one side, which are able to react with the single lysine of the ligand, as well as a DBCO group on the other side. The DBCO group can undergo a SPAAC with an azide group of the reaction partner resulting in an orthogonal, fast, and high yield click conjugation.

This reaction pathway has the advantage over the conventional copper-catalysed azide-alkyne cycloaddition that – due to its ring strain – DBCO is highly reactive and no metal is required to catalyse the reaction [174]. We successfully conjugated the K-EGF^{RR} equipped with the DBCO linker to Cy5 and D2 containing an azide group. The linker used here can be either non-cleavable or cleavable under reducing or acidic conditions. The cleavable linkers have the advantage of cargo release in the target organelles, for example when the pH decreases in the endosomes during the endosomal pathway. In this case the ligand has no effect on the activity of the drug. In summary, the EGF variant K-EGF^{RR} has been shown to have a binding affinity comparable to that of the wild-type EGF and to exhibit uptake mediated by the EGF receptor. In addition, the single conjugation site equipped with a DBCO linker was successfully conjugated to either a dye, a dendron or a toxin. These findings make K-EGF^{RR} an interesting target for further evaluations and a promising candidate for targeted therapies. We demonstrated in this thesis that the mutations in which the lysines are replaced by arginines and an artificial lysine is added at the N-terminus have no effect on the ability of EGF to bind to its receptor and to be internalized.

4.2 SPPS – so simple and yet so many options

Non-viral vectors are promising carrier alternatives for gene delivery as the viral drug delivery platforms demonstrate immunogenicity and cytotoxicity. Dendrimers have gained prominence in this field due to their defined structure, targeted surface modifications and reduction of side effects. A well-established dendrimer is PAMAM, which exhibits polycationic properties to condense the genetic material. The high surface charge not only provides better loading capacity but also leads to higher cytotoxicity. The surface functional groups can be modified to reduce toxicity, to allow conjugation of a targeting moiety, or to increase transfection efficiency. However, the position and the number of surface modifications per dendrimer are not predictable, resulting in a non-homogeneous product. Therefore, the aim of this work was to synthesise different dendrons with a defined number of functional groups to generate a more defined and less toxic non-viral gene delivery platform. The dendrons were composed of amino acids, mainly lysines, and can therefore be classified as dendritic polylysines. The first dendritic polylysine was synthesized in solution by Denkewalter *et al.* [52]. We decided to use the SPPS methodology, which has the advantage of being highly efficient and reducing or completely suppressing side reactions compared to solution-based synthesis. In addition, the SPPS allows easy purification by washing and filtration between reaction steps. The four polylysine dendrons (D1–D4) were successfully and reproducibly prepared by SPPS, purified by HPLC, and analysed by MALDI-TOF-MS (Figure S5–Figure S8).

The resin used in this work was a polystyrene (PS)-based Wang resin, but there are other resins described in literature like polyacrylamide or polyethylene glycol (PEG) based. Swali *et al.* [175] used the PEG-PS resin, TentaGel®, for the first SPPS of PAMAM. The advantage of PEGylated PS resins is that they are amphiphilic, which means that they are soluble in polar as well as non-polar solvents. Furthermore, the PEG can be used as a spacer between the PS core and the linker, resulting in higher flexibility and less steric hindrance, which is beneficial for dendron synthesis [69].

Another important aspect in our synthesis strategy is the linker which is attached to the resin. It can be either integral, where the functionality is attached directly to the solid support, or non-integral, where an additional reactive moiety is attached [176]. Non-integral linkers offer a greater variety of functionalities and are more likely to be used for longer or dendritic peptides as they are more flexible. The acid labile Wang linker, which was used in this thesis, and the Rink-amide linker are the two most commonly used non-integral linkers for Fmoc-strategy [177], whereas, for the Boc strategy, 4-methylbenzhydrylamine hydrochloride (MBHA) or Merrifield are the preferred linkers [178]. In this thesis the Wang resin was used as it produces a carboxylic acid product when cleaved. This additional functionality might be of use for further modifications. In case of the Rink-amid linker, an amine would be obtained after cleavage in addition to the already existing surface amines.

Additionally, the loading capacity of the linker-equipped resin is important. Although high loading resins contain more reactive sites and therefore leading to higher product yield, the size of the dendron increases with each generation and so does the steric hindrance. As this can lead to incomplete reactions a lower loading is preferred for dendrimeric SPPS.

The Boc/Blz and Fmoc/tBu strategies are the two main strategies used in SPPS. In this work, the amino groups of lysine were protected with the base labile Fmoc. It is preferred over the acid labile Boc group, as the final cleavage of the resin is also performed under acidic conditions [179, 180]. Cysteines were incorporated into the polylysine dendron to introduce additional thiol groups for the conjugation of EEE SO1861. This requires another orthogonal protecting group in addition to Fmoc. For the first experiments we used Fmoc-Cys-(tBu). The thiol group is simultaneously deprotected during cleavage of the dendron from the resin under acidic conditions. Since deprotected thiol groups tend to form disulphide bridges which lead to aggregation of the dendrons, Fmoc-Cys-S(tBu) was used instead for the final experiments. The disulphide bridge is not acid labile and can be cleaved under reductive conditions, for example tris-2-carboxyethyl phosphine (TCEP).

The next and important steps in SPPS are activation and coupling of the new amino acid. A wide range of coupling reagents are available to support this reaction. One of the most common groups of coupling reagents are carbodiimides, such as N,N′-diisopropylcarbodiimide (DIC) or N,N′-dicyclohexylcarbodiimide (DCC), which have been used since the early days of SPPS [65]. Even quite popular, they also have some drawbacks, such as not having a very high coupling rate, or deactivating the activated species by rearranging into an N-acyl urea. For this reason, they are often used together with additives such as HOBt or HOAt to avoid such problems [181, 182] Another group are phosphonium and uranium/aminium salts. These include acylphosphonium (BOP, PyBOP) and acyluronium/aminium salts (HATU, HBTU, TATU, TBTU) [183-186].They convert amino acids into active OAt or OBt esters under basic conditions where DIPEA is often used as a base. There is also an increasing demand for reagents which are safer and more environmentally friendly. Regarding these aspects reagents like 1-[(1-(cyano-2-ethoxy-2-oxoethylideneaminooxy)-dimethylamino-morpholino)] uronium hexafluorophosphate (COMU), propylene carbonate (PC) and dimethyl carbonate (DMC) have already shown promising results for the successful use in SPPS [187-189]. The first dendritic polylysine synthesis by SPPS was performed by Tam *et al.* using a Pam resin, the Boc strategy and only DCC as a coupling reagent. Other conditions for SPPS leading to polylysine dendrimers are listed in Table 13.

Table 13: SPPS conditions used to generate dendritic polylysines.

Linker	Strategy	Coupling reagents	Ref.
Pam	Boc	DCC	Tam *et al.* [190]
Rink amide	Fmoc	DIC, HOBt	Wang *et al.* [191]
Rink amide	Fmoc	HBTU, NMM, DIPEA	Liao *et al.* [192]
MBHA	Fmoc	DCC, HOBt	Eom *et al.* [193]
MBHA	Boc	DIC, HOBt	Sheveleva *et al.* [194]
Rink amide MBHA	Fmoc	HBTU, DIPEA	Deng *et al.* [195]
Wang	Fmoc	HBTU, HOBt, DIPEA, NMP	Bellassai *et al.* [196]
Wang	Fmoc	HATU, DIPEA	This thesis.

In this work, we performed the synthesis of the desired dendrons with the Wang resin already containing the first amino acid following the Fmoc strategy and using HATU and DIPEA as coupling reagents. In our experiments HATU was chosen as it is a more potent agent than HBTU leading to higher yields. The dendritic polylysines D1–D4 were successfully synthesized under reproducible conditions. The dendrimers were purified by HPLC and further used for the formation of polyplexes. In summary, we were able to show that SPPS and the applied strategies are well suited to synthesise several polylysine dendrons with a defined number of different functional groups in a reproducible manner.

4.3 Does size really matters and what about the shape?

In this thesis we also studied the ability of the synthesised dendrons D1–D4 to deliver plasmid DNA into cells and finally into the nucleus using eGFP and luciferase plasmids. The expression level of eGFP or luciferase was determined by Incucyte measurements or luciferase assay. The results revealed that transfection was unsuccessful in both cases. In this section, the possible reasons and factors influencing successful delivery and transfection are evaluated and discussed.

The success of gene delivery depends mainly on the delivery vehicle. Cationic polymers or dendrimers encapsulate the negatively charged DNA via electrostatic interactions. Thus, the number of amine groups and hence the amount of positive charge on the surface is critical and increases with the number of generations. The dendrons used in this work contain either 17 (D1, D2), 9 (D3, D4) or 8 amino groups (D5). The gene loading capacity of the previously synthesised dendrons (D1–D4) was evaluated using either the agarose gel retardation assay or the Pico488 assay. In both cases, levels of free DNA were determined. The studies demonstrated that all dendrons were able to complex the whole eGFP plasmid at an N/P ratio of 16 (Figure 25, Figure S9). However, D3 and D5 did not complex the same amount of genetic material at N/P 8 like D1, D2 and D4. This trend was also observed by Ohsaki *et al.* [197] when a hyperbranched polylysine with 8 amino groups was complexed with pDNA at N/P 8. Only the higher generations with 16 or more amino groups were able to condense the whole amount of plasmid at this N/P ratio. It was further described that higher generations of dendritic polylysines were found to have a higher DNA condensation capacity [198].

We also investigated the influence of ligand incorporation by electrostatic interactions or covalent binding on DNA complexation. No effect of EGF on the successful formation of polyplexes was observed for D1, D5 and D2, either polyplexed or covalently bound (Figure 28 A, B, Figure S14). For D4 [N/P 16, EGF 10] more than 60% of the DNA was found to be free, whereas for D3 [N/P 16, EGF 10] 90% of the DNA was not polyplexed (Figure 28 A). This tendency could be due to the lower number of amines and therefore the reduced positive charge. In addition, the thiol groups, although still protected, could influence the binding when EGF is involved. No interference was detected for D5, which has only one terminal thiol group, whereas the amount of free DNA increases with the amount of thiol groups (D3 = 4; D4 = 2). Both factors lead to a weaker binding of the DNA and thus EGF can interfere more easily.

The size of the polyplexed particles is another important factor in successful drug delivery. A particle size of not more than 100–200 nm is considered as optimal, as it is small enough to avoid spleen filtration but large enough to avoid liver uptake. Particles in the range of 1–10 µm are similar to the size of bacteria and are therefore often taken up by macrophages.

All our polyplexes containing polylysine dendrons that were tested *in vitro* have a size range of 270–1023 nm. It might be that the polyplexes are too large to enter cells via the endosomal pathway, given the size ranges for cell uptake. They should be able to interact with the receptor and enter the cells via clathrin-mediated endocytosis, as they are equipped with the targeting ligand EGF. However, the particle size is limited to 200 nm when using this pathway [199]. Since the polyplexes are not in the endosome, this may explain why the endosomal escape enhancer SO1861 has no effect on transfection efficiency. Larger particles enter cells by macro-pinocytosis or phagocytosis. In particular, cationic dendrimers have the ability to interact electrostatically with the cell membrane and to enter the cell via adsorptive pinocytosis [200].

Looking at the experiments performed in this work, some trends can be observed. The particle size decreases as the N/P ratio increases (Figure 26, Figure 31). In particular, the size of D3 [N/P 8] is larger than the others, which were unable to complex the total amount of DNA. This is in agreement with the study of Alazzo *et al.* [201], where the size of hyperbranched polylysine is larger at low N/P ratios, especially for those where free DNA was detected in the agarose gel.

Size also increases with incorporation of EGF into the polyplexes. It is important to note that not only the size of D1–D4 [N/P 16, EGF 0.1–10] changed, but also the size of D1–D4 [N/P 16, EGF 0] changed compared to D1–D4 [N/P 16] due to the different solvents used in the experiments. D1–D4 [N/P 16] was dissolved in HEPES (10 mM) only, while D1–D4 [N/P 16, EGF 0] also contains DPBS. The same volume of DPBS was used for D1–D4 [N/P 16, EGF 0] as EGF solution for D1–D4 [N/P 16, EGF 0.1–10]. Together with the observation in all DLS measurements that adding NaCl (150 nM) causes the polyplexes to become significantly larger it cannot be excluded that the change in size is due to the buffer, already containing NaCl, rather than EGF. Coelho *et al.* [202] also described that NaCl and the timepoint when it is added can have an effect on polyplex size. When NaCl was added after polyplex formation, the particles were smaller compared to when NaCl was already present during the polyplex formation. This was despite the fact that the final salt concentration was the same for both routes. Interestingly, D2 [N/P 16, EGF (after, before)] polyplexes (Figure 30) with EGF covalently bound to the dendron are smaller than D2 [N/P 16, EGF (pp)] (Figure 29). The covalent EGF apparently enables D2 to form denser DNA polyplexes.

Looking at the polyplexes where two different dendrons are involved, it becomes clear that the number of amines has an impact not only on the loading capacity but also on the size. The two polyplexes used were D1, which contains 16 amines, and D5, which contains 8 amines. D1+5 [N/P 16, D1/D5 4:1] with more D1 has a smaller size than D1+5 [N/P 16, D1/D5 1:4] with more D5. This can be explained by the higher cationic character of these polyplexes resulting in a denser polyplex formation.

Although Pezzoli *et al.* [203] observed a significant size difference depending on different mixing methods, we could not confirm this observation in our studies with D1+5 [N/P 16, D1/D5 4:1, M1–4 (mixed or vortexed)]. Here neither the order of the reactants nor the mixing method had an influence on the size.

The next factor to consider is the shape of the dendrons. In this work the dendrons were based on polylysine, which exists in different shapes like linear, hyperbranched or dendritic. In most cases, studies on polylysine dendrimers describe a barbell shape. This is because they are synthesised in a symmetrical way starting from a bifunctional core unit. As our dendrons are synthesized via SPPS using the convergent strategy and are afterwards not conjugated to a core molecule together with other dendrons to from a dendrimer, it would be still classified as a dendron. However, Gorzkiewicz *et al.* [204] described their constructs as polylysine dendrimers, which have a similar structure to our dendrons. Their dendrons transfect cells as well as or even better than lipofectamine. However, they also contain additional amino acids, like arginine or histidine, as spacers or to obtain higher charged molecules. Kadlecova *et al.* [205] compared linear, hyperbranched and dendritic polylysines of different generations. When comparing different shapes with comparable molecular mass, the hyperbranched polylysine shows a significantly better transfection of cells (10% (linear, dendritic) vs. 40% (hyperbranched) at N/P 7). Surprisingly, the size of the polyplexes also increases with higher N/P ratios and, for all forms with comparable molecular mass, a size of 500–550 nm (N/P 8) and 110–150 nm (N/P 1) was determined. It appears that the size of the particles does not limit the delivery of genetic material to the nucleus. However, they found that in the case of dendritic polylysines, a minimum of generation six is required to show a transfection efficiency of more than 10%. Ohsaki *et al.* also reported that even when the size of dendritic polylysine G3 was 257 nm and this dendrimer was able to complex DNA at N/P 2, dendritic polylysines of generation lower than four were unable to successfully deliver the gene. This is in line with a study by Li *et al.* who compared different generations of polylysine dendrimers with 23 kDa linear polylysine. They found that G3 of the dendritic polylysine was incapable of transfecting cells, while for G4–G5 transfection was observed. The transfection efficiency was lower compared to the linear polylysine. However, the dendritic polylysines were less toxic (70% cell viability versus 25%).

As there are several factors that can influence the successful delivery of genes into the cell, it is difficult to say which factor limited the transfection in this work. Since larger polyplexes can also be taken up by the cells, transfection is not strictly limited by these factors. However, there is an interplay between several factors that can influence each other. For example, the lower charge may lead to poorer complexation of the DNA, resulting in a larger particle size and ultimately poorer transfection. The structure of the polymer may also play a role.

In this thesis, we demonstrated that PAMAM loaded with EGF and eGFP plasmid can successfully transfect the genetic material, even when the polyplex has a size of 364 nm. Furthermore, especially when using the targeted EEE (SO1861-EGF), the transfection efficiency was increased. This demonstrates that SO1861 enhances endosomal escape and that cationic dendrimers equipped with K-EGF^{RR} can be used to successfully deliver genetic material into cells.

4.4 EGF – too powerful for targeted drug delivery?

The mortality rate of cancer increased over the recent years and is now a leading cause of death worldwide [206]. Conventional treatments such as surgery, chemotherapy and radiotherapy are successful in treating many malignancies. However, chemo- and radiation therapy also cause side effects due to their non-specificity affecting healthy cells as well [207]. Targeted therapy is a promising way to overcome this disadvantage. The EGF receptor (EGFR), which is known to be overexpressed on cancer cells, has been identified as a promising candidate for active targeting of several types of cancer. This receptor can be targeted using either fully human antibodies, antibody fragments, peptides or EGF itself as targeting ligand.

In this work, EGF was used as a targeting moiety for non-viral gene delivery. We attached the EGF to dendron polyplexes either electrostatically (D1–D4) or covalently using strain-promoted azide-alkyne cycloaddition (SPAAC) click chemistry (D2, Figure 27). Blessing *et al.* [208], Buñanles *et al.* [209] and Li *et al.* [146] also used these methods to create a targeted gene delivery vehicle. Li *et al.* incorporated EGF into the polyplexes containing luciferase plasmid and generation 5 PAMAM, through electrostatic interactions. They were evaluating the transfection efficiency of the gene on HepG2 (4.4 nTMP), HeLa (26.4 nTPM) and MDA-MB 231 (61.6 nTPM) cells using a polyplex with an N/P ratio of 20 and EGF/DNA ratio of 2. In all cases, they observed a significant increase in luciferase expression in the EGF polyplexes compared to the untargeted polyplexes. They also tested the polyplexes *in vivo*, where they were able to detect a higher luminescence signal in the tumour for the targeted polyplex [146]. Similar *in vitro* and *in vivo* results were reported by Buñanles *et al.* [209], who used self-assembled polyplexes containing luciferase plasmid, EGF and liposomes and tested them on HepG2 (4.4 nTPM) and rat DHDK12 cells. On the other hand, Blessing *et al.* [208] covalently attached murine EGF with a SPDP linker to thiol-functionalised polyethylene imine (PEI) with and without PEG. They tested their constructs on the mouse cell lines Renca-EGFR and CMT-93 and on human epidermoid KB cells. They observed a 300-fold higher level of luciferase expression in PEI polyplexes with EGF than in those without.

They also formed polyplexes in which PEI was PEGylated. Here, the luciferase expression level and thus the transfection efficiency of EGF-PEG-PEI was 10–100 times higher than for PEG-PEI.

Unfortunately, transfection of eGFP or luciferase plasmids was not observed in case of our polyplexes. Neither for the targeted polylysine dendron polyplex nor for the untargeted. For the GFP transfection assay, eGFP encoding plasmid was used and the polyplex was tested on the EGFR-overexpressing cell lines A431 (5282.1 nTPM) and MDA-MB 468 (613.3 nTPM) and the off-target cell line HEK293-FT (3.6 nTPM). Green fluorescence was indeed detected, but also a cytotoxic effect on the cells treated with D1–D4 [N/P 16, EGF 10 or 1] and when additionally treated with SO1861-EGF (Figure 36, Figure S15–Figure S17). Except for the lipofectamine control, no luciferase expression was observed in the luciferase assay on PC-9 cells (Figure 38, Figure 39). The MTS assay confirmed the cytotoxic effect of EGF and SO1861-EGF on A431 and MDA-MB 468. No toxic effect was observed for PC-9 (180 nTPM) and HEK293-FT (Figure 37). It can therefore be concluded that the increased fluorescence signal of the EGF polyplexes compared to the negative control (DMEM) in the GFP assay is due to autofluorescence. It is known that dead cells have a tendency to show a higher autofluorescence than living cells [210]. This raises the question of whether EGF is too potent for targeted therapy.

Kawamoto *et al.* [211] and Filmus *et al.* [212] have investigated the effect of EGF on EGFR-overexpressing cells such as A431 and MDA-MB 468. They found that EGF can inhibit cell growth or even lead to cell death. Kawamoto also showed that there is a threshold above which cell growth is impaired by reducing the amount of EGFR in some A431 clones. Nevertheless, there have been several studies in which EGF has been successfully used as a target ligand. Conjugation of EGF to polycaprolactone (PCL) [213], high-density lipoprotein (HDL)-mimicking nanoparticles [214, 215] and carboxymethyl dextran (CMDx)-coated magnetic iron oxide nanoparticles [216] have demonstrated EGFR-mediated uptake *in vitro*. Sandoval *et al.* [217] and Shimada *et al.* [218] have used EGF conjugated lipid nanoparticles loaded with the cytostatic drugs gemcitabine or paclitaxel *in vivo*. They showed a reduction of tumour volume or growth inhibition. It is important to note that the studies described above were designed to kill cancer cells. In addition, they did not include a control in which the cells or mice were treated with EGF alone. Therefore, it cannot be excluded that the cytotoxic effect of the target constructs is solely due to EGF. A noteworthy study has been published by Zhang *et al.* [166], already mentioned in section 4.1. They conjugated the EGF mutants to gold nanoparticles and tested their cytotoxicity. Surprisingly, cell viability of over 75% was achieved in cells treated with 48 or 96 nM EGF. This is not consistent with our results, where the IC_{50} of EGF on A431 was 4.91 nM.

Other studies also differ from Zhangs observation, as they reported a viability of only 25% when using 10 nM EGF [212]. However, Zhang was able to observe that the cytotoxic effect of EGF can be increased when it is conjugated to gold nanoparticles leading to a cell viability of 30%. In order to treat cancer, this supposed disadvantage of EGFs cytotoxic effect on highly EGFR-overexpressing cells is used to their advantage. EGF has also been used by Gonzalez *et al.* [219] together with the carrier protein P64K for the treatment of non-small cell lung cancer (NSCLC) or squamous cell carcinoma of the head and neck. This vaccine, also known as CIMAvax, is currently in a phase II trial. The treatment is designed to induce the formation of EGF antibodies, resulting in EGF deprivation.

In summary, EGF is a powerful tool in the fight against cancer. Either as an agent by itself or together with a cancer drug, which can even enhance its effect. However, as a targeting ligand in the context of gene therapy, the cell line or cancer type to be targeted should be chosen carefully. The early death of the cells can result in unsuccessful transfection of the genetic material and therefore lead to a less effective therapy, especially when the approach is not aiming for cell death.

5 Conclusion & Outlook

The aim of this work was to develop a dendritic non-viral gene delivery platform with a defined number of functional groups to reduce heterogeneity. These dendrons should be equipped with a targeting moiety and an endosomal escape enhancer. For this reason, the single conjugation side ligands K-EGF^{RR} and C-ApoA1 were chosen to target cancer and liver cells respectively. Recombinant expression in *E. coli* of these two ligands was successful and both were equipped with a dye and/or a heterobifunctional PEG linker. Furthermore, EGF was conjugated to dendron D2 and SO1861. Binding studies demonstrated that the binding affinity of the EGF variant K-EGF^{RR} to its receptor is as good as or better than the one of the wild type. However, no binding to SR-BI was observed for C-ApoA1 or the wild type. Therefore, further binding experiments should be performed with the addition of lipids such as cholesterol. This has been shown in previous studies to lead to successful binding of ApoA1. The novel polylysine dendrons used in this work were reproducibly synthesised by SPPS and successfully purified by HPLC. Polyplex formation was then carried out at different N/P ratios, with N/P 16 proving to complex the full amount of DNA for all dendrons. K-EGF^{RR} was also incorporated into these polyplexes either electrostatically or covalently. The size of the polyplexes was analysed by DLS and was in the range of 270–1412 nm with an increase in size when EGF and NaCl were present. To further understand the composition of the polyplexes, the zeta potential and the behaviour of the polyplexes in different buffers need to be investigated. Unfortunately, the use of dendron polyplexes D1–D4 [N/P 16, EGF 0–10] as well as D1+D5 [N/P 16, EGF 0–10] did not lead to successful transfection of eGFP or luciferase plasmid. This was the case even when the polyplex was targeted and EEE SO1861 was added. As discussed above, several factors may be responsible for this observation, such as size, charge and dendron formation. Therefore, a reduction in the size of the polyplexes should be the subject of further experiments. Increasing the generation and thus the total charge could be a promising approach. For generations greater than three, a low loaded resin can be used to reduce the steric hindrance during chain-elongation. In addition, the surface lysines of the dendrons can be modified or replaced by arginines, which have been shown to have a positive effect on transfection efficiency. Furthermore, the guanidinium groups of the dendrons allow them to act as cell-penetrating peptides at low pH, for example in endosomes. Other dendrons and dendron combinations, such as the D1+D5 polyplexes, which provide different functional groups for polyplexing and click chemistry modifications, also need to be investigated. The ability of the K-EGF^{RR} and the targeted SO1861-EGF to enhance transfection efficiency was demonstrated using PAMAM polyplexes. This makes the targeted cationic dendrimers a very promising vehicle for the successful delivery of genes and SO1861 a very successful endosomal escape enhancer.

6 References

1. Liu X, Liu M, Wu L, Liang D: Gene Therapy for Hemophilia and Duchenne Muscular Dystrophy in China. *Hum Gene Ther* 2018, **29**(2):146-150.
2. Liras A, Segovia C, Gabán AS: Advanced therapies for the treatment of hemophilia: future perspectives. *Orphanet J Rare Dis* 2012, **7**:97.
3. Bhattacharyya NP: Huntington's disease: a monogenic disorder with cellular and biochemical complexities. *Febs j* 2008, **275**(17):4251.
4. Favorova OO, Kulakova OG, Boĭko AN: Multiple sclerosis as a polygenic disease: an update. *Genetika* 2010, **46**(3):302-313.
5. van Rheenen W, Peyrot WJ, Schork AJ, Lee SH, Wray NR: Genetic correlations of polygenic disease traits: from theory to practice. *Nat Rev Genet* 2019, **20**(10):567-581.
6. Mahdieh N, Rabbani B: An overview of mutation detection methods in genetic disorders. *Iran J Pediatr* 2013, **23**(4):375-388.
7. Bick D, Bick SL, Dimmock DP, Fowler TA, Caulfield MJ, Scott RH: An online compendium of treatable genetic disorders. *Am J Med Genet C Semin Med Genet* 2021, **187**(1):48-54.
8. Bhatia S: Long-term health impacts of hematopoietic stem cell transplantation inform recommendations for follow-up. *Expert Rev Hematol* 2011, **4**(4):437-452; quiz 453-434.
9. Patel P, Suzuki Y, Tanaka A, Yabe H, Kato S, Shimada T, Mason RW, Orii KE, Fukao T, Orii T *et al*: Impact of Enzyme Replacement Therapy and Hematopoietic Stem Cell Therapy on Growth in Patients with Hunter Syndrome. *Mol Genet Metab Rep* 2014, **1**:184-196.
10. Pan X, Veroniaina H, Su N, Sha K, Jiang F, Wu Z, Qi X: Applications and developments of gene therapy drug delivery systems for genetic diseases. *Asian J Pharm Sci* 2021, **16**(6):687-703.
11. Hardee CL, Arévalo-Soliz LM, Hornstein BD, Zechiedrich L: Advances in Non-Viral DNA Vectors for Gene Therapy. *Genes (Basel)* 2017, **8**(2).
12. Tai W: Chemical modulation of siRNA lipophilicity for efficient delivery. *J Control Release* 2019, **307**:98-107.
13. Barrangou R, Doudna JA: Applications of CRISPR technologies in research and beyond. *Nat Biotechnol* 2016, **34**(9):933-941.
14. Gupta A, Andresen JL, Manan RS, Langer R: Nucleic acid delivery for therapeutic applications. *Adv Drug Deliv Rev* 2021, **178**:113834.
15. Xu S, Yang K, Li R, Zhang L: mRNA Vaccine Era-Mechanisms, Drug Platform and Clinical Prospection. *Int J Mol Sci* 2020, **21**(18).
16. Lara AR, Ramírez OT, Wunderlich M: Plasmid DNA production for therapeutic applications. *Methods Mol Biol* 2012, **824**:271-303.
17. Yin H, Kanasty RL, Eltoukhy AA, Vegas AJ, Dorkin JR, Anderson DG: Non-viral vectors for gene-based therapy. *Nature Reviews Genetics* 2014, **15**(8):541-555.
18. Mao CQ, Du JZ, Sun TM, Yao YD, Zhang PZ, Song EW, Wang J: A biodegradable amphiphilic and cationic triblock copolymer for the delivery of siRNA targeting the acid ceramidase gene for cancer therapy. *Biomaterials* 2011, **32**(11):3124-3133.
19. Chen C, Yang Z, Tang X: Chemical modifications of nucleic acid drugs and their delivery systems for gene-based therapy. *Med Res Rev* 2018, **38**(3):829-869.
20. Khorkova O, Wahlestedt C: Oligonucleotide therapies for disorders of the nervous system. *Nat Biotechnol* 2017, **35**(3):249-263.
21. Yin H, Kanasty RL, Eltoukhy AA, Vegas AJ, Dorkin JR, Anderson DG: Non-viral vectors for gene-based therapy. *Nat Rev Genet* 2014, **15**(8):541-555.
22. Pahle J, Walther W: Vectors and strategies for nonviral cancer gene therapy. *Expert Opin Biol Ther* 2016, **16**(4):443-461.
23. Lachmann R: Herpes simplex virus-based vectors. *Int J Exp Pathol* 2004, **85**(4):177-190.

24. Deregowski V, Canalis E: Gene delivery by retroviruses. *Methods Mol Biol* 2008, **455**:157-162.
25. Kaliberov SA, Kaliberova LN, Yan H, Kapoor V, Hallahan DE: Retargeted adenoviruses for radiation-guided gene delivery. *Cancer Gene Ther* 2016, **23**(9):303-314.
26. Merentie M, Lottonen-Raikaslehto L, Parviainen V, Huusko J, Pikkarainen S, Mendel M, Laham-Karam N, Kärjä V, Rissanen R, Hedman M *et al*: Efficacy and safety of myocardial gene transfer of adenovirus, adeno-associated virus and lentivirus vectors in the mouse heart. *Gene Ther* 2016, **23**(3):296-305.
27. Prokofjeva MM, Proshkina GM, Lebedev TD, Shulgin AA, Spirin PV, Prassolov VS, Deyev SM: Lentiviral gene delivery to plasmolipin-expressing cells using Mus caroli endogenous retrovirus envelope protein. *Biochimie* 2017, **142**:226-233.
28. Kulkarni JA, Witzigmann D, Thomson SB, Chen S, Leavitt BR, Cullis PR, van der Meel R: The current landscape of nucleic acid therapeutics. *Nature Nanotechnology* 2021, **16**(6):630-643.
29. Singh V, Khan N, Jayandharan GR: Vector engineering, strategies and targets in cancer gene therapy. *Cancer Gene Therapy* 2022, **29**(5):402-417.
30. Balazs DA, Godbey W: Liposomes for use in gene delivery. *J Drug Deliv* 2011, **2011**:326497.
31. Yousefpour Marzbali M, Yari Khosroushahi A: Polymeric micelles as mighty nanocarriers for cancer gene therapy: a review. *Cancer Chemother Pharmacol* 2017, **79**(4):637-649.
32. Ghosn Y, Kamareddine MH, Tawk A, Elia C, El Mahmoud A, Terro K, El Harake N, El-Baba B, Makdessi J, Farhat S: Inorganic Nanoparticles as Drug Delivery Systems and Their Potential Role in the Treatment of Chronic Myelogenous Leukaemia. *Technol Cancer Res Treat* 2019, **18**:1-9.
33. Barua S, Ramos J, Potta T, Taylor D, Huang HC, Montanez G, Rege K: Discovery of cationic polymers for non-viral gene delivery using combinatorial approaches. *Comb Chem High Throughput Screen* 2011, **14**(10):908-924.
34. Guimarães D, Cavaco-Paulo A, Nogueira E: Design of liposomes as drug delivery system for therapeutic applications. *Int J Pharm* 2021, **601**:120571.
35. Mathiyazhakan M, Wiraja C, Xu C: A Concise Review of Gold Nanoparticles-Based Photo-Responsive Liposomes for Controlled Drug Delivery. *Nanomicro Lett* 2018, **10**(1):10.
36. Kapoor M, Lee SL, Tyner KM: Liposomal Drug Product Development and Quality: Current US Experience and Perspective. *Aaps j* 2017, **19**(3):632-641.
37. Ita K: Polyplexes for gene and nucleic acid delivery: Progress and bottlenecks. *Eur J Pharm Sci* 2020, **150**:105358.
38. Ramamoorth M, Narvekar A: Non viral vectors in gene therapy- an overview. *J Clin Diagn Res* 2015, **9**(1):Ge01-06.
39. Del Pozo-Rodríguez A, Solinís M, Rodríguez-Gascón A: Applications of lipid nanoparticles in gene therapy. *Eur J Pharm Biopharm* 2016, **109**:184-193.
40. Boussif O, Lezoualc'h F, Zanta MA, Mergny MD, Scherman D, Demeneix B, Behr JP: A versatile vector for gene and oligonucleotide transfer into cells in culture and in vivo: polyethylenimine. *Proc Natl Acad Sci U S A* 1995, **92**(16):7297-7301.
41. Jiang C, Chen J, Li Z, Wang Z, Zhang W, Liu J: Recent advances in the development of polyethylenimine-based gene vectors for safe and efficient gene delivery. *Expert Opin Drug Deliv* 2019, **16**(4):363-376.
42. Abedi-Gaballu F, Dehghan G, Ghaffari M, Yekta R, Abbaspour-Ravasjani S, Baradaran B, Dolatabadi JEN, Hamblin MR: PAMAM dendrimers as efficient drug and gene delivery nanosystems for cancer therapy. *Appl Mater Today* 2018, **12**:177-190.
43. Wojnilowicz M, Glab A, Bertucci A, Caruso F, Cavalieri F: Super-resolution Imaging of Proton Sponge-Triggered Rupture of Endosomes and Cytosolic Release of Small Interfering RNA. *ACS Nano* 2019, **13**(1):187-202.
44. Kazemi Oskuee R, Dabbaghi M, Gholami L, Taheri-Bojd S, Balali-Mood M, Mousavi SH, Malaekeh-Nikouei B: Investigating the influence of polyplex size on toxicity properties of polyethylenimine mediated gene delivery. *Life Sci* 2018, **197**:101-108.

45. Buhleier E, Wehner WD, Voegtle F: ‚Cascade'- and ‚nonskid-chain-like' syntheses of molecular cavity topologies *Synthesis* 1978, **1978**:155-158.
46. Gillani SS, Munawar MA, Khan KM, Chaudhary JA: Synthesis, characterization and applications of poly-aliphatic amine dendrimers and dendrons. *Journal of the Iranian Chemical Society* 2020, **17**(11):2717-2736.
47. Hsu H-J, Bugno J, Lee S-r, Hong S: Dendrimer-based nanocarriers: a versatile platform for drug delivery. *WIREs Nanomedicine and Nanobiotechnology* 2017, **9**(1):e1409.
48. Madaan K, Kumar S, Poonia N, Lather V, Pandita D: Dendrimers in drug delivery and targeting: Drug-dendrimer interactions and toxicity issues. *J Pharm Bioallied Sci* 2014, **6**(3):139-150.
49. Kesharwani P, Jain K, Jain NK: Dendrimer as nanocarrier for drug delivery. *Progress in Polymer Science* 2014, **39**(2):268-307.
50. Contin M, Garcia C, Dobrecky C, Lucangioli S, D'Accorso N: Advances in drug delivery, gene delivery and therapeutic agents based on dendritic materials. *Future Med Chem* 2019, **11**(14):1791-1810.
51. Sapra R, Verma RP, Maurya GP, Dhawan S, Babu J, Haridas V: Designer Peptide and Protein Dendrimers: A Cross-Sectional Analysis. *Chemical Reviews* 2019, **119**(21):11391-11441.
52. Robert G. Denkewalter JK, Lukasavage WJ. : Macromolecular highly branched homogenerous compound based on lysine units. In: *United States Patent.* 1981.
53. de Brabander-van den Berg EMM, Meijer EW: Poly(propylene imine) Dendrimers: Large-Scale Synthesis by Hetereogeneously Catalyzed Hydrogenations. *Angewandte Chemie International Edition in English* 1993, **32**(9):1308-1311.
54. Tomalia D, Baker HQ, Dewald JR, Mj H, Kallos G, Martin S, Roeck J, Ryder J, Smith P: A New Class of Polymers: Starburst-Dendritic Macromolecules. *Polymer Journal* 1985, **17**:117-132.
55. Choi YJ, Kang SJ, Kim YJ, Lim YB, Chung HW: Comparative studies on the genotoxicity and cytotoxicity of polymeric gene carriers polyethylenimine (PEI) and polyamidoamine (PAMAM) dendrimer in Jurkat T-cells. *Drug Chem Toxicol* 2010, **33**(4):357-366.
56. Kannan RM, Nance E, Kannan S, Tomalia DA: Emerging concepts in dendrimer-based nanomedicine: from design principles to clinical applications. *J Intern Med* 2014, **276**(6):579-617.
57. Surekha B, Kommana NS, Dubey SK, Kumar AVP, Shukla R, Kesharwani P: PAMAM dendrimer as a talented multifunctional biomimetic nanocarrier for cancer diagnosis and therapy. *Colloids Surf B Biointerfaces* 2021, **204**:111837.
58. Ho MN, Bach LG, Nguyen DH, Nguyen CH, Nguyen CK, Tran NQ, Nguyen NV, Hoang Thi TT: PEGylated PAMAM dendrimers loading oxaliplatin with prolonged release and high payload without burst effect. *Biopolymers* 2019, **110**(7):e23272.
59. Chaplot SP, Rupenthal ID: Dendrimers for gene delivery--a potential approach for ocular therapy? *J Pharm Pharmacol* 2014, **66**(4):542-556.
60. Shi C, He Y, Feng X, Fu D: ε-Polylysine and next-generation dendrigraft poly-L-lysine: chemistry, activity, and applications in biopharmaceuticals. *Journal of Biomaterials Science, Polymer Edition* 2015, **26**(18):1343-1356.
61. Zhu H, Liu R, Shang Y, Sun L: Polylysine complexes and their biomedical applications. *Engineered Regeneration* 2023, **4**(1):20-27.
62. Lächelt U, Wagner E: Nucleic Acid Therapeutics Using Polyplexes: A Journey of 50 Years (and Beyond). *Chemical Reviews* 2015, **115**(19):11043-11078.
63. Manouchehri S, Zarrintaj P, Saeb MR, Ramsey JD: Advanced Delivery Systems Based on Lysine or Lysine Polymers. *Molecular Pharmaceutics* 2021, **18**(10):3652-3670.
64. Merrifield RB: Solid-phase peptide synthesis. *Adv Enzymol Relat Areas Mol Biol* 1969, **32**:221-296.
65. Merrifield RB: Solid-Phase Peptide Synthesis. III. An Improved Synthesis of Bradykinin*. *Biochemistry* 1964, **3**(9):1385-1390.

66. Carpino LA, Han GY: 9-Fluorenylmethoxycarbonyl function, a new base-sensitive amino-protecting group. *Journal of the American Chemical Society* 1970, **92**(19):5748-5749.
67. Carpino LA, Han GY: 9-Fluorenylmethoxycarbonyl amino-protecting group. *The Journal of Organic Chemistry* 1972, **37**(22):3404-3409.
68. Coin I, Beyermann M, Bienert M: Solid-phase peptide synthesis: from standard procedures to the synthesis of difficult sequences. *Nature Protocols* 2007, **2**(12):3247-3256.
69. Ya-Ting Huang A, Kao CL, Selvaraj A, Peng L: Solid-phase dendrimer synthesis: a promising approach to transform dendrimer construction. *Materials Today Chemistry* 2023, **27**:101285.
70. Kaiser E, Colescott RL, Bossinger CD, Cook PI: Color test for detection of free terminal amino groups in the solid-phase synthesis of peptides. *Anal Biochem* 1970, **34**(2):595-598.
71. Maeda H, Wu J, Sawa T, Matsumura Y, Hori K: Tumor vascular permeability and the EPR effect in macromolecular therapeutics: a review. *J Control Release* 2000, **65**:271-284.
72. Matsumura Y, Maeda H: A New Concept for Macromolecular Therapeutics in Cancer Chemotherapy: Mechanism of Tumoritropic Accumulation of Proteins and the Antitumor Agent Smancs. *Cancer Research* 1986, **46**(12 Part 1):6387.
73. Gerber DE: Targeted therapies: a new generation of cancer treatments. *Am Fam Physician* 2008, **77**(3):311-319.
74. Liu H, Bolleddula J, Nichols A, Tang L, Zhao Z, Prakash C: Metabolism of bioconjugate therapeutics: why, when, and how? *Drug Metab Rev* 2020, **52**(1):66-124.
75. Pun SH, Tack F, Bellocq NC, Cheng J, Grubbs BH, Jensen GS, Davis ME, Brewster M, Janicot M, Janssens B *et al*: Targeted delivery of RNA-cleaving DNA enzyme (DNAzyme) to tumor tissue by transferrin-modified, cyclodextrin-based particles. *Cancer Biol Ther* 2004, **3**(7):641-650.
76. Grandis JR, Sok JC: Signaling through the epidermal growth factor receptor during the development of malignancy. *Pharmacol Ther* 2004, **102**(1):37-46.
77. Master AM, Sen Gupta A: EGF receptor-targeted nanocarriers for enhanced cancer treatment. *Nanomedicine (Lond)* 2012, **7**(12):1895-1906.
78. Yewale C, Baradia D, Vhora I, Patil S, Misra A: Epidermal growth factor receptor targeting in cancer: a review of trends and strategies. *Biomaterials* 2013, **34**(34):8690-8707.
79. Yarden Y: The EGFR family and its ligands in human cancer. signalling mechanisms and therapeutic opportunities. *Eur J Cancer* 2001, **37 Suppl 4**:S3-8.
80. Nyati MK, Morgan MA, Feng FY, Lawrence TS: Integration of EGFR inhibitors with radiochemotherapy. *Nat Rev Cancer* 2006, **6**(11):876-885.
81. Park J-H, Iwamoto M, Yun J-H, Uchikubo-Kamo T, Son D, Jin Z, Yoshida H, Ohki M, Ishimoto N, Mizutani K *et al*: Structural insights into the HBV receptor and bile acid transporter NTCP. *Nature* 2022, **606**(7916):1027-1031.
82. Yan H, Zhong G, Xu G, He W, Jing Z, Gao Z, Huang Y, Qi Y, Peng B, Wang H *et al*: Sodium taurocholate cotransporting polypeptide is a functional receptor for human hepatitis B and D virus. *Elife* 2012, **1**:e00049.
83. Yao X, Gordon EM, Figueroa DM, Barochia AV, Levine SJ: Emerging Roles of Apolipoprotein E and Apolipoprotein A-I in the Pathogenesis and Treatment of Lung Disease. *Am J Respir Cell Mol Biol* 2016, **55**(2):159-169.
84. Ritter MC, Scanus AM: Role of apolipoprotein A-I in the structure of human serum high density lipoproteins. Reconstitution studies. *Journal of Biological Chemistry* 1977, **252**(4):1208-1216.
85. Williams DL, de La Llera-Moya M, Thuahnai ST, Lund-Katz S, Connelly MA, Azhar S, Anantharamaiah GM, Phillips MC: Binding and cross-linking studies show that scavenger receptor BI interacts with multiple sites in apolipoprotein A-I and identify the class A amphipathic alpha-helix as a recognition motif. *J Biol Chem* 2000, **275**(25):18897-18904.

86. Xu S, Laccotripe M, Huang X, Rigotti A, Zannis VI, Krieger M: Apolipoproteins of HDL can directly mediate binding to the scavenger receptor SR-BI, an HDL receptor that mediates selective lipid uptake. *J Lipid Res* 1997, **38**(7):1289-1298.
87. Li Z, Zhao R, Wu X, Sun Y, Yao M, Li J, Xu Y, Gu J: Identification and characterization of a novel peptide ligand of epidermal growth factor receptor for targeted delivery of therapeutics. *The FASEB Journal* 2005, **19**(14):1978-1985.
88. Trabulo S, Aires A, Aicher A, Heeschen C, Cortajarena AL: Multifunctionalized iron oxide nanoparticles for selective targeting of pancreatic cancer cells. *Biochimica et Biophysica Acta (BBA) - General Subjects* 2017, **1861**(6):1597-1605.
89. Christensen MV, Høgdall CK, Jochumsen KM, Høgdall EVS: Annexin A2 and cancer: A systematic review. *Int J Oncol* 2018, **52**(1):5-18.
90. Wang Y, Chen X, Tian B, Liu J, Yang L, Zeng L, Chen T, Hong A, Wang X: Nucleolin-targeted Extracellular Vesicles as a Versatile Platform for Biologics Delivery to Breast Cancer. *Theranostics* 2017, **7**(5):1360-1372.
91. Poturnayová A, Dzubinová Ľ, Buríková M, Bízik J, Hianik T: Detection of Breast Cancer Cells Using Acoustics Aptasensor Specific to HER2 Receptors. *Biosensors* 2019, **9**(2):72.
92. Varshosaz J, Hassanzadeh F, Sadeghi H, Khadem M: Galactosylated nanostructured lipid carriers for delivery of 5-FU to hepatocellular carcinoma. *Journal of Liposome Research* 2012, **22**(3):224-236.
93. Kwon MY, Wang C, Galarraga JH, Puré E, Han L, Burdick JA: Influence of hyaluronic acid modification on CD44 binding towards the design of hydrogel biomaterials. *Biomaterials* 2019, **222**:119451.
94. Mattheolabakis G, Milane L, Singh A, Amiji MM: Hyaluronic acid targeting of CD44 for cancer therapy: from receptor biology to nanomedicine. *Journal of Drug Targeting* 2015, **23**(7-8):605-618.
95. Frigerio B, Bizzoni C, Jansen G, Leamon CP, Peters GJ, Low PS, Matherly LH, Figini M: Folate receptors and transporters: biological role and diagnostic/therapeutic targets in cancer and other diseases. *Journal of Experimental & Clinical Cancer Research* 2019, **38**(1):125.
96. Cirulli V, Beattie GM, Klier G, Ellisman M, Ricordi C, Quaranta V, Frasier F, Ishii JK, Hayek A, Salomon DR: Expression and function of alpha(v)beta(3) and alpha(v)beta(5) integrins in the developing pancreas: roles in the adhesion and migration of putative endocrine progenitor cells. *J Cell Biol* 2000, **150**(6):1445-1460.
97. Li S, McGuire MJ, Lin M, Liu YH, Oyama T, Sun X, Brown KC: Synthesis and characterization of a high-affinity {alpha}v{beta}6-specific ligand for in vitro and in vivo applications. *Mol Cancer Ther* 2009, **8**(5):1239-1249.
98. Kojima R, Bojar D, Rizzi G, Hamri GC-E, El-Baba MD, Saxena P, Ausländer S, Tan KR, Fussenegger M: Designer exosomes produced by implanted cells intracerebrally deliver therapeutic cargo for Parkinson's disease treatment. *Nature Communications* 2018, **9**(1):1305.
99. Moreno P, Ramos-Álvarez I, Moody TW, Jensen RT: Bombesin related peptides/receptors and their promising therapeutic roles in cancer imaging, targeting and treatment. *Expert Opinion on Therapeutic Targets* 2016, **20**(9):1055-1073.
100. Pasqualini R, Koivunen E, Kain R, Lahdenranta J, Sakamoto M, Stryhn A, Ashmun RA, Shapiro LH, Arap W, Ruoslahti E: Aminopeptidase N is a receptor for tumor-homing peptides and a target for inhibiting angiogenesis. *Cancer Res* 2000, **60**(3):722-727.
101. Daniels TR, Bernabeu E, Rodríguez JA, Patel S, Kozman M, Chiappetta DA, Holler E, Ljubimova JY, Helguera G, Penichet ML: The transferrin receptor and the targeted delivery of therapeutic agents against cancer. *Biochimica et Biophysica Acta (BBA) - General Subjects* 2012, **1820**(3):291-317.
102. Ohno S-i, Takanashi M, Sudo K, Ueda S, Ishikawa A, Matsuyama N, Fujita K, Mizutani T, Ohgi T, Ochiya T *et al*: Systemically Injected Exosomes Targeted to EGFR Deliver Antitumor MicroRNA to Breast Cancer Cells. *Molecular Therapy* 2013, **21**(1):185-191.
103. Yang N, Ye Z, Li F, Mahato RI: HPMA polymer-based site-specific delivery of oligonucleotides to hepatic stellate cells. *Bioconjug Chem* 2009, **20**(2):213-221.

104. Du SL, Pan H, Lu WY, Wang J, Wu J, Wang JY: Cyclic Arg-Gly-Asp peptide-labeled liposomes for targeting drug therapy of hepatic fibrosis in rats. *J Pharmacol Exp Ther* 2007, **322**(2):560-568.
105. Hagens WI, Mattos A, Greupink R, de Jager-Krikken A, Reker-Smit C, van Loenen-Weemaes A, Gouw IA, Poelstra K, Beljaars L: Targeting 15d-prostaglandin J2 to hepatic stellate cells: two options evaluated. *Pharm Res* 2007, **24**(3):566-574.
106. Adrian JE, Poelstra K, Scherphof GL, Meijer DK, van Loenen-Weemaes AM, Reker-Smit C, Morselt HW, Zwiers P, Kamps JA: Effects of a new bioactive lipid-based drug carrier on cultured hepatic stellate cells and liver fibrosis in bile duct-ligated rats. *J Pharmacol Exp Ther* 2007, **321**(2):536-543.
107. Li C, Zhang D, Guo H, Hao L, Zheng D, Liu G, Shen J, Tian X, Zhang Q: Preparation and characterization of galactosylated bovine serum albumin nanoparticles for liver-targeted delivery of oridonin. *Int J Pharm* 2013, **448**(1):79-86.
108. Liang HF, Chen CT, Chen SC, Kulkarni AR, Chiu YL, Chen MC, Sung HW: Paclitaxel-loaded poly(gamma-glutamic acid)-poly(lactide) nanoparticles as a targeted drug delivery system for the treatment of liver cancer. *Biomaterials* 2006, **27**(9):2051-2059.
109. Cheong SJ, Lee CM, Kim SL, Jeong HJ, Kim EM, Park EH, Kim DW, Lim ST, Sohn MH: Superparamagnetic iron oxide nanoparticles-loaded chitosan-linoleic acid nanoparticles as an effective hepatocyte-targeted gene delivery system. *Int J Pharm* 2009, **372**(1-2):169-176.
110. Kim SI, Shin D, Choi TH, Lee JC, Cheon GJ, Kim KY, Park M, Kim M: Systemic and specific delivery of small interfering RNAs to the liver mediated by apolipoprotein A-I. *Mol Ther* 2007, **15**(6):1145-1152.
111. Miyata R, Ueda M, Jinno H, Konno T, Ishihara K, Ando N, Kitagawa Y: Selective targeting by preS1 domain of hepatitis B surface antigen conjugated with phosphorylcholine-based amphiphilic block copolymer micelles as a biocompatible, drug delivery carrier for treatment of human hepatocellular carcinoma with paclitaxel. *Int J Cancer* 2009, **124**(10):2460-2467.
112. Lin A, Liu Y, Huang Y, Sun J, Wu Z, Zhang X, Ping Q: Glycyrrhizin surface-modified chitosan nanoparticles for hepatocyte-targeted delivery. *Int J Pharm* 2008, **359**(1-2):247-253.
113. Stewart MP, Langer R, Jensen KF: Intracellular Delivery by Membrane Disruption: Mechanisms, Strategies, and Concepts. *Chemical Reviews* 2018, **118**(16):7409-7531.
114. Stahl P, Schwartz AL: Receptor-mediated endocytosis. *The Journal of clinical investigation* 1986, **77**(3):657-662.
115. Mellman I, Fuchs R, Helenius A: Acidification of the endocytic and exocytic pathways. *Annu Rev Biochem* 1986, **55**:663-700.
116. Gilleron J, Querbes W, Zeigerer A, Borodovsky A, Marsico G, Schubert U, Manygoats K, Seifert S, Andree C, Stöter M *et al*: Image-based analysis of lipid nanoparticle-mediated siRNA delivery, intracellular trafficking and endosomal escape. *Nat Biotechnol* 2013, **31**(7):638-646.
117. Weng A, Thakur M, Beceren-Braun F, Bachran D, Bachran C, Riese SB, Jenett-Siems K, Gilabert-Oriol R, Melzig MF, Fuchs H: The toxin component of targeted anti-tumor toxins determines their efficacy increase by saponins. *Mol Oncol* 2012:323 - 332.
118. Gilabert-Oriol R, Weng A, Trautner A, Weise C, Schmid D, Bhargava C, Niesler N, Wookey PJ, Fuchs H, Thakur M: Combinatorial approach to increase efficacy of Cetuximab, Panitumumab and Trastuzumab by dianthin conjugation and co-application of SO1861. . *Biochemical pharmacology* 2015, **97**:247 - 255.
119. Bachran D, Schneider S, Bachran C, Weng A, Melzig MF, Fuchs H: The Endocytic Uptake Pathways of Targeted Toxins Are Influenced by Synergistically Acting Gypsophila Saponins. *Molecular Pharmaceutics* 2011, **8**(6):2262-2272.
120. Holmes SEB, C.; Fuchs, H.; Weng, A.; Melzig, M.F.; Flavell, S.U.; Flavell, D.J. : Triterpenoid saponin augmention of saporin-based immunotoxin cytotoxicity for human leukaemia and lymphoma cells is partially immunospecific and target molecule dependent. *Immunopharmacology and immunotoxicology* 2015, **37**:42-55.

121. Moghimipour E, Handali S: Saponin: Properties, Methods of Evaluation and Applications, vol. 5; 2015.
122. Gilabert-Oriol R, Thakur M, von Mallinckrodt B, Hug T, Wiesner B, Eichhorst J, Melzig MF, Fuchs H, A. W: Modified trastuzumab and cetuximab mediate efficient toxin delivery while retaining antibody-dependent cell-mediated cytotoxicity in target cells. *Mol Pharm* 2013, **10**:4347 - 4357.
123. Fuchs H, Niesler N, Trautner A, Sama S, Jerz G, Panjideh H, Weng A: Glycosylated Triterpenoids as Endosomal Escape Enhancers in Targeted Tumor Therapies. *Biomedicines* 2017, **5**(2):14.
124. Heisler I, Sutherland M, Bachran C, Hebestreit P, Schnitger A, Melzig MF, Fuchs H: Combined application of saponin and chimeric toxins drastically enhances the targeted cytotoxicity on tumor cells. *J Control Release* 2005, **106**:123 - 137.
125. Bachran DS, S.; Bachran, C.; Urban, R.;Weng, A.; Melzig, M.F.; Hoffmann, C.; Kaufmann, A.M.;, Fuchs H: Epidermal growth factor receptor expression affects the efficacy of the combined application of saponin and a targeted toxin on human cervical carcinoma cells. *Int J Cancer* 2010, **127**:1453 - 1461.
126. Weng A, Thakur M, Beceren-Braun F, Bachran D, Bachran C, Riese SB, Jenett-Siems K, Gilabert-Oriol R, Melzig MF, Fuchs H: The toxin component of targeted anti-tumor toxins determinestheir efficacy increase by saponins. *Mol Oncol* 2012, **6**(3):323-332.
127. Fuchs H, Weng A, Gilabert-Oriol R: Augmenting the Efficacy of Immunotoxins and Other Targeted Protein Toxins by Endosomal Escape Enhancers. *Toxins* 2016, **8**(7):200.
128. Kolb HC, Finn MG, Sharpless KB: Click-Chemie: diverse chemische Funktionalität mit einer Handvoll guter Reaktionen. *Angewandte Chemie* 2001, **113**(11):2056-2075.
129. Lang K, Chin JW: Cellular Incorporation of Unnatural Amino Acids and Bioorthogonal Labeling of Proteins. *Chemical Reviews* 2014, **114**(9):4764-4806.
130. Boutureira O, Bernardes GJL: Advances in Chemical Protein Modification. *Chemical Reviews* 2015, **115**(5):2174-2195.
131. Rostovtsev V, Green L, Fokin V, Sharpless K: A Stepwise Huisgen Cycloaddition Process: Copper(I)-Catalyzed Regioselective "Ligation" of Azides and Terminal Alkynes. *Angew Chem Int Ed* 2002, **41**(14):2596-2599.
132. Tornøe CW, Christensen C, Meldal M: Peptidotriazoles on Solid Phase: [1,2,3]-Triazoles by Regiospecific Copper(I)-Catalyzed 1,3-Dipolar Cycloadditions of Terminal Alkynes to Azides. *The Journal of Organic Chemistry* 2002, **67**(9):3057-3064.
133. Agard NJ, Prescher JA, Bertozzi CR: A Strain-Promoted [3 + 2] Azide−Alkyne Cycloaddition for Covalent Modification of Biomolecules in Living Systems. *Journal of the American Chemical Society* 2004, **126**(46):15046-15047.
134. Dommerholt J, Rutjes FPJT, van Delft FL: Strain-Promoted 1,3-Dipolar Cycloaddition of Cycloalkynes and Organic Azides. *Top Curr Chem* 2016, **374**(16).
135. Oliveira BL, Guo Z, Bernardes GJL: Inverse electron demand Diels–Alder reactions in chemical biology. *Chemical Society Reviews* 2017, **46**(16):4895-4950.
136. Hoyle CE, Bowman CN: Thiol–Ene Click Chemistry. *Angewandte Chemie International Edition* 2010, **49**(9):1540-1573.
137. Posner T: Beiträge zur Kenntniss der ungesättigten Verbindungen. II. Ueber die Addition von Mercaptanen an ungesättigte Kohlenwasserstoffe. *Berichte der deutschen chemischen Gesellschaft* 1905, **38**(1):646-657.
138. Arslan M, Gevrek TN, Sanyal A, Sanyal R: Cyclodextrin mediated polymer coupling via thiol–maleimide conjugation: facile access to functionalizable hydrogels. *RSC Advances* 2014, **4**(101):57834-57841.
139. Sun Y, Liu H, Cheng L, Zhu S, Cai C, Yang T, Yang L, Ding P: Thiol Michael addition reaction: a facile tool for introducing peptides into polymer-based gene delivery systems. 2018, **67**(1):25-31.
140. Lowe AB: Thiol-ene "click" reactions and recent applications in polymer and materials synthesis. *Polymer Chemistry* 2010, **1**(1):17-36.

141. Nair DP, Podgórski M, Chatani S, Gong T, Xi W, Fenoli CR, Bowman CN: The Thiol-Michael Addition Click Reaction: A Powerful and Widely Used Tool in Materials Chemistry. *Chemistry of Materials* 2014, **26**(1):724-744.
142. Adzima BJ, Bowman CN: The emerging role of click reactions in chemical and biological engineering. *AIChE Journal* 2012, **58**(10):2952-2965.
143. Patra AK, Gahlay GK, Reddy BV, Gupta SK, Panda AK: Refolding, structural transition and spermatozoa-binding of recombinant bonnet monkey (Macaca radiata) zona pellucida glycoprotein-C expressed in Escherichia coli. *Eur J Biochem* 2000, **267**(24):7075-7081.
144. Bachran C, Schneider S, Riese SB, Bachran D, Urban R, Schellmann N, Zahn C, Sutherland M, Fuchs H: A lysine-free mutant of epidermal growth factor as targeting moiety of a targeted toxin. *Life Sciences* 2011, **88**(5):226-232.
145. Uhlén M, Fagerberg L, Hallström BM, Lindskog C, Oksvold P, Mardinoglu A, Sivertsson Å, Kampf C, Sjöstedt E, Asplund A *et al*: Proteomics. Tissue-based map of the human proteome. *Science* 2015, **347**(6220):1260419.
146. Li J, Chen L, Liu N, Li S, Hao Y, Zhang X: EGF-coated nano-dendriplexes for tumor-targeted nucleic acid delivery in vivo. *Drug Delivery* 2016, **23**(5):1718-1725.
147. Marzec E: Development and in vitro evaluation of a non-viral dendron-based gene delivery platform. Charité – Universitätsmedizin Berlin; 2023.
148. Lin Y, Liu YX, Cislo T, Mason BL, Yu MY: Expression and characterization of the preS1 peptide of hepatitis B surface antigen in Escherichia coli. *J Med Virol* 1991, **33**(3):181-187.
149. Mi Z, Guo J, Feng F, Chen W, Zhang X, Tong Y: Expression of HBV Pre S1 peptide in E. coli and product characterization. *Chin Med Sci J* 1997, **12**(1):37-40.
150. Qian B, Shen H, Xiong J, Chen L, Zhang L, Jia J, Wang Y, Zhang Z, Yuan Z, Cao K *et al*: Expression and purification of the synthetic preS1 gene of Hepatitis B Virus with preferred Escherichia coli codon preference. *Protein Expression and Purification* 2006, **48**(1):74-80.
151. Deng Q, Kong YY, Xie YH, Wang Y: Expression and purification of the complete PreS region of hepatitis B Virus. *World J Gastroenterol* 2005, **11**(20):3060-3064.
152. di Guan C, Li P, Riggs PD, Inouye H: Vectors that facilitate the expression and purification of foreign peptides in Escherichia coli by fusion to maltose-binding protein. *Gene* 1988, **67**(1):21-30.
153. Dharra R, Talwar S, Singh Y, Gupta R, Cirillo JD, Pandey AK, Kulharia M, Mehta PK: Rational design of drug-like compounds targeting Mycobacterium marinum MelF protein. *PLOS ONE* 2017, **12**(9):e0183060.
154. de Beer MC, Durbin DM, Cai L, Jonas A, de Beer FC, van der Westhuyzen DR: Apolipoprotein A-I conformation markedly influences HDL interaction with scavenger receptor BI. *Journal of Lipid Research* 2001, **42**(2):309-313.
155. George-Nascimento C, Gyenes A, Halloran SM, Merryweather J, Valenzuela P, Steimer KS, Masiarz FR, Randolph A: Characterization of recombinant human epidermal growth factor produced in yeast. *Biochemistry* 1988, **27**(2):797-802.
156. Hamsa PV, Kachroo P, Chattoo BB: Production and secretion of biologically active human epidermal growth factor in Yarrowia lipolytica. *Curr Genet* 1998, **33**(3):231-237.
157. Heo JH, Won HS, Kang HA, Rhee SK, Chung BH: Purification of recombinant human epidermal growth factor secreted from the methylotrophic yeast Hansenula polymorpha. *Protein Expr Purif* 2002, **24**(1):117-122.
158. Su Z, Huang Y, Zhou Q, Wu Z, Wu X, Zheng Q, Ding C, Li X: High-level expression and purification of human epidermal growth factor with SUMO fusion in Escherichia coli. *Protein Pept Lett* 2006, **13**(8):785-792.
159. Ma Y, Yu J, Lin J, Wu S, Li S, Wang J: High Efficient Expression, Purification, and Functional Characterization of Native Human Epidermal Growth Factor in Escherichia coli. *BioMed Research International* 2016, **2016**:3758941.
160. Tegel H, Tourle S, Ottosson J, Persson A: Increased levels of recombinant human proteins with the Escherichia coli strain Rosetta(DE3). *Protein Expression and Purification* 2010, **69**(2):159-167.

161. Kane JF, Hartley DL: Formation of recombinant protein inclusion bodies in Escherichia coli. *Trends in Biotechnology* 1988, **6**(5):95-101.
162. Przybycien TM, Dunn JP, Valax P, Georgiou G: Secondary structure characterization of beta-lactamase inclusion bodies. *Protein Eng* 1994, **7**(1):131-136.
163. Khan RH, Rao KB, Eshwari AN, Totey SM, Panda AK: Solubilization of recombinant ovine growth hormone with retention of native-like secondary structure and its refolding from the inclusion bodies of Escherichia coli. *Biotechnol Prog* 1998, **14**(5):722-728.
164. Zou Q, Habermann-Rottinghaus SM, Murphy KP: Urea effects on protein stability: hydrogen bonding and the hydrophobic effect. *Proteins* 1998, **31**(2):107-115.
165. Bach M, Hölig P, Schlosser E, Völkel T, Graser A, Müller R, Kontermann RE: Isolation from phage display libraries of lysine-deficient human epidermal growth factor variants for directional conjugation as targeting ligands. *Protein Engineering, Design and Selection* 2003, **16**(12):1107-1113.
166. Zhang A, Nakanishi J: Improved anti-cancer effect of epidermal growth factor-gold nanoparticle conjugates by protein orientation through site-specific mutagenesis. *Sci Technol Adv Mater* 2021, **22**(1):616-626.
167. Gilabert-Oriol R, Thakur M, Weise C, Dernedde J, von Mallinckrodt B, Fuchs H, Weng A: Small structural differences of targeted anti-tumor toxins result in strong variation of protein expression. *Protein Expression and Purification* 2013, **91**(1):54-60.
168. von Mallinckrodt B, Thakur M, Weng A, Gilabert-Oriol R, Dürkop H, Brenner W, Lukas M, Beindorff N, Melzig MF, Fuchs H: Dianthin-EGF is an effective tumor targeted toxin in combination with saponins in a xenograft model for colon carcinoma. *Future Oncol* 2014, **10**(14):2161-2175.
169. Panowski S, Bhakta S, Raab H, Polakis P, Junutula JR: Site-specific antibody drug conjugates for cancer therapy. *MAbs* 2014, **6**(1):34-45.
170. Boylan NJ, Zhou W, Proos RJ, Tolbert TJ, Wolfe JL, Laurence JS: Conjugation site heterogeneity causes variable electrostatic properties in Fc conjugates. *Bioconjug Chem* 2013, **24**(6):1008-1016.
171. Axup JY, Bajjuri KM, Ritland M, Hutchins BM, Kim CH, Kazane SA, Halder R, Forsyth JS, Santidrian AF, Stafin K *et al*: Synthesis of site-specific antibody-drug conjugates using unnatural amino acids. *Proc Natl Acad Sci U S A* 2012, **109**(40):16101-16106.
172. van Geel R, Wijdeven MA, Heesbeen R, Verkade JM, Wasiel AA, van Berkel SS, van Delft FL: Chemoenzymatic Conjugation of Toxic Payloads to the Globally Conserved N-Glycan of Native mAbs Provides Homogeneous and Highly Efficacious Antibody-Drug Conjugates. *Bioconjug Chem* 2015, **26**(11):2233-2242.
173. Levashova Z, Backer MV, Horng G, Felsher D, Backer JM, Blankenberg FG: SPECT and PET Imaging of EGF Receptors with Site-Specifically Labeled EGF and Dimeric EGF. *Bioconjugate Chemistry* 2009, **20**(4):742-749.
174. Mbua NE, Guo J, Wolfert MA, Steet R, Boons GJ: Strain-promoted alkyne-azide cycloadditions (SPAAC) reveal new features of glycoconjugate biosynthesis. *Chembiochem* 2011, **12**(12):1912-1921.
175. Swali V, Wells NJ, Langley GJ, Bradley M: Solid-Phase Dendrimer Synthesis and the Generation of Super-High-Loading Resin Beads for Combinatorial Chemistry. *The Journal of Organic Chemistry* 1997, **62**(15):4902-4903.
176. Guillier F, Orain D, Bradley M: Linkers and cleavage strategies in solid-phase organic synthesis and combinatorial chemistry. *Chem Rev* 2000, **100**(6):2091-2158.
177. Castro V, Rodriguez H, Albericio F: Wang Linker Free of Side Reactions. *Organic Letters* 2013, **15**(2):246-249.
178. Deng F-K, Mandal K, Luisier S, Kent SBH: Synthesis and comparative properties of two amide-generating resin linkers for use in solid phase peptide synthesis. *Journal of Peptide Science* 2010, **16**(10):545-550.
179. Sakakibara S, Shimonishi Y, Kishida Y, Okada M, Sugihara H: Use of anhydrous hydrogen fluoride in peptide synthesis. I. Behavior of various protective groups in anhydrous hydrogen fluoride. *Bull Chem Soc Jpn* 1967, **40**(9):2164-2167.

180. Raz R, Burlina F, Ismail M, Downward J, Li J, Smerdon SJ, Quibell M, White PD, Offer J: HF-Free Boc Synthesis of Peptide Thioesters for Ligation and Cyclization. *Angewandte Chemie International Edition* 2016, **55**(42):13174-13179.
181. König W, Geiger R: A new method for synthesis of peptides: activation of the carboxyl group with dicyclohexylcarbodiimide using 1-hydroxybenzotriazoles as additives. *Chem Ber* 1970, **103**(3):788-798.
182. Carpino LA: 1-Hydroxy-7-azabenzotriazole. An efficient peptide coupling additive. *Journal of the American Chemical Society* 1993, **115**(10):4397-4398.
183. Castro B, Dormoy JR, Evin G, Selve C: Reactifs de couplage peptidique I (1) - l'hexafluorophosphate de benzotriazolyl N-oxytrisdimethylamino phosphonium (B.O.P.). *Tetrahedron Letters* 1975, **16**(14):1219-1222.
184. Coste J, Le-Nguyen D, Castro B: PyBOP®: A new peptide coupling reagent devoid of toxic by-product. *Tetrahedron Letters* 1990, **31**(2):205-208.
185. Carpino LA, Ionescu D, El-Faham A: Peptide Coupling in the Presence of Highly Hindered Tertiary Amines. *The Journal of Organic Chemistry* 1996, **61**(7):2460-2465.
186. Poulain RF, Tartar AL, Déprez BtP: Parallel synthesis of 1,2,4-oxadiazoles from carboxylic acids using an improved, uronium-based, activation. *Tetrahedron Letters* 2001, **42**(8):1495-1498.
187. El-Faham A, Albericio F: COMU: a third generation of uronium-type coupling reagents. *J Pept Sci* 2010, **16**(1):6-9.
188. MacMillan DS, Murray J, Sneddon HF, Jamieson C, Watson AJB: Evaluation of alternative solvents in common amide coupling reactions: replacement of dichloromethane and N,N-dimethylformamide. *Green Chemistry* 2013, **15**(3):596-600.
189. Lawrenson SB, Arav R, North M: The greening of peptide synthesis. *Green Chemistry* 2017, **19**(7):1685-1691.
190. Tam JP: Synthetic peptide vaccine design: synthesis and properties of a high-density multiple antigenic peptide system. *Proceedings of the National Academy of Sciences* 1988, **85**(15):5409-5413.
191. Wang L, Ji X, Guo D, Shi C, Luo J: Facial Solid-Phase Synthesis of Well-Defined Zwitterionic Amphiphiles for Enhanced Anticancer Drug Delivery. *Molecular Pharmaceutics* 2021, **18**(6):2349-2359.
192. Liao Y, Chan Y-T, Molakaseema V, Selvaraj A, Chen H-T, Wang Y-M, Choo Y-M, Kao C-L: Facile Solid-Phase Synthesis of Well-Defined Defect Lysine Dendrimers. *ACS Omega* 2022, **7**(26):22896-22905.
193. Eom KD, Park SM, Tran HD, Kim MS, Yu RN, Yoo H: Dendritic alpha,epsilon-poly(L-lysine)s as delivery agents for antisense oligonucleotides. *Pharm Res* 2007, **24**(8):1581-1589.
194. Sheveleva Nadezhda N, Markelov DA, Vovk MA, Mikhailova ME, Tarasenko II, Tolstoy PM, Neelov IM, Lähderanta E: Lysine-based dendrimer with double arginine residues. *RSC Advances* 2019, **9**(31):18018-18026.
195. Deng X, Li X, Chen W, Zhao T, Huang W, Qian H: Design, synthesis and biological evaluation of peptide dendrimers with wound healing promoting activity. *Medicinal Chemistry Research* 2017, **26**(3):580-586.
196. Bellassai N, Marti A, Spoto G, Huskens J: Low-fouling, mixed-charge poly-l-lysine polymers with anionic oligopeptide side-chains. *Journal of Materials Chemistry B* 2018, **6**(46):7662-7673.
197. Ohsaki M, Okuda T, Wada A, Hirayama T, Niidome T, Aoyagi H: In vitro gene transfection using dendritic poly(L-lysine). *Bioconjug Chem* 2002, **13**(3):510-517.
198. Nair A, Bu J, Bugno J, Rawding PA, Kubiatowicz LJ, Jeong WJ, Hong S: Size-Dependent Drug Loading, Gene Complexation, Cell Uptake, and Transfection of a Novel Dendron-Lipid Nanoparticle for Drug/Gene Co-delivery. *Biomacromolecules* 2021, **22**(9):3746-3755.
199. Rejman J, Oberle V, Zuhorn IS, Hoekstra D: Size-dependent internalization of particles via the pathways of clathrin- and caveolae-mediated endocytosis. *Biochem J* 2004, **377**(Pt 1):159-169.

200. Mislick KA, Baldeschwieler JD: Evidence for the role of proteoglycans in cation-mediated gene transfer. *Proc Natl Acad Sci U S A* 1996, **93**(22):12349-12354.
201. Alazzo A, Lovato T, Collins H, Taresco V, Stolnik S, Soliman M, Spriggs K, Alexander C: Structural variations in hyperbranched polymers prepared via thermal polycondensation of lysine and histidine and their effects on DNA delivery. *Journal of Interdisciplinary Nanomedicine* 2018, **3**(2):38-54.
202. Coelho F, Botelho C, Paris JL, Marques EF, Silva BFB: Influence of the media ionic strength on the formation and in vitro biological performance of polycation-DNA complexes. *Journal of Molecular Liquids* 2021, **344**:117930.
203. Pezzoli D, Giupponi E, Mantovani D, Candiani G: Size matters for in vitro gene delivery: investigating the relationships among complexation protocol, transfection medium, size and sedimentation. *Sci Rep* 2017, **7**:44134.
204. Gorzkiewicz M, Kopeć O, Janaszewska A, Konopka M, Pędziwiatr-Werbicka E, Tarasenko II, Bezrodnyi VV, Neelov IM, Klajnert-Maculewicz B: Poly(lysine) Dendrimers Form Complexes with siRNA and Provide Its Efficient Uptake by Myeloid Cells: Model Studies for Therapeutic Nucleic Acid Delivery. *International Journal of Molecular Sciences* 2020, **21**(9):3138.
205. Kadlecova Z, Baldi L, Hacker D, Wurm FM, Klok H-A: Comparative Study on the In Vitro Cytotoxicity of Linear, Dendritic, and Hyperbranched Polylysine Analogues. *Biomacromolecules* 2012, **13**(10):3127-3137.
206. ReFaey K, Tripathi S, Grewal SS, Bhargav AG, Quinones DJ, Chaichana KL, Antwi SO, Cooper LT, Meyer FB, Dronca RS *et al*: Cancer Mortality Rates Increasing vs Cardiovascular Disease Mortality Decreasing in the World: Future Implications. *Mayo Clinic Proceedings: Innovations, Quality & Outcomes* 2021, **5**(3):645-653.
207. Aslam M, Naveed S, Ahmad A, Abbas Z, Gull I, Athar M: Side Effects of Chemotherapy in Cancer Patients and Evaluation of Patients Opinion about Starvation Based Differential Chemotherapy. *Journal of Cancer Therapy* 2014, **5**:817-822.
208. Blessing T, Kursa M, Holzhauser R, Kircheis R, Wagner E: Different Strategies for Formation of PEGylated EGF-Conjugated PEI/DNA Complexes for Targeted Gene Delivery. *Bioconjugate Chemistry* 2001, **12**(4):529-537.
209. Buñuales M, Düzgüneş N, Zalba S, Garrido MJ, ILarduya CTd: Efficient gene delivery by EGF-lipoplexes in vitro and in vivo. *Nanomedicine* 2011, **6**(1):89-98.
210. Surre J, Saint-Ruf C, Collin V, Orenga S, Ramjeet M, Matic I: Strong increase in the autofluorescence of cells signals struggle for survival. *Scientific Reports* 2018, **8**(1):12088.
211. Kawamoto T, Mendelsohn J, Le A, Sato GH, Lazar CS, Gill GN: Relation of epidermal growth factor receptor concentration to growth of human epidermoid carcinoma A431 cells. *J Biol Chem* 1984, **259**(12):7761-7766.
212. Filmus J, Pollak MN, Cailleau R, Buick RN: MDA-468, a human breast cancer cell line with a high number of epidermal growth factor (EGF) receptors, has an amplified EGF receptor gene and is growth inhibited by EGF. *Biochemical and Biophysical Research Communications* 1985, **128**(2):898-905.
213. Fonge H, Lee H, Reilly RM, Allen C: Multifunctional block copolymer micelles for the delivery of 111In to EGFR-positive breast cancer cells for targeted Auger electron radiotherapy. *Mol Pharm* 2010, **7**(1):177-186.
214. Zhang Z, Chen J, Ding L, Jin H, Lovell JF, Corbin IR, Cao W, Lo PC, Yang M, Tsao MS *et al*: HDL-mimicking peptide-lipid nanoparticles with improved tumor targeting. *Small* 2010, **6**(3):430-437.
215. Jin H, Lovell JF, Chen J, Ng K, Cao W, Ding L, Zhang Z, Zheng G: Investigating the specific uptake of EGF-conjugated nanoparticles in lung cancer cells using fluorescence imaging. *Cancer Nanotechnology* 2010, **1**(1):71-78.
216. Creixell M, Herrera AP, Ayala V, Latorre-Esteves M, Pérez-Torres M, Torres-Lugo M, Rinaldi C: Preparation of epidermal growth factor (EGF) conjugated iron oxide nanoparticles and their internalization into colon cancer cells. *Journal of Magnetism and Magnetic Materials* 2010, **322**(15):2244-2250.

217. Sandoval MA, Sloat BR, Lansakara PD, Kumar A, Rodriguez BL, Kiguchi K, Digiovanni J, Cui Z: EGFR-targeted stearoyl gemcitabine nanoparticles show enhanced anti-tumor activity. *J Control Release* 2012, **157**(2):287-296.
218. Shimada T, Ueda M, Jinno H, Chiba N, Wada M, Watanabe J, Ishihara K, Kitagawa Y: Development of Targeted Therapy with Paclitaxel Incorporated into EGF-conjugated Nanoparticles. *Anticancer Research* 2009, **29**(4):1009-1014.
219. Gonzalez G, Crombet T, Lage A: Chronic Vaccination with a Therapeutic EGF-Based Cancer Vaccine: A Review of Patients Receiving Long Lasting Treatment. *Current Cancer Drug Targets* 2011, **11**(1):103-110.

7 Appendix

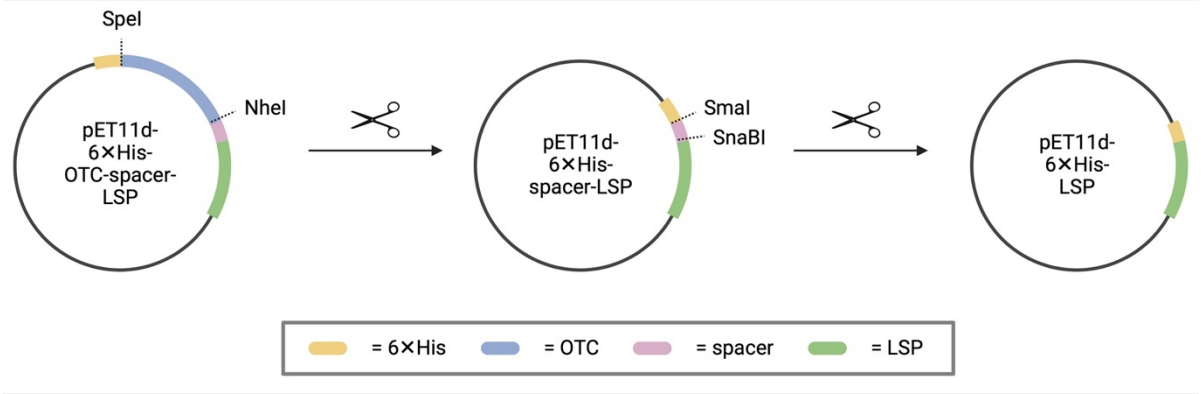

Figure S1: Developing of pET11d-6×His-LSP plasmid using restriction enzyme digestion. *6×His-OTC-spacer-LSP in pET11d vector was digested using the restriction enzymes SpeI and NheI to cut out OTC and create 6×His-OTC-spacer-LSP. This plasmid was digested with SmaI and SnaBI to obtain 6×His-LSP in the pET11d vector. OTC = ornithine transcarbamylase, LSP = large surface protein. Created with BioRender.com.*

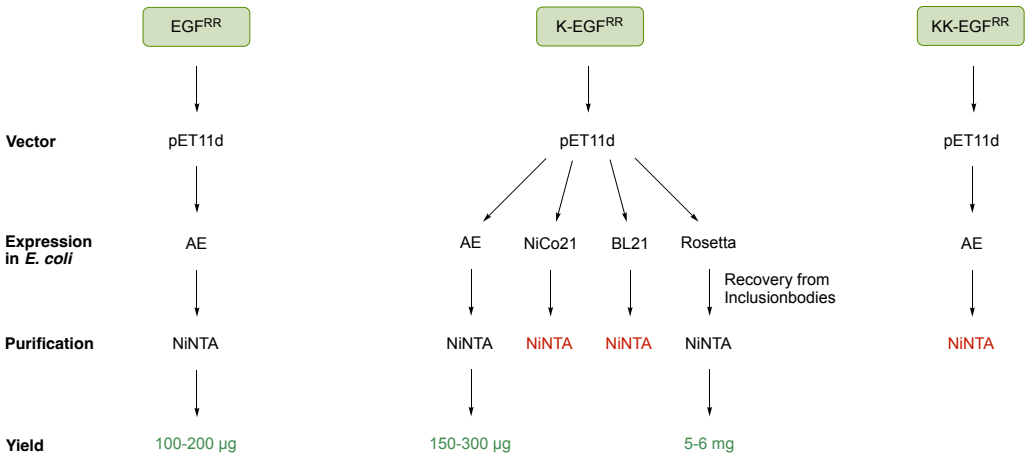

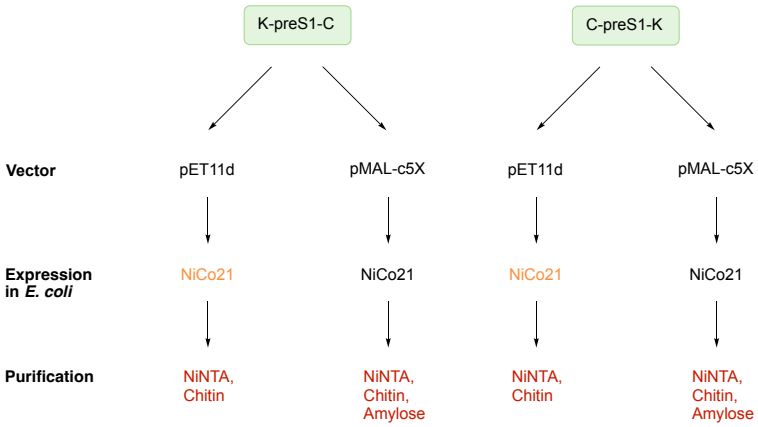

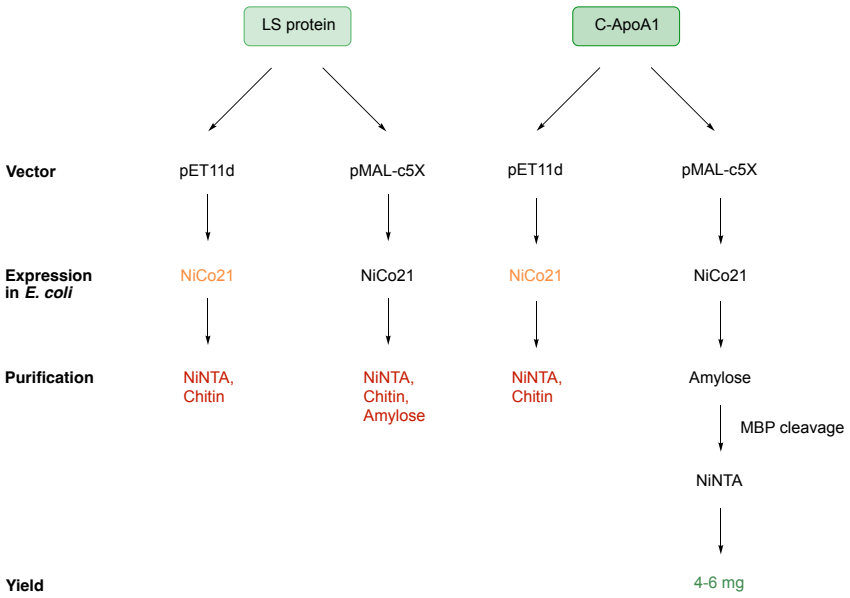

Figure S2: Overview of the recombinant expression outcome of the targeting ligands.
Cancer targeting: EGF^{RR}, K-EGF^{RR}, KK-EGF^{RR}; liver targeting: K-preS1-C, C-preS1-K, LS protein, C-ApoA1. Red indicates that this step was not successful and therefore the expression and purification was cancelled at this point. Orange indicates that at this point it was not quite clear if the desired product was obtained. Green indicates the final yield per 1 L expression approach and that the expression and purification was successful for this ligand.

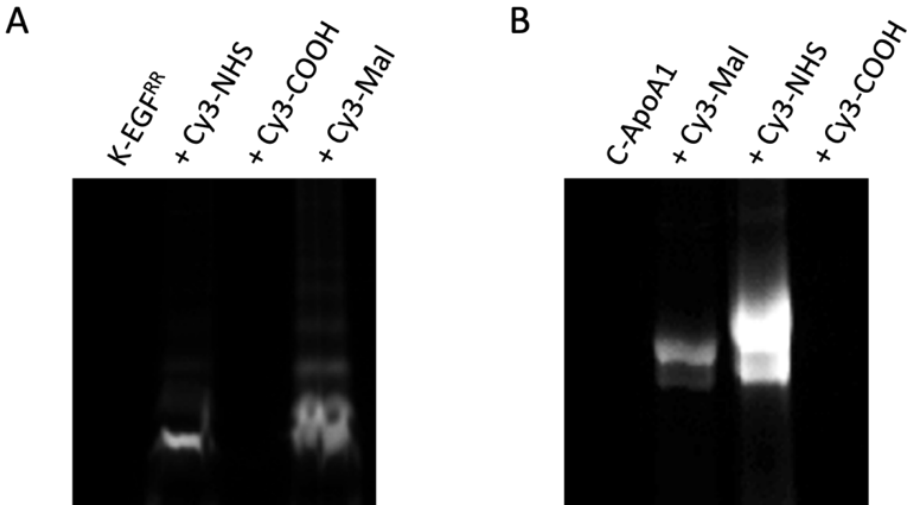

Figure S3: Accessibility evaluation of the ligand variants.
SDS-PAGE of the conjugation of Cy3-dyes to K-EGF^{RR} (A) and C-ApoA1 (B) to confirm the accessibility of the functional groups. The image was obtained by using the Cy3-channel of a VersaDoc device.

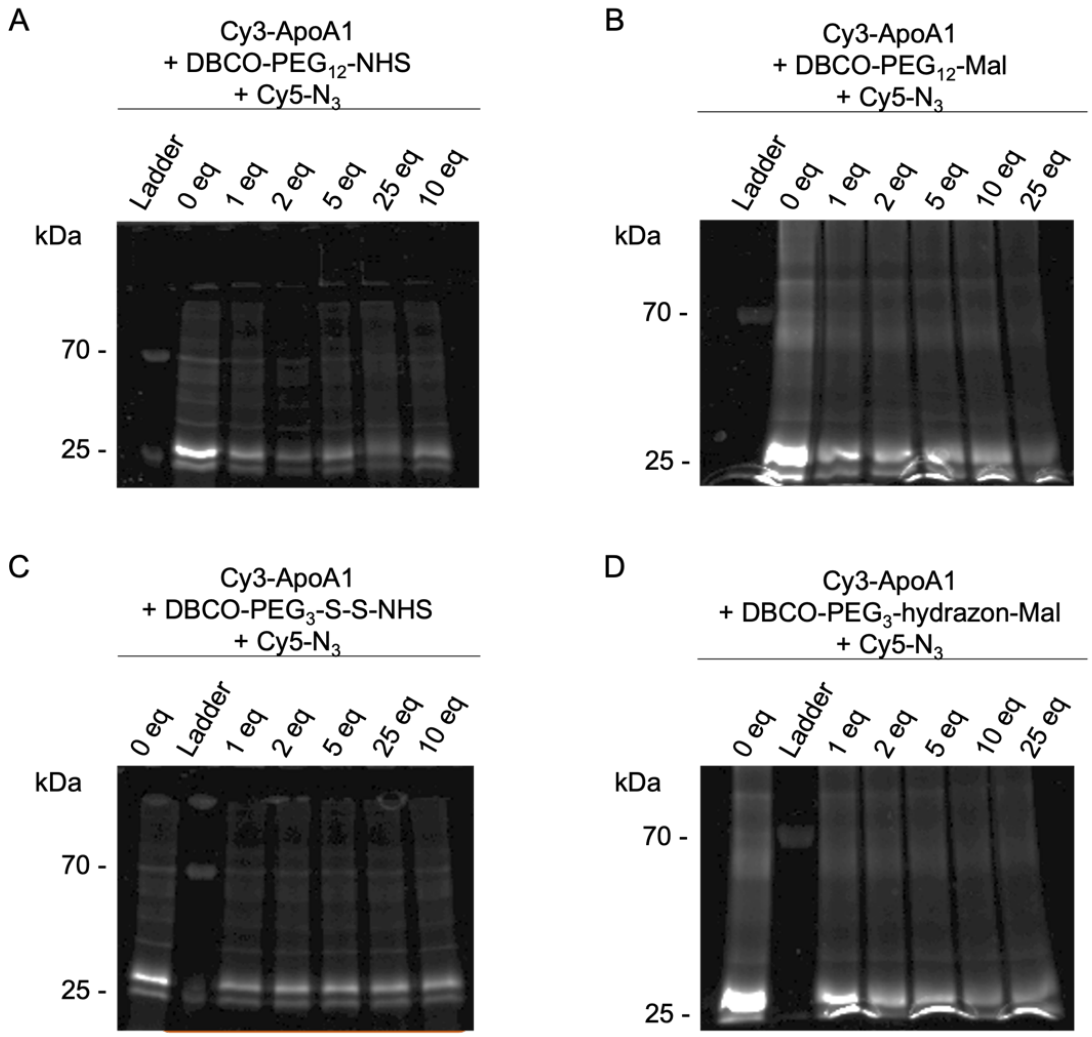

Figure S4: Verification of the successful conjugation of the linker to Cy3-C-ApoA1.
Conjugation of (A) non-cleavable and (B) cleavable DBCO-PEG-Mal linker at Cy3-C-ApoA1 with different equivalents of linker. Conjugation of (C) non-cleavable and (D) cleavable DBCO-PEG-NHS linker at Cy3-C-ApoA1 with different equivalents of linker. Afterwards the Cy3-C-ApoA1-Linker conjugates were incubated with Cy5-N_3, to check if the conjugation of the linker was successful. The image was obtained by using the Cy3-channel of a VersaDoc device.

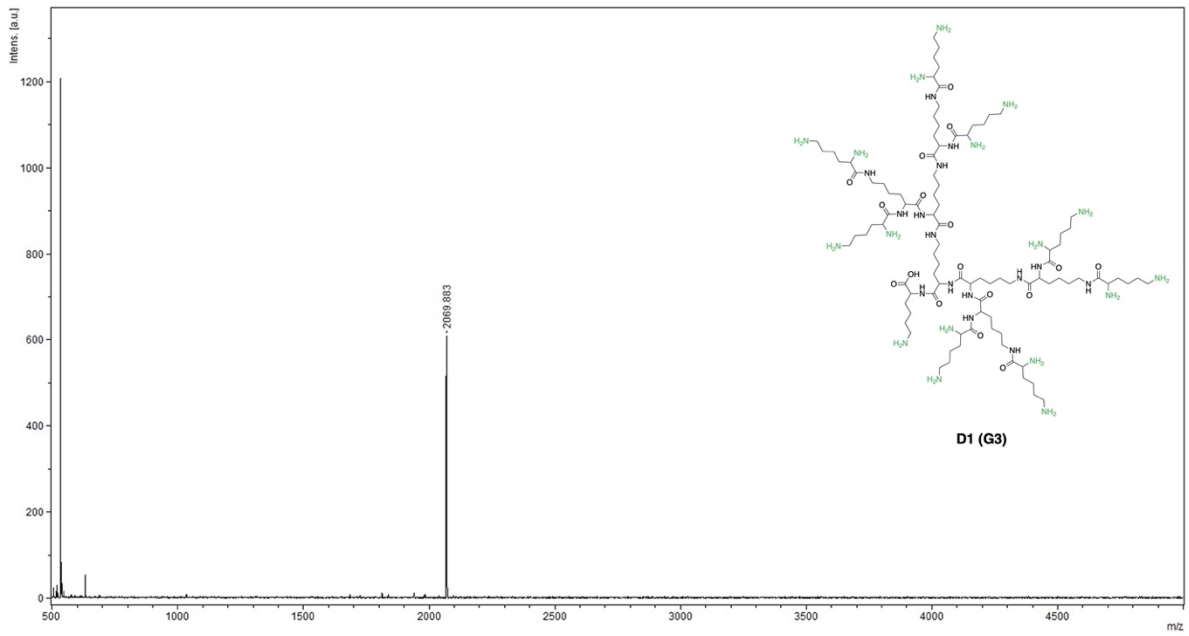

Figure S5: MALDI-TOF-MS of D1 (G3) after HPLC purification.
m/z = 2069.883 ([M+H]⁺

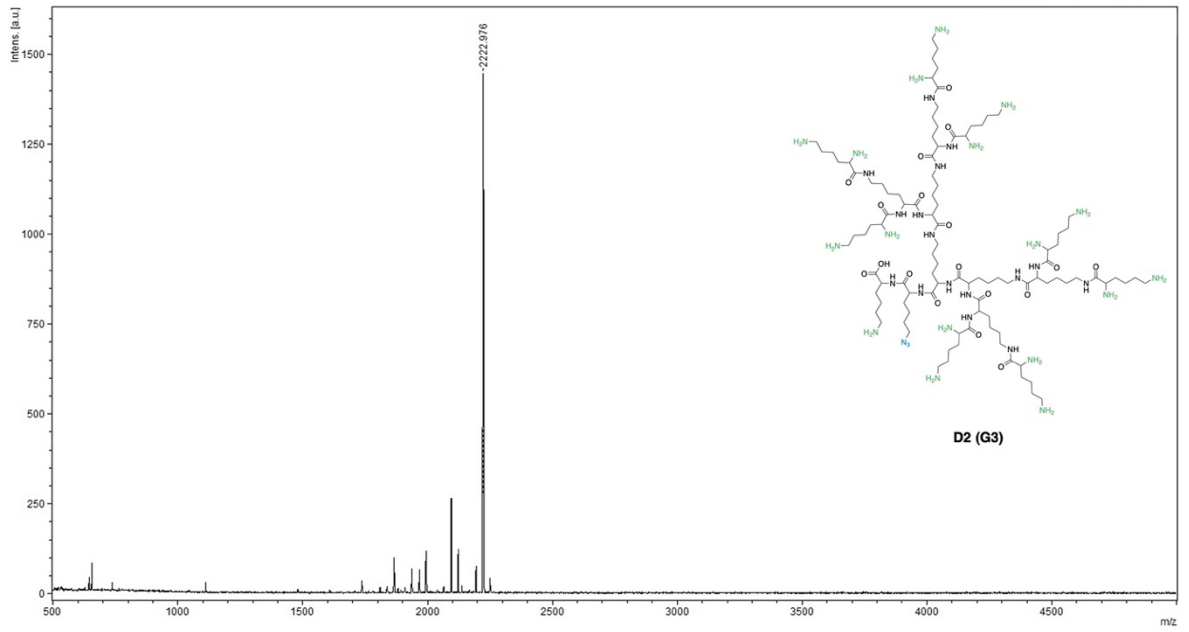

Figure S6: MALDI-TOF-MS of D2 (G3) after HPLC purification.
m/z = 2222.976 ([M+H]⁺)

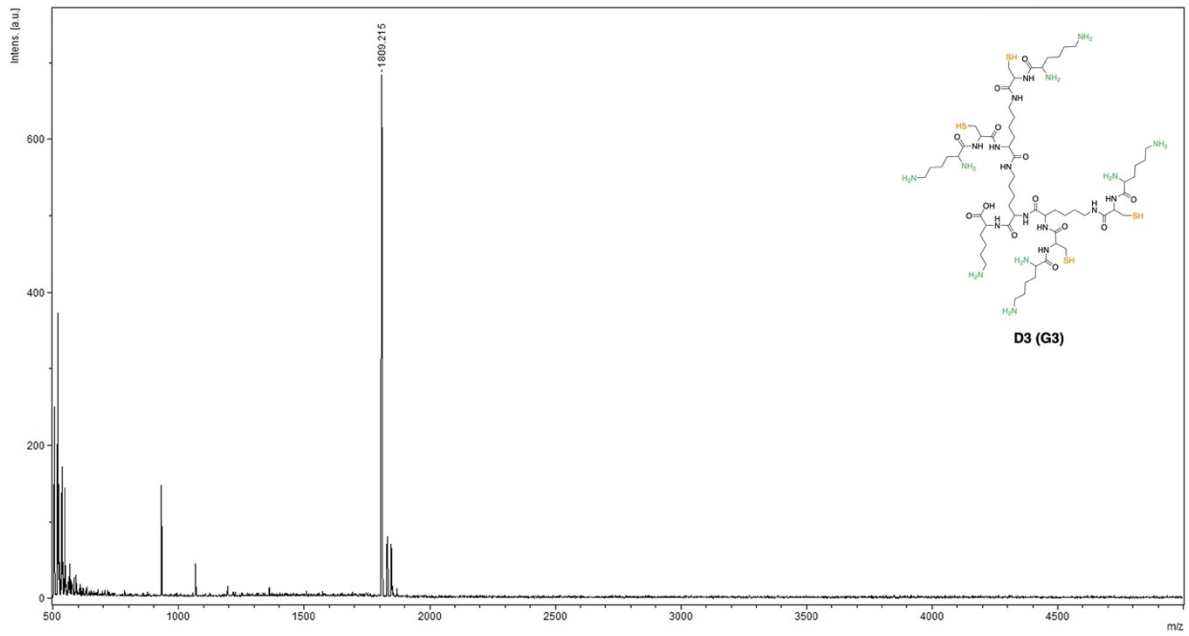

Figure S7: MALDI-TOF-MS of D3 (G3) after HPLC purification.
m/z = 1809.215 ($[M+H]^+$)

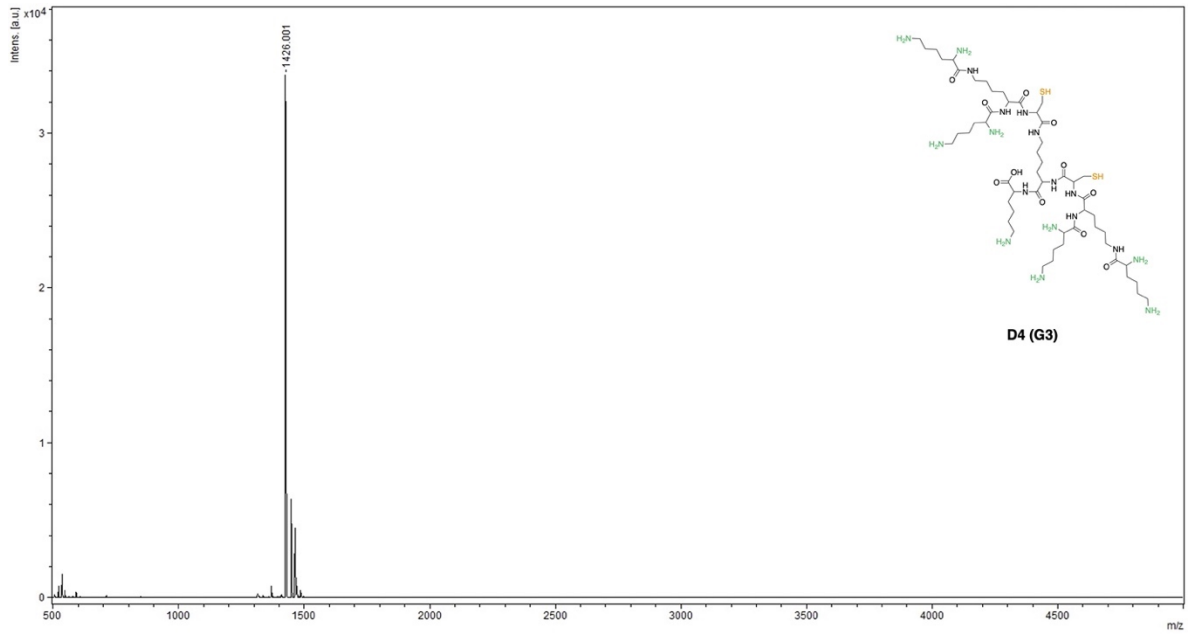

Figure S8: MALDI-TOF-MS of D4 (G3) after HPLC purification.
m/z = 1426.001 ($[M+H]^+$)

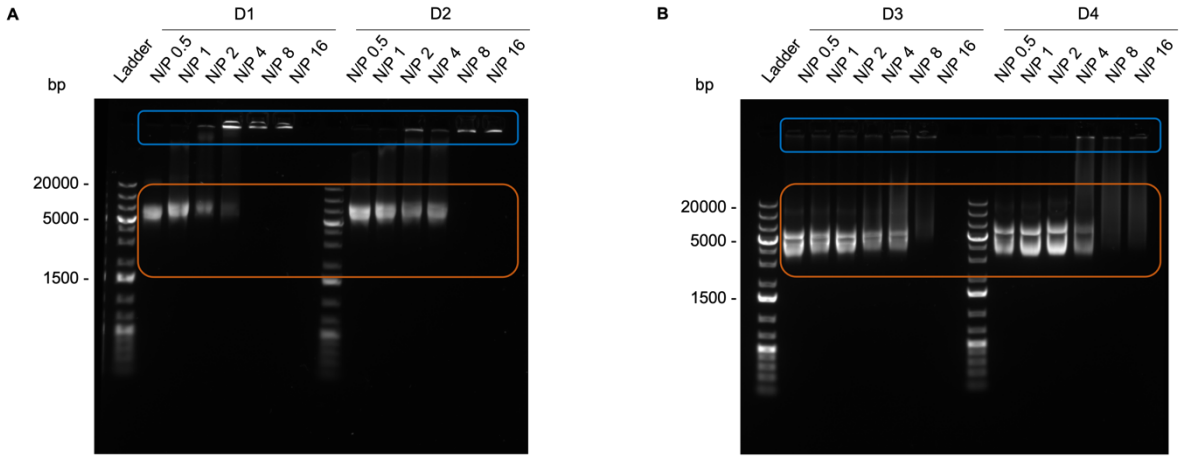

Figure S9: Agarose gel retardation assay of D1–D4 [N/P 0.5–16].
Blue indicates polyplexed eGFP plasmid, whereas orange indicates free eGFP plasmid.

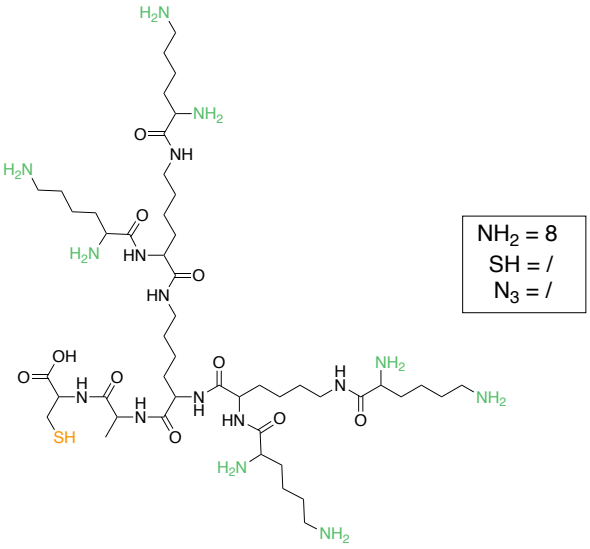

D5 (G2)

Figure S10: Structure of D5 (G2).

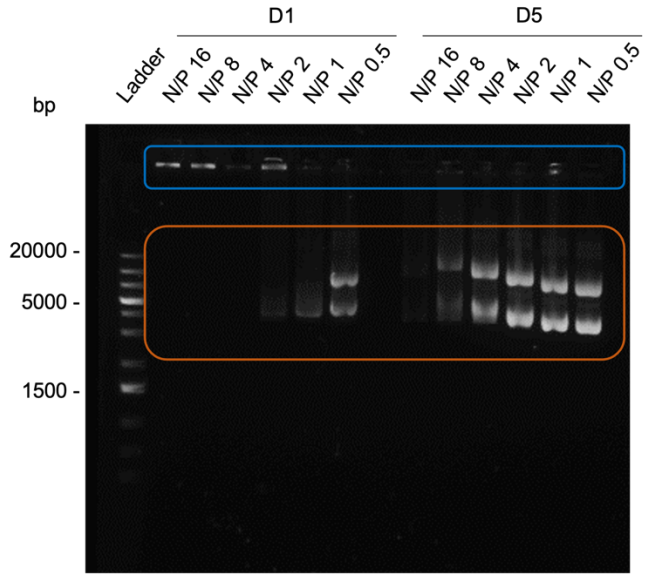

Figure S11: Agarose gel retardation assay of D1 [N/P 0.5–16] and D5 [N/P 0.5–16].
Blue indicates polyplexed eGFP plasmid, whereas orange indicates free eGFP plasmid.

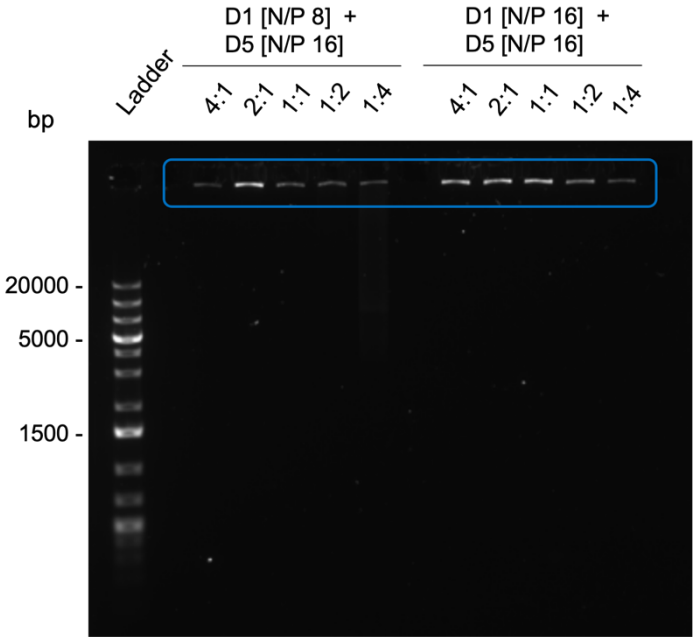

Figure S12: Agarose gel retardation assay of D1+D5 [N/P 8+16, D1/D5] and D1+D5 [N/P 16+16, D1/D5].
Blue indicates polyplexed eGFP plasmid.

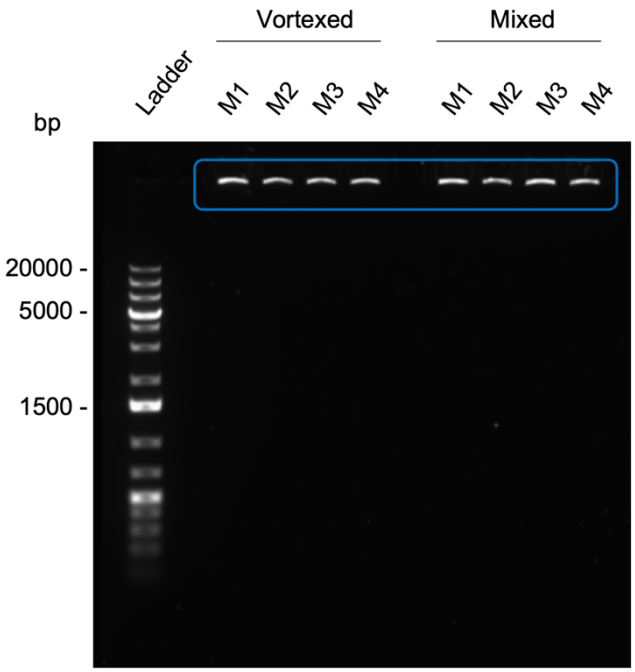

Figure S13: Agarose gel retardation assay of D1+D5 [N/P 16+16, D:D 4:1, M1-4 (vortexed)] and D5 [N/P 16+16, D:D 4:1, M1-4 (mixed)].
Blue indicates polyplexed eGFP plasmid.

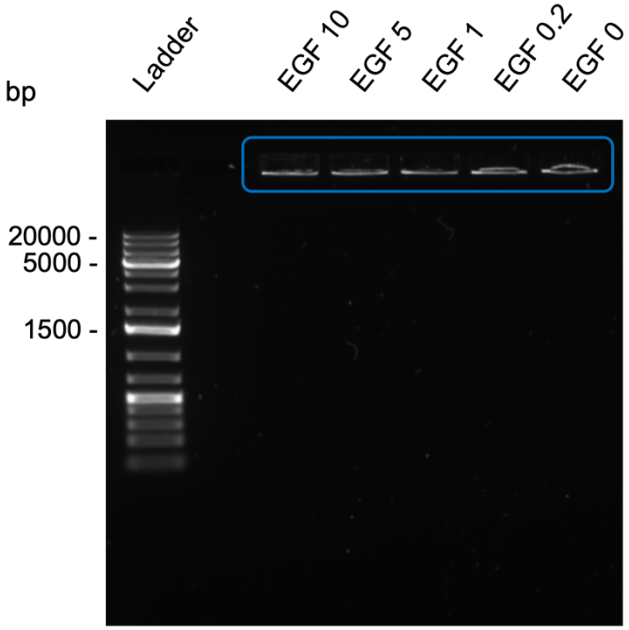

Figure S14: Agarose gel retardation assay of D1+D5 [N/P 16+16, D:D 4:1, M1 (vortexed), EGF].
Blue indicates polyplexed eGFP plasmid

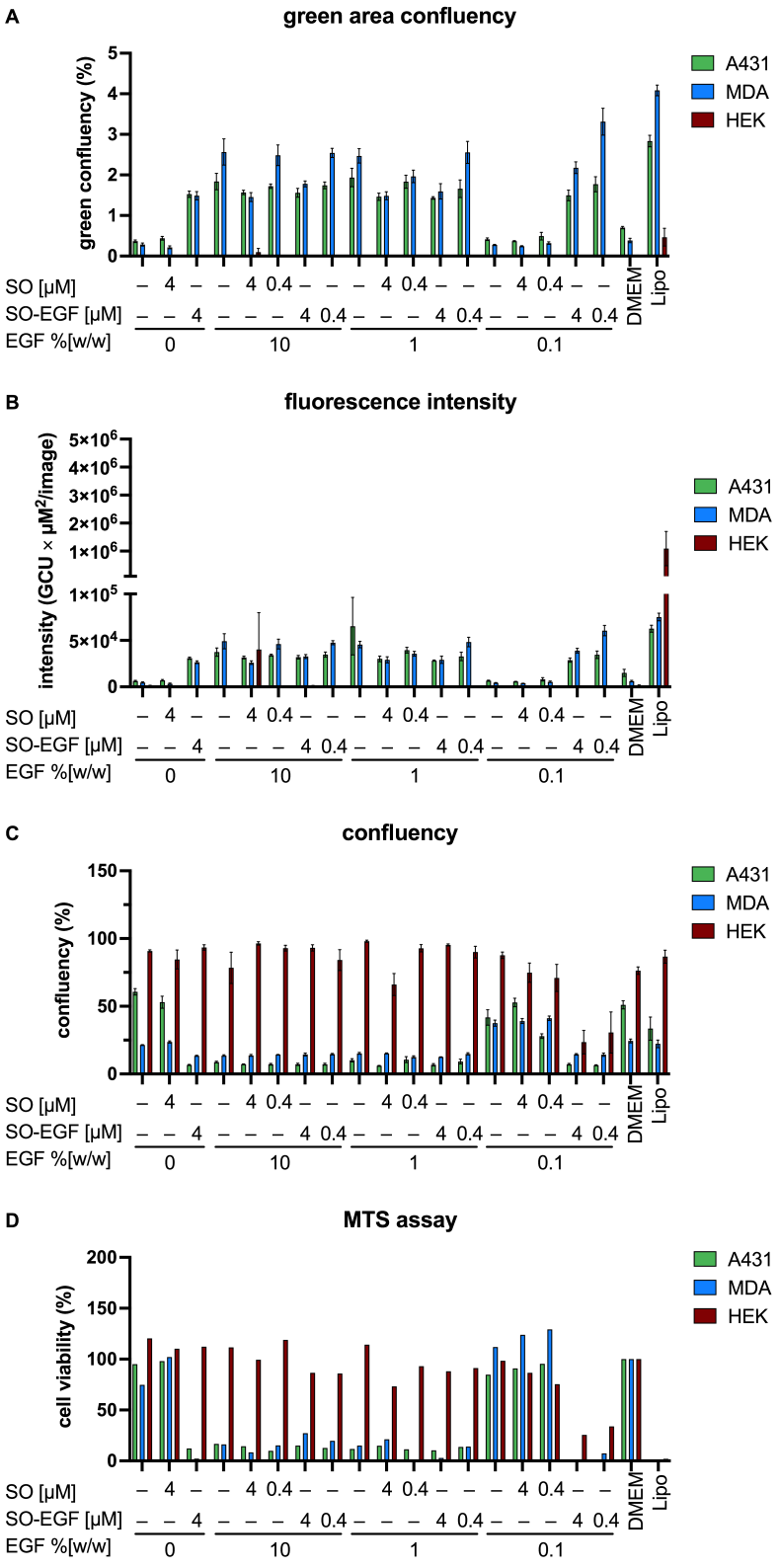

Figure S15: Transfection efficiency of eGFP plasmid and cytotoxicity of D2 [N/P 16, EGF 0–10 (pp)] with and without additional SO1861 or SO1861-EGF.
The assay was performed on EGFR positive cell lines A431 (green) and MDA-MB 468 (blue) as well as on EGFR negative cell line HEK293-FT (red). Analysis of (A) green area confluency, (B) fluorescence intensity and (C) confluency were performed by Incucyte measurements. (D) The absorbance of MTS proliferation assay was determined by SpectraMax 340. The mean value ± SEM is shown (N = 1, n = 3).

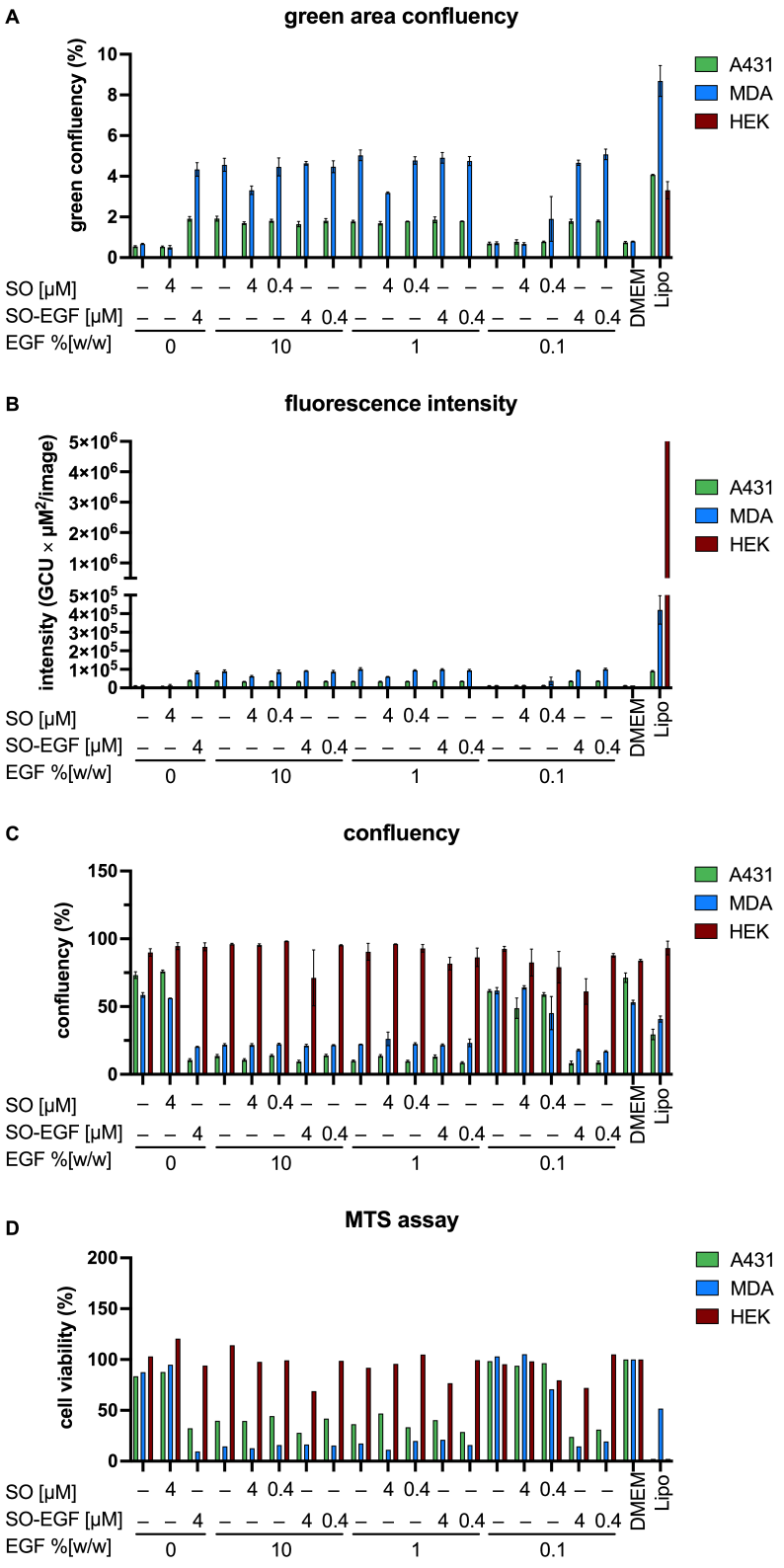

Figure S16: Transfection efficiency of eGFP plasmid and cytotoxicity of D2 [N/P 16, EGF 0–10 (before)] with and without additional SO1861 or SO1861-EGF.
The assay was performed on EGFR positive cell lines A431 (green) and MDA-MB 468 (blue) as well as on EGFR negative cell line HEK293-FT (red). Analysis of (A) green area confluency, (B) fluorescence intensity and (C) confluency were performed by Incucyte measurements. (D) The absorbance of MTS proliferation assay was determined by SpectraMax 340. The mean value ± SEM is shown (N = 1, n = 3).

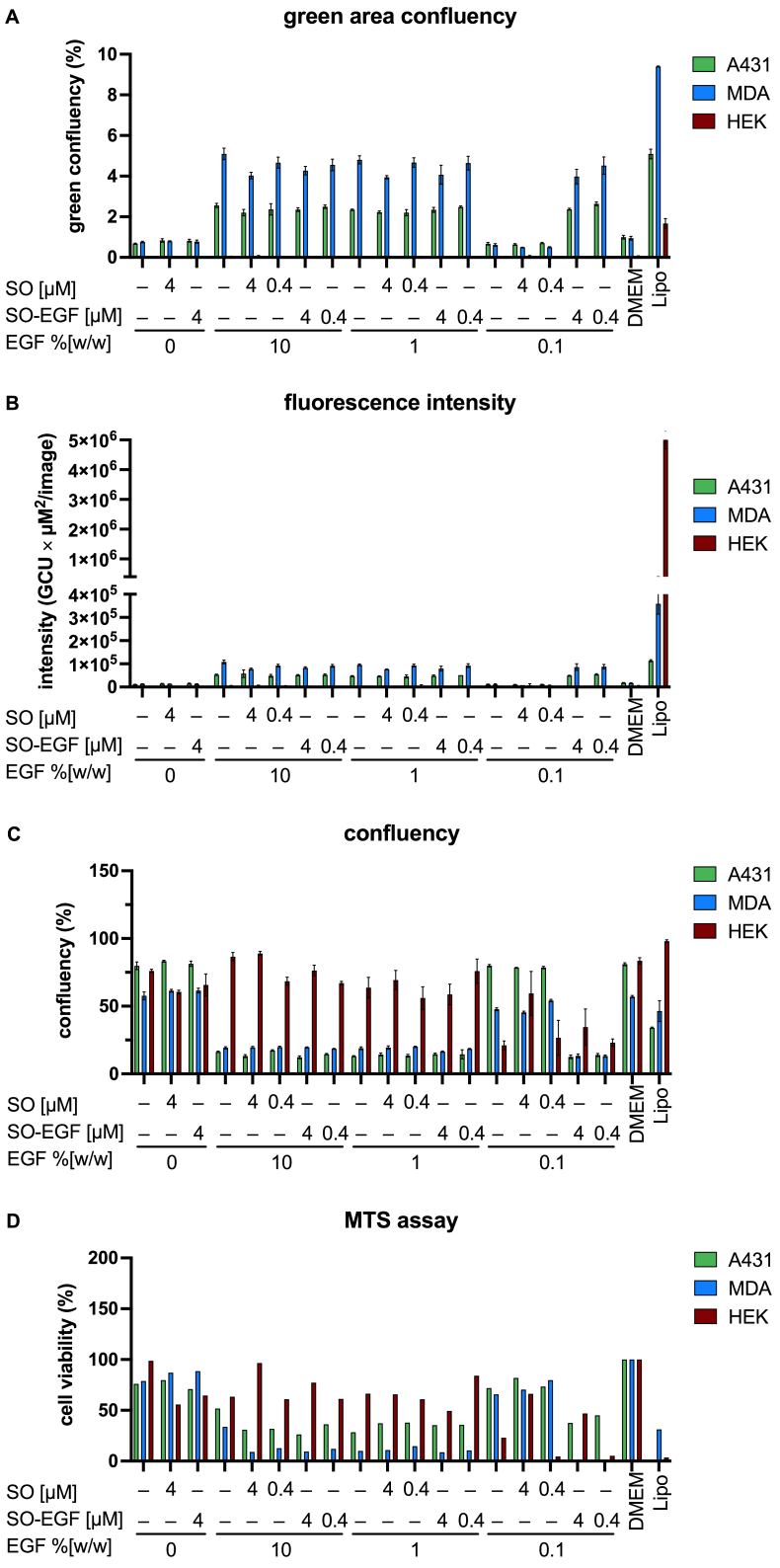

Figure S17: Transfection efficiency of eGFP plasmid and cytotoxicity of D2 [N/P 16, EGF 0–10 (after)] with and without additional SO1861 or SO1861-EGF.
The assay was performed on EGFR positive cell lines A431 (green) and MDA-MB 468 (blue) as well as on EGFR negative cell line HEK293-FT (red). Analysis of (A) green area confluency, (B) fluorescence intensity and (C) confluency were performed by Incucyte measurements. (D) The absorbance of MTS proliferation assay was determined by SpectraMax 340. The mean value ± SEM is shown (N = 1, n = 3).

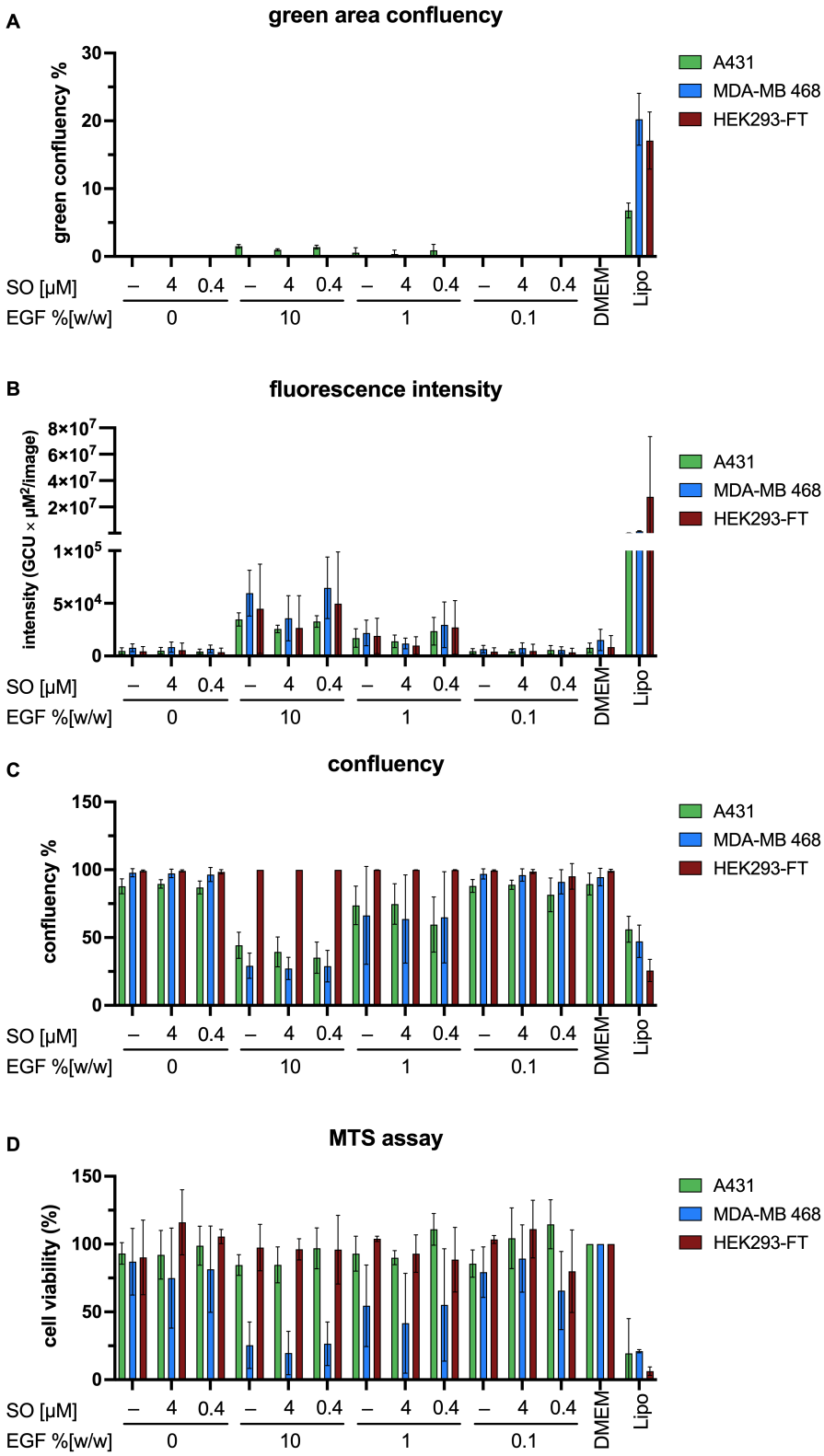

Figure S18: Transfection efficiency of eGFP plasmid and cytotoxicity of D1+5 [N/P 16, EGF 0–10 (pp)] with and without additional SO1861 or SO1861-EGF.
The assay was performed on EGFR positive cell lines A431 (green) and MDA-MB 468 (blue) as well as on EGFR negative cell line HEK293-FT (red). Analysis of (A) green area confluency, (B) fluorescence intensity and (C) confluency were performed by Incucyte measurements. (D) The absorbance of MTS proliferation assay was determined by SpectraMax 340. The mean value ± SEM is shown (N = 1, n = 3).

This project has received funding from the European Union's Horizon 2020 research and innovation programme under grant agreement No 825730.